



**HAL**  
open science

# Cryo-electron microscopy study of translation initiation complexes from *Staphylococcus aureus*

Margarita Belinite

► **To cite this version:**

Margarita Belinite. Cryo-electron microscopy study of translation initiation complexes from *Staphylococcus aureus*. Genomics [q-bio.GN]. Université de Strasbourg, 2019. English. NNT : 2019STRAJ082 . tel-02974666

**HAL Id: tel-02974666**

**<https://theses.hal.science/tel-02974666>**

Submitted on 22 Oct 2020

**HAL** is a multi-disciplinary open access archive for the deposit and dissemination of scientific research documents, whether they are published or not. The documents may come from teaching and research institutions in France or abroad, or from public or private research centers.

L'archive ouverte pluridisciplinaire **HAL**, est destinée au dépôt et à la diffusion de documents scientifiques de niveau recherche, publiés ou non, émanant des établissements d'enseignement et de recherche français ou étrangers, des laboratoires publics ou privés.

**ÉCOLE DOCTORALE DES SCIENCES DE LA VIE ET DE LA SANTÉ**  
**IGBMC – CNRS UMR 7104 – Inserm U 964**

**THÈSE** présentée par :  
**Margarita BELINITE**

soutenue le : 21 octobre 2019

pour obtenir le grade de : **Docteur de l'université de Strasbourg**

Discipline/ Spécialité : Biophysique et biologie structurale

(Biophysics and Structural biology)

**Cryo-electron microscopy study of  
translation initiation complexes from  
*Staphylococcus aureus***

**Etude en microscopie cryogénique des  
complexes d'initiation de la traduction de  
*Staphylococcus aureus***

**THÈSE dirigée par :**

**Dr Yaser HASHEM**  
**Dr Marat YUSUPOV**

Chargé de recherches, Université de Bordeaux  
Directeur de recherche, Université de Strasbourg

**RAPPORTEURS :**

**Pr Yves MECHULAM**  
**Dr Fabien DARFEUILLE**

Directeur de recherche, École Polytechnique (Paris)  
Chargé de recherches, Université de Bordeaux

**AUTRES MEMBRES DU JURY :**

**Dr Celia PLISSON-CHASTANG**  
**Dr Gulnara YUSUPOVA**

Chargé de recherches, Université Paul Sabatier (Toulouse)  
Directeur de recherche, Université de Strasbourg

## ACKNOWLEDGEMENTS

This thesis describe the work that I have been doing since 2015 under the supervision of several people.

First of all, I would like to thank my jury members **Pr. Yves Mechulam, Dr. Fabien Darfeuille, Dr. Celia Plisson-Chastang** and **Dr. Gulnara Yusupova** who agreed to evaluate my PhD work. I am very grateful to meet them in Strasbourg and to discuss.

I am grateful to my PhD supervisor **Yaser Hashem** for giving me a chance to work in his team, for all our discussions, for his help and motivation. Every day I learned a lot while working in his laboratory. Also, I met so many wonderful people in Strasbourg and in Bordeaux. It was a pleasure to work in your lab.

I am thankful to my co-supervisor **Marat Yusupov** for his support and patience. Time spent in his laboratory was productive and useful for me.

I express my gratitude to **Stefano** and **Angelita** for sharing their experience with me, for helping me with my main project and for all our discussions.

Special thanks to **Pascale Romby** for all our discussions that gave me a fresh view on my project.

I would like to thank everyone in all three labs I worked in, starting from **Iskander** and **Simone** for teaching me and helping me with my projects. Then, to **Jay, Quentin** and **Anthony** for all our useful discussions and your contribution in my main project, to **Clair** and **Adeline** for technical support. Thanks to people from my second lab: **Alexey, Nemanja, Sasha, Justine, Mélanie** and **Lasse** for all their useful advices and to **Irina, Salvatore, Olga, Yury** and **Mumin** for their constant support. Also, thanks to people from my third lab in Bordeaux: **Marie, Camila, Stéphanie, Florian, Aline, Mayara, Ewelina** for their support during my last year of PhD. Special thanks to **Anthony** and **Florent** for your help in the last part of my PhD and to **Heddy** for grids preparations, data acquisition and image processing and also our useful discussions. Without all these people it would be much more difficult to do my projects.

Thanks to Pascale Romby's (**Isabelle, Anne-Catherine, Emma, Laura** and **Lucas**) and Axel Innis (**Alba, Mélanie, Elodie, Natacha, Mecit, Aitor** and **Anne-Xander**) laboratories for the opportunity to sometimes work in their labs.

**Danièle** and **Léandra** for the incredible support and help with all my documents.

**Johana, Lauriane** and **Philippe** for the mass spec analysis of my samples. Without their commitment and effort this work would not be possible.

Many thanks to my friends **Irina, Lyuba, Elena, Fatima, Salvatore, Olga** and **Yury** for your support and incredible time spent together.

Also, thanks to my friends in Kazan: **Elena, Elvira, Anastasia, Ekaterina, Anastasia, Alina** and **Sofia** for always being happy to see me, no matter how much time had passed.

Most importantly, I would like to thank my family. I am very grateful to my parents **Marina** and **Aleksander**, who accepted my intention to come to France. To my sister **Ekaterina**, whom I wish good luck in China. I am proud of you. And especially to my husband **Anatolii**, who supported me and moved with me first to Strasbourg, and then to Bordeaux.

My PhD would not have been possible without the support and participation of all these people. Thank you!

# TABLE OF CONTENTS

<b>ACKNOWLEDGEMENTS</b> .....	<b>2</b>
<b>TABLE OF CONTENTS</b> .....	<b>4</b>
<b>TABLE OF FIGURES AND TABLES</b> .....	<b>6</b>
<b>ABBREVIATIONS</b> .....	<b>9</b>
<b>INTRODUCTION</b> .....	<b>10</b>
<b>The Ribosome</b> .....	<b>11</b>
<b>Core of the ribosome</b> .....	11
<b>Features of prokaryotic and eukaryotic ribosomes</b> .....	12
Eukaryotic-specific ribosomal proteins and extensions .....	14
RNA expansion segments (ES) .....	14
<b>Protein synthesis</b> .....	<b>21</b>
<b>Initiation</b> .....	21
<b>Elongation</b> .....	22
<b>Termination and recycling</b> .....	23
<b>Translation initiation in bacteria</b> .....	<b>25</b>
<b>Components of initiation complex in bacteria</b> .....	26
<b>IF1</b> .....	26
<b>IF2</b> .....	27
<b>IF3</b> .....	28
<b>fMet-tRNA<sup>fMet</sup></b> .....	29
<b>mRNA</b> .....	31
<b>Translation regulation in S. aureus</b> .....	<b>32</b>
<b>Specific features of the protein synthesizing apparatus of Staphylococcus aureus</b> .....	33
<b>S1</b> .....	34
<b>Initiation factors</b> .....	34
<b>Antibiotics</b> .....	<b>36</b>
Selective membrane permeability .....	36
Protein synthesis inhibitors .....	36
Antibiotics that inhibit the synthesis of nucleic acids .....	38
Fatty acid synthesis inhibitors .....	39
<b>Current drugs against S. aureus</b> .....	39
<b>Project 1: Assembly pathway of the S. aureus initiation complex</b> .....	<b>41</b>
<b>Project 2: Crystallogensis of Candida albicans 80S</b> .....	<b>42</b>
<b>Specific features of Candida albicans ribosome</b> .....	42
<b>RESEARCH PROJECT 1</b> .....	<b>44</b>
<b>Translation initiation complex from S. aureus</b> .....	<b>44</b>
<b>In vitro reconstruction of translation initiation complex</b> .....	45
<b>MATERIALS AND METHODS</b> .....	45
<b>RESULTS</b> .....	76
<b>Ex vivo experiments</b> .....	96
<b>DISCUSSION</b> .....	99
<b>PERSPECTIVES</b> .....	104

CONCLUDING REMARKS .....	105
<b>RESEARCH PROJECT 2 .....</b>	<b>106</b>
<b>Structure determination of Candida albicans ribosome .....</b>	<b>106</b>
<b>MATERIALS AND METHODS.....</b>	<b>107</b>
<b>80S PURIFICATION .....</b>	<b>107</b>
<b>X-RAY CRYSTALLOGRAPHY .....</b>	<b>109</b>
<b>RESULTS.....</b>	<b>112</b>
<b>Mass spectrometry.....</b>	<b>112</b>
<b>Analytical ultracentrifugation .....</b>	<b>115</b>
<b>Crystallization.....</b>	<b>116</b>
<b>Post-crystallization treatment.....</b>	<b>118</b>
<b>DISCUSSION .....</b>	<b>120</b>
<b>PERSPECTIVES.....</b>	<b>121</b>
<b>CONCLUDING REMARKS .....</b>	<b>121</b>
<b>RESUME DE THESE EN FRANÇAIS .....</b>	<b>122</b>
<b>BIBLIOGRAPHY.....</b>	<b>127</b>

## TABLE OF FIGURES AND TABLES

<b>Figure 1.</b>	The small ribosomal subunit with tRNA binding sites and decoding center	12
<b>Figure 2.</b>	The large subunit major functional sites are the tRNA binding sites, the peptide exit tunnel that extends through the body of the large subunit and the peptidyl transferase center.	12
<b>Figure 3.</b>	Composition of bacterial and eukaryotic ribosomes	13
<b>Figure 4.</b>	Ribosomal proteins of the 40S subunit	18
<b>Figure 5.</b>	Ribosomal proteins of the 60S subunit	18
<b>Figure 6.</b>	Sequence and secondary structure of rRNA of LSU from <i>S. cerevisiae</i>	19
<b>Figure 7.</b>	Sequence and secondary structure of rRNA of 18S from <i>S. cerevisiae</i>	20
<b>Figure 8.</b>	Scheme of the initiation process in bacteria	21
<b>Figure 9.</b>	Translation initiation process in eukaryotes	22
<b>Figure 10.</b>	Conservative elongation process of protein synthesis in all kingdoms	22
<b>Figure 11.</b>	The diagram shows the last 2 steps of translation termination and recycling for prokaryotes	23
<b>Figure 12.</b>	The diagram shows termination and recycling processes for eukaryotes that are different from prokaryotes	23
<b>Figure 13.</b>	Schematic diagram of translation cycle in bacteria	24
<b>Figure 14.</b>	The translation cycle for eukaryotes which is divided into four main steps: initiation (including preinitiation), elongation, termination and recycling	24
<b>Figure 15.</b>	The process of the initiation complex formation based on FRET experiments	25
<b>Figure 16.</b>	The assembly of the initiation complex, based on cryo-EM structures	26
<b>Figure 17.</b>	The structure of IF1 from <i>S. aureus</i> determined with multidimensional NMR spectroscopy	26
<b>Figure 18.</b>	X-ray structure of translation IF2 from <i>Methanothermobacter thermautotrophicus</i>	28
<b>Figure 19.</b>	Cryo-EM structure of IF3 from <i>Thermus thermophilus</i>	29
<b>Figure 20.</b>	Comparison of initiator and elongator methionine tRNAs	30
<b>Figure 21.</b>	RNA-mediated mechanism used in virulence gene regulation. The mechanism of action of <i>S. aureus</i> RNAIII on <i>spa</i> expression	33
<b>Figure 22.</b>	Scheme of the initiation factor 2 structure from <i>T. thermophilus</i> , <i>S. aureus</i> and <i>E. coli</i>	35
<b>Figure 23.</b>	A scheme shows at which stage of protein synthesis different antibiotics bind to the ribosome	37
<b>Figure 24.</b>	Sucrose gradient profile of 70S from <i>S. aureus</i>	47
<b>Figure 25.</b>	One-dimensional PAGE of <i>S. aureus</i> 70S ribosome	48
<b>Figure 26.</b>	Agarose gel in native and denaturing conditions	49
<b>Figure 27.</b>	Crystals of 70S ribosome from <i>S. aureus</i>	52
<b>Figure 28.</b>	Sucrose gradient profile of 30S from <i>S. aureus</i>	53
<b>Figure 29.</b>	One-dimensional PAGE of <i>S. aureus</i> 30S ribosome	54
<b>Figure 30.</b>	Agarose gel of 30S ribosome	54
<b>Figure 31.</b>	Formation of simplified translation initiation complex by toeprinting assays	55
<b>Figure 32.</b>	One-dimensional PAGE of initiation factors	61
<b>Figure 33.</b>	Structure of <i>spa</i> mRNA	62
<b>Figure 34.</b>	6% PAGE of <i>spa</i> mRNA	63

<b>Figure 35.</b>	One-dimensional PAGE of MetRS	65
<b>Figure 36.</b>	One-dimensional PAGE of MTF	66
<b>Figure 37.</b>	6% PAGE of tRNA	68
<b>Figure 38.</b>	Schematic representation of basic composition of electron microscope	71
<b>Figure 39.</b>	Representation of the cryo-EM grid at different scales	72
<b>Figure 40.</b>	Scheme of sample analysis by cryo-electron microscopy	72
<b>Figure 41.</b>	Principle steps of image processing in CryoSparc	75
<b>Figure 42.</b>	Formation of simplified initiation complex with IF1 and IF2 by toeprinting assays	77
<b>Figure 43.</b>	The quantification of the toeprint (given in %) was first normalized according to the full-length extension product bands using the ImageQuant TL software	77
<b>Figure 44.</b>	Formation of simplified initiation complex with IF2 by toeprinting assays	78
<b>Figure 45.</b>	The quantification of the toeprint (given in %) was first normalized according to the full-length extension product bands using the ImageQuant TL software	78
<b>Figure 46.</b>	Formation of initiation complex with fMet-tRNA <sup>fMet</sup> and Lys-tRNA by toeprinting assays	79
<b>Figure 47.</b>	The quantification of the toeprint (given in %) was first normalized according to the full-length extension product bands using the ImageQuant TL software	80
<b>Figure 48.</b>	Sucrose gradient profile and agarose gel of 30S	80
<b>Figure 49.</b>	Micrograph of SSU from <i>S. aureus</i>	82
<b>Figure 50.</b>	3D classification of 643532 particles divided into 10 classes	83
<b>Figure 51.</b>	Sucrose gradient profiles of 30S	83
<b>Figure 52.</b>	15% polyacrylamide gel	84
<b>Figure 53.</b>	Sucrose gradient profile and agarose gel of 16S rRNA	84
<b>Figure 54.</b>	3D classification of 479872 particles divided into 10 classes. Obtained 1 class with 60000 particles was reclassified into 6 classes	85
<b>Figure 55.</b>	Sucrose gradient profile and agarose gel of 16S rRNA	86
<b>Figure 56.</b>	During 3D classification 1 class with 40000 particles was obtained and reclassified into 4 classes	86
<b>Figure 57.</b>	Sucrose gradient profiles	87
<b>Figure 58.</b>	Scheme of stepwise assembling of initiation complex	88
<b>Figure 59.</b>	Structures obtained after 4 <sup>th</sup> data collection: 30S without spermidine	89
<b>Figure 60.</b>	Structure obtained after 4 <sup>th</sup> data collection: 30S with spermidine	89
<b>Figure 61.</b>	Structure obtained after 5 <sup>th</sup> data collection	90
<b>Figure 62.</b>	Cryo-EM reconstruction of 30S, mRNA and spermidine complex	90
<b>Figure 63.</b>	Structure obtained after 6 <sup>th</sup> data acquisition	91
<b>Figure 64.</b>	Structure obtained after 6 <sup>th</sup> data acquisition	91
<b>Figure 65.</b>	Structure obtained after 6 <sup>th</sup> data acquisition	92
<b>Figure 66.</b>	Cryo-EM reconstruction of 30S with mRNA and IF3 complex	93
<b>Figure 67.</b>	Structure obtained after 6 <sup>th</sup> data collection: 30S with mRNA, fMet-tRNA <sup>fMet</sup> and IF3	93
<b>Figure 68.</b>	Structure obtained after 6 <sup>th</sup> data collection: 30S with mRNA and IF3	93
<b>Figure 69.</b>	Structure obtained after 6 <sup>th</sup> data collection: 30S with mRNA, fMet-tRNA <sup>fMet</sup> and IF3	94
<b>Figure 70.</b>	Scheme of stepwise assembling of initiation complex	95
<b>Figure 71.</b>	Sucrose gradient profile	96

<b>Figure 72.</b>	15% polyacrylamide gel	97
<b>Figure 73.</b>	Agarose gel in native conditions of sample from III gradient	97
<b>Figure 74.</b>	Structure obtained after 7 <sup>th</sup> data collection	98
<b>Figure 75.</b>	Atomic model of <i>E. coli</i> ribosome (Noeske et al., 2015)	101
<b>Figure 76.</b>	Comparison of two 30S structures: without and with spermidine	101
<b>Figure 77.</b>	Comparison of two 30S with mRNA structures: without and with spermidine	101
<b>Figure 78.</b>	Comparison of two 30S with mRNA and IF3 (different incubation)	102
<b>Figure 79.</b>	Comparison of two 30S-mRNA structures: without and with IF3	103
<b>Figure 80.</b>	Sucrose gradient profile of <i>C. albicans</i> ribosome	108
<b>Figure 81.</b>	A schematic phase diagram showing the solubility of a protein in solution as a function of the concentration of the precipitant present	110
<b>Figure 82.</b>	Schematic representation of diffraction experiment	111
<b>Figure 83.</b>	One-dimensional 15% PAGE of 80S from <i>C. albicans</i> and <i>S. cerevisiae</i>	112
<b>Figure 84.</b>	Agarose gel of 80S from <i>C. albicans</i> and <i>S. cerevisiae</i>	112
<b>Figure 85.</b>	Comparison of sedimentation profiles of <i>C. albicans</i> ribosome and <i>S. cerevisiae</i> ribosome	116
<b>Figure 86.</b>	Crystals of 80S from <i>C. albicans</i>	118
<b>Figure 87.</b>	Scheme of post-crystallization treatment	119
<b>Table 1.</b>	Composition and characteristics of ribosome from different species	13
<b>Table 2.</b>	List of ribosomal proteins from <i>Candida albicans</i>	15
<b>Table 3.</b>	Mechanisms of action and resistance mechanisms of selected ribosome-targeting antibiotics	38
<b>Table 4.</b>	Antibiotics used against <i>S. aureus</i> and the mechanism of their resistance	40
<b>Table 5.</b>	List of ribosomal proteins found in <i>S. aureus</i> ribosome sample by LC-MS/MS analysis	49
<b>Table 6.</b>	List of non-ribosomal proteins found in <i>S. aureus</i> ribosome sample by LC-MS/MS analysis	51
<b>Table 7.</b>	Characteristics of microscopes used for data acquisition	73
<b>Table 8.</b>	List of proteins found in <i>S. aureus</i> 30S ribosome sample by LC-MS/MS analysis	81
<b>Table 9.</b>	Variations of prepared complexes collected on Talos microscope and processed CryoSparc software	92
<b>Table 10.</b>	List of proteins found in <i>C. albicans</i> 80S ribosome sample by LC-MS/MS analysis	113
<b>Table 11.</b>	Summary of tried crystallization conditions	116

# ABBREVIATIONS

## Methods :

NMR	nuclear magnetic resonance
Cryo-EM	cryo-electron microscopy
FRET	Förster resonance energy transfer
LC-MS/MS	liquid chromatography coupled mass spectrometry
PAGE	polyacrylamide gel electrophoresis

## S. aureus :

<i>S. aureus</i>	<i>Staphylococcus aureus</i>
<i>E. coli</i>	<i>Escherichia coli</i>
<i>B. subtilis</i>	<i>Bacillus subtilis</i>
<i>T. thermophilus</i>	<i>Thermus thermophilus</i>
<i>B. stearothermophilus</i>	<i>Bacillus stearothermophilus</i>
MRSA	methicillin-resistant <i>S. aureus</i>
MSSA	methicillin-susceptible <i>S. aureus</i>
TSS	toxic shock syndrome

## Ribosome :

aa-tRNA	aminoacyl-tRNA
A-site	aminoacyl site
EF	elongation factor (eIF – eukaryotic IF)
E-site	exit site
IF	initiation factor
mRNA	messenger ribonucleic acid
PTC	peptidyl transferase center
P-site	peptidyl site
RF	release factor
RRF	ribosome recycling factor
rRNA	ribosomal ribonucleic acid
SD	Shine-Dalgarno
tRNA	transfer ribonucleic acid

## Cryo-electron microscopy:

CTF	contrast transfer function
DDD	direct detector device
FEG	field emission gun
FSC	Fourier shell correlation
TEM	transmission electron microscopy

## Reagents:

DTT	dithiothreitol
EDTA	ethylenediaminetetraacetic acid
GDP	guanosine diphosphate
GTP	guanosine triphosphate
LB	lysogeny broth
PEG	polyethylene glycol
SDS	sodium dodecyl sulfate

Amino acids are described according to the standard nomenclature with three letters. All ribosomal proteins named according to the current nomenclature (Ban et al., 2014).

## INTRODUCTION

---

---

## The Ribosome

---

Protein synthesis, also called mRNA translation, is a conserved process that is carried out by the ribosome in all living cells.

For the first time, ribosomes were observed by cell biologist George Emil Palade in the mid-1950s. A few years later the term “ribosome” was proposed by Richard B. Roberts. In 1974, Albert Claude, Christian de Duve and George Emil Palade were awarded the Nobel Prize for the discovery of the ribosome. Later, in 2009, Venkatraman Ramakrishnan, Thomas A. Steitz and Ada E. Yonath got the Nobel Prize in Chemistry for determining the detailed structure of ribosome. Since the 1960s, biochemical and mutational studies of the ribosome have made it possible to describe many of its functional and structural features.

In 2009, Konstantin Bokov and Sergey Steinberg, based on the 3D-structure of the ribosomal RNA from *Escherichia coli*, suggested that ribosome could be formed as a result of a gradual evolution from a very simple small RNA molecule (proto-ribosome). Each new ribosome insert was sequentially added, making the ribosome more stable (Bokov and Steinberg, 2009).

### Core of the ribosome

The ribosome is an important machine and is a major link between genes and proteins. It has an asymmetric structure with a common core between prokaryotic and eukaryotic organisms. Structurally and functionally, the ribosome includes a large and a small subunits that are hybrid molecules made of ribonucleic acid (ribosomal RNA) and proteins. The average ratio between rRNA(s) and proteins is 2:1 in bacteria and about 1:1 in eukaryotes. In the mitochondrial and chloroplast ribosomes ratios are 1:2 and 3:2 respectively (Sharma and Agrawal, 2012).

Small ribosomal subunits (SSU) from prokaryotes (30S) and eukaryotes (40S) have similar shapes, and some of their landmarks as dubbed in anthropomorphic terms such as ‘head’, ‘body’, ‘beak’ and ‘shoulder’. They are responsible for selection of the aminoacyl-tRNA (aa-tRNA) according to the mRNA sequence and have a functional mRNA and tRNA binding sites: aminoacyl-tRNA (A-site), peptidyl-tRNA (P-site) and the exit site for the

deacylated-tRNA (E-site) (Fig. 1). During translation, tRNAs are translocated from the A- to the P-site and from the P- to the E-site.

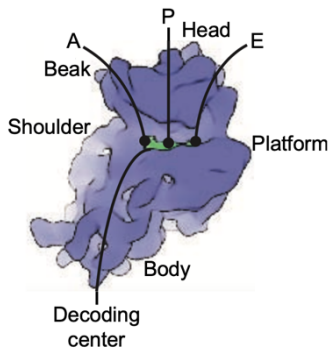


**Figure 1.** The small ribosomal subunit with tRNA binding sites (A, P and E) and decoding center.

The large ribosomal subunits (LSU) from different species also have similar features, which include the ‘central protuberance’, ‘L1-stalk’ and the ‘L7/L12- stalk’ (‘P-stalk’ in eukaryotes). This subunit has the three tRNA-binding sites (A, P and E) and the peptidyl transferase center (PTC) (Fig 2). The function of large subunit is to catalyze the formation of peptide bonds between amino acids, through the PTC.

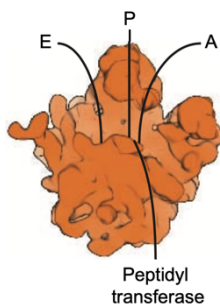


**Figure 2.** The large subunit major functional sites are the tRNA binding sites (A, P and E), the peptide exit tunnel that extends through the body of the large subunit, and the peptidyl transferase center (PTC) (Melnikov et al., 2012).

### Features of prokaryotic and eukaryotic ribosomes

Despite significant similarities in the structure of ribosomes between prokaryotes and eukaryotes, there are many peculiarities in structures and regulation mechanisms of ribosomes from different organisms and also in the process of protein synthesis in general. The prokaryotic ribosome is formed by some 54 ribosomal proteins and 3 ribosomal RNAs (16S, 23S and 5S), while the eukaryotic ribosome is composed of some 79 ribosomal proteins and 4 ribosomal RNAs (18S, 25S, 5.8S and 5S). The fully assembled prokaryotic ribosome has a sedimentation coefficient (particle deposition rate during ultracentrifugation) of 70S, its LSU of 50S and SSU of 30S, whereas the eukaryotic ribosome is an 80S because of its ~40% molecular weight, consisting of an LSU of 60S and an SSU of 40S (Fig. 3). The archaeal

ribosome have a size and composition similar to bacterial ribosomes: they contain three rRNA molecules (16S, 23S and 5S) and 50-70 proteins depending on the species. However, the primary structures of archaeal rRNA and r-proteins are closer to eukaryotes (Table 1).

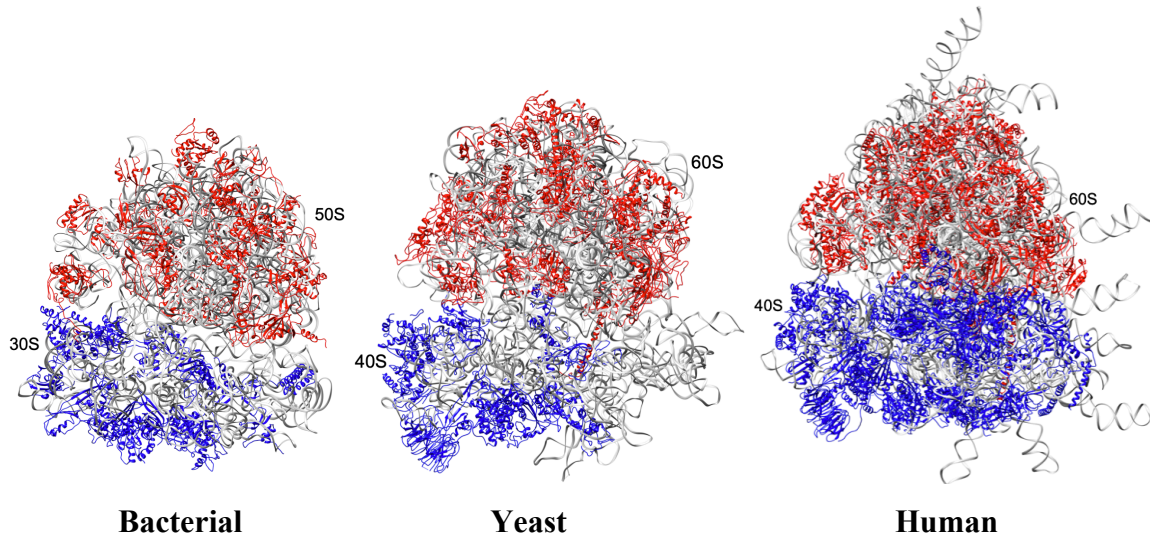


**Figure 3.** Composition of bacterial and eukaryotic ribosomes: RNA in light grey, proteins of small ribosomal subunit in blue and proteins of large ribosomal subunit in red. The figures are based on X-ray and Cryo-EM structures from Jenner et al., 2013, Ben-Shem et al., 2010, Armache et al., 2010.

**Table 1.** Composition and characteristics of ribosome from different species (Yusupov et al., 2001, Spahn et al., 2004, Schuwirth et al., 2005, Ben-Shem et al., 2010, Armache et al., 2013).

	Bacteria	Archaea	Yeast	H. sapiens
Ribosome	70S	70S	80S	80S
Molecular weight	2.3 MDa	2.5 MDa	3.3 MDa	4.3 MDa
Number of rRNAs	3	3	4	4
Number of r-proteins	54	up to 68	79	80
Large subunit	50S	50S	60S	60S
rRNA	23S, 5S	23S, 5S	25S, 5.8S, 5S	28S, 5.8S, 5S
r-proteins	33	27	46	47
Small subunit	30S	30S	40S	40S
rRNA	16S	16S	18S	18S
r-proteins	21	~20	33	33

Briefly, the 80S ribosome presents many features that are not found in the bacterial ribosomes. For instance, additional rRNA helices (also called expansion segments), additional ribosomal proteins and protein extensions organized in tails.

#### *Eukaryotic-specific ribosomal proteins and extensions*

In the eukaryotic ribosome, specific proteins for the small ribosomal subunit are S1, S4, S6, S8, S10, S12, S17, S19 - S31 (Fig. 4). For the large ribosomal subunit specific proteins are L6, L8, L13, L14, L15, L18, L19 - L22, L24, L27, L30, L31 – L43 (Table 2, Fig. 5).

There are a group of proteins with unusual folds long tails and extending loops (S3, L4, L22, L23 and L29). With the determination of ribosome structures from different organisms, it became clear that these unusual protein folds are even more abundant in eukaryotes than in bacteria. The function of these insertions and extensions is to interact with other eukaryotic-specific proteins and rRNA extension segments, which may facilitate the assembly of eukaryotic-specific components.

#### *RNA expansion segments (ES)*

Expansion segments (ESs) can be defined as the additional rRNA insertions the eukaryotic ribosome compared to their bacterial counterpart. They can be found on both the SSU (labeled with an “S”) and the LSU (labeled with an “L”), accordingly. Some of ESs can be accompanied by ribosomal proteins extensions and tails, such as in *S. cerevisiae* where the expansion segments ES31L and ES39L embed stretches of single-stranded rRNA and are surrounded by several ribosomal proteins.

Other ESs can be long flexible naked rRNA helices. An example of such ESs are ES7L, ES15L, ES27L and ES39L. The functions of most of these segments are still poorly understood. Although it has been shown that ES act as platforms for the binding of proteins that modulate translation across evolution (Armache et al., 2010, Fujii et al., 2018, Fig. 6 and 7).

**Table 2.** List of ribosomal proteins from *Candida albicans* (www.uniprot.org), where e – eukaryotic-specific ribosomal proteins, u – universal proteins, MW - molecular weight, pI - isoelectric point.

Small ribosomal subunit				Large ribosomal subunit			
Name of protein	Name of gene	MW	pI	Name of protein	Name of gene	MW	pI
eS1	RPS1	29,0	10,04	uL1	RPL1	24,4	9,76
uS2	RPS0	28,7	4,91	uL2	RPL2	27,3	10,71
uS3	RPS3	27,3	9,23	uL3	RPL3	43,9	10,26
uS4	RPS9	21,7	10,20	uL4	RPL4	39,2	10,74
eS4	RPS4	29,4	10,15	uL5	RPL11	19,8	9,95
uS5	RPS2	26,9	10,24	uL6	RPL9	21,7	9,51
eS6	RPS6	27,1	10,15	eL6	RPL6	19,8	10,21
eS7	RPS7	21,2	9,92	eL8	RPL8	28,5	10,05
uS7	RPS5	25,2	8,7	uL10	RPP0	33,3	4,83
eS8	RPS8	22,7	11,09	uL11	RPL12	17,8	9,51
uS8	RPS22	14,8	9,88	uL13	RPL16	22,6	10,32
uS9	RPS16	15,7	10,29	eL13	RPL13	23,0	10,61
eS10	RPS10	13,8	9,83	eL14	RPL14	14,7	10,90

uS10	RPS20	13,3	9,94	uL14	RPL23	13,3	10,07
uS11	RPS14	14,0	10,90	eL15	RPL15	24,3	11,34
uS12	RPS23	16,0	10,81	uL15	RPL28	16,7	10,42
eS12	RPS12	15,7	4,70	uL16	RPL10	25,1	10,08
uS13	RPS18	17,0	10,35	eL18	RPL18	20,8	11,8
uS14	RPS29	6,6	9,76	uL18	RPL5	34,4	7,64
uS15	RPS13	16,9	10,23	eL19	RPL19	21,6	11,12
uS17	RPS11	17,6	10,43	eL20	RPL20	20,3	10,24
eS17	RPS17	15,7	10,46	eL21	RPL21	18,0	10,33
uS19	RPS15	15,9	10,32	eL22	RPL22	14,1	5,36
eS19	RPS19	16,1	9,42	uL22	RPL17	21,0	10,77
eS21	RPS21	9,6	8,15	uL23	RPL25	15,8	10,15
eS24	RPS24	15,5	10,87	eL24	RPL24	17,4	11,37
eS25	RPS25	11,6	10,15	uL24	RPL26	14,2	10,48
eS26	RPS26	13,6	10,89	eL27	RPL27	15,5	10,18
eS27	RPS27	9,0	8,73	uL29	RPL35	14,1	11,24

eS28	RPS28	7,5	10,36	eL30	RPL30	11,5	9,70
eS30	RPS30	7,1	11,47	uL30	RPL7	27,4	10,24
eS31	RPS31	16,8	10,48	eL31	RPL31	13,0	9,82
P1		10,7	4,02	eL32	RPL32	14,9	10,54
P2		10,9	3,93	eL33	RPL33	12,1	10,78
				eL34	RPL24	13,7	10,74
				eL36	RPL36	11,1	11,4
				eL37	RPL37	9,9	11,63
				eL38	RPL38	8,9	10,46
				eL40	RPL40	17,3	9,85
				eL42	RPL41	12,2	10,37
				eL43	RPL43	10,1	10,68

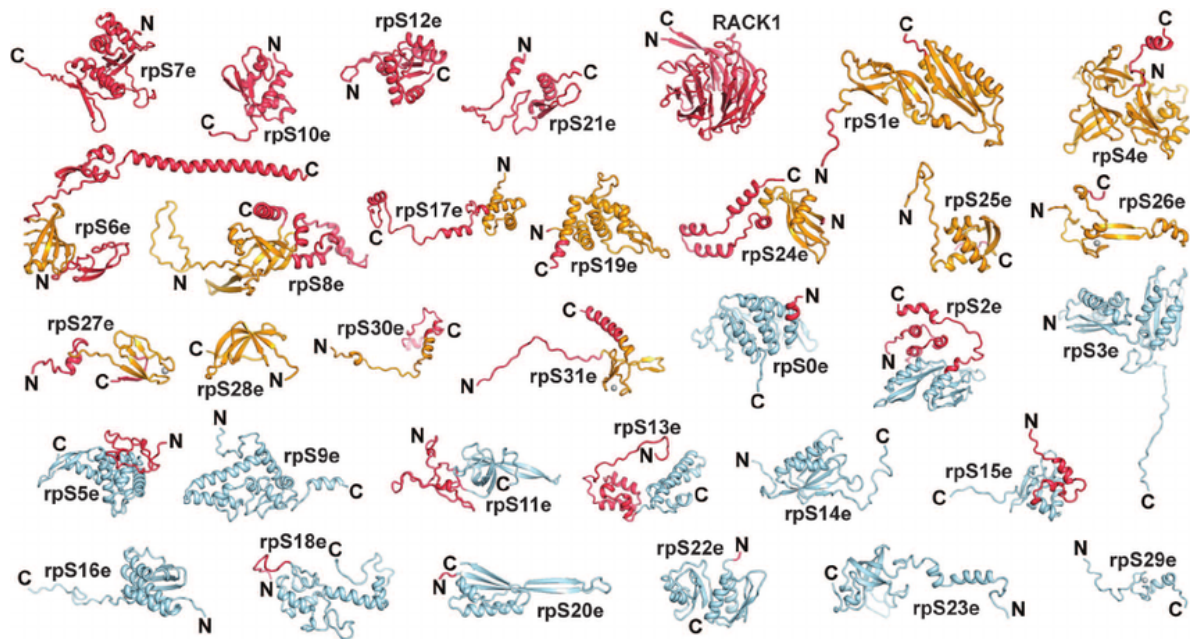


**Figure 4.** Ribosomal proteins of the 40S subunit that are colored according to conservation: protein cores found in all kingdoms are in light blue, proteins with archaeal homologs are in gold and unique for eukaryotes protein extensions are in red (Rabl et al., 2011).

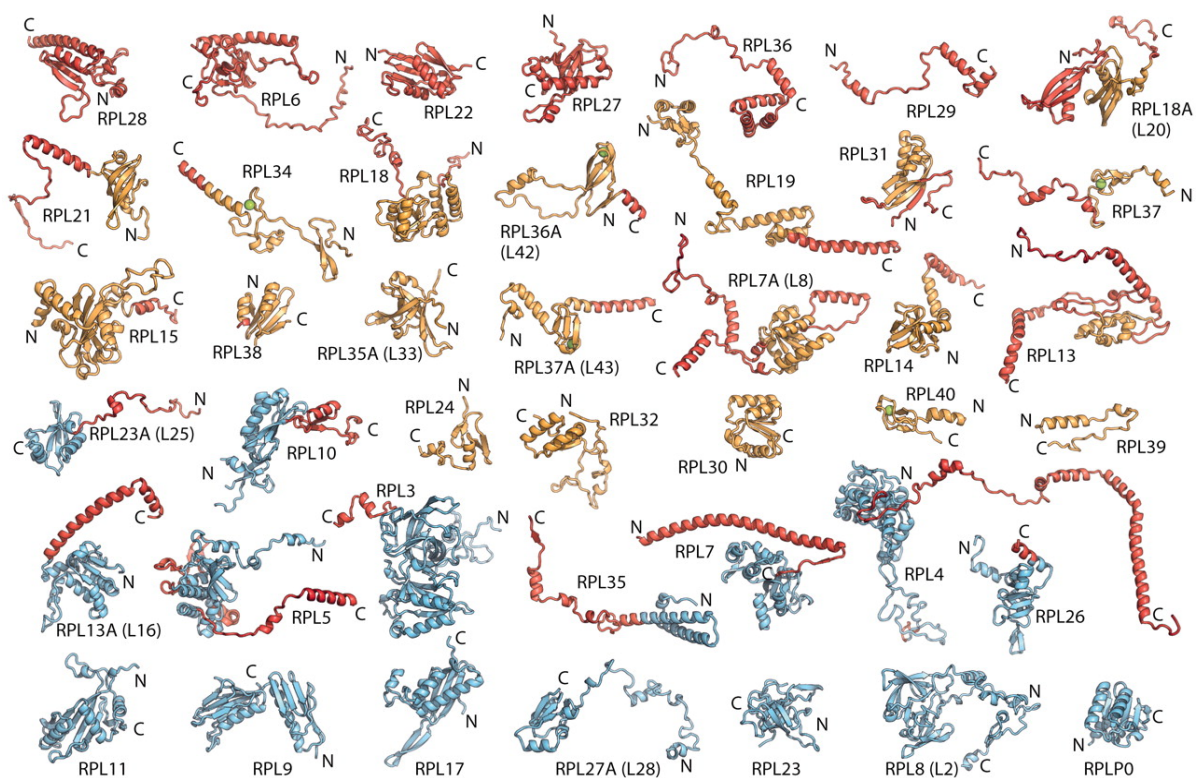


**Figure 5** Ribosomal proteins of the 60S subunit that are colored according to conservation: protein cores found in all kingdoms are in light blue, proteins with archaeal homologs are in gold and unique for eukaryotes proteins extensions are in red. Zinc ions are shown as green spheres (Klinge et al., 2011).

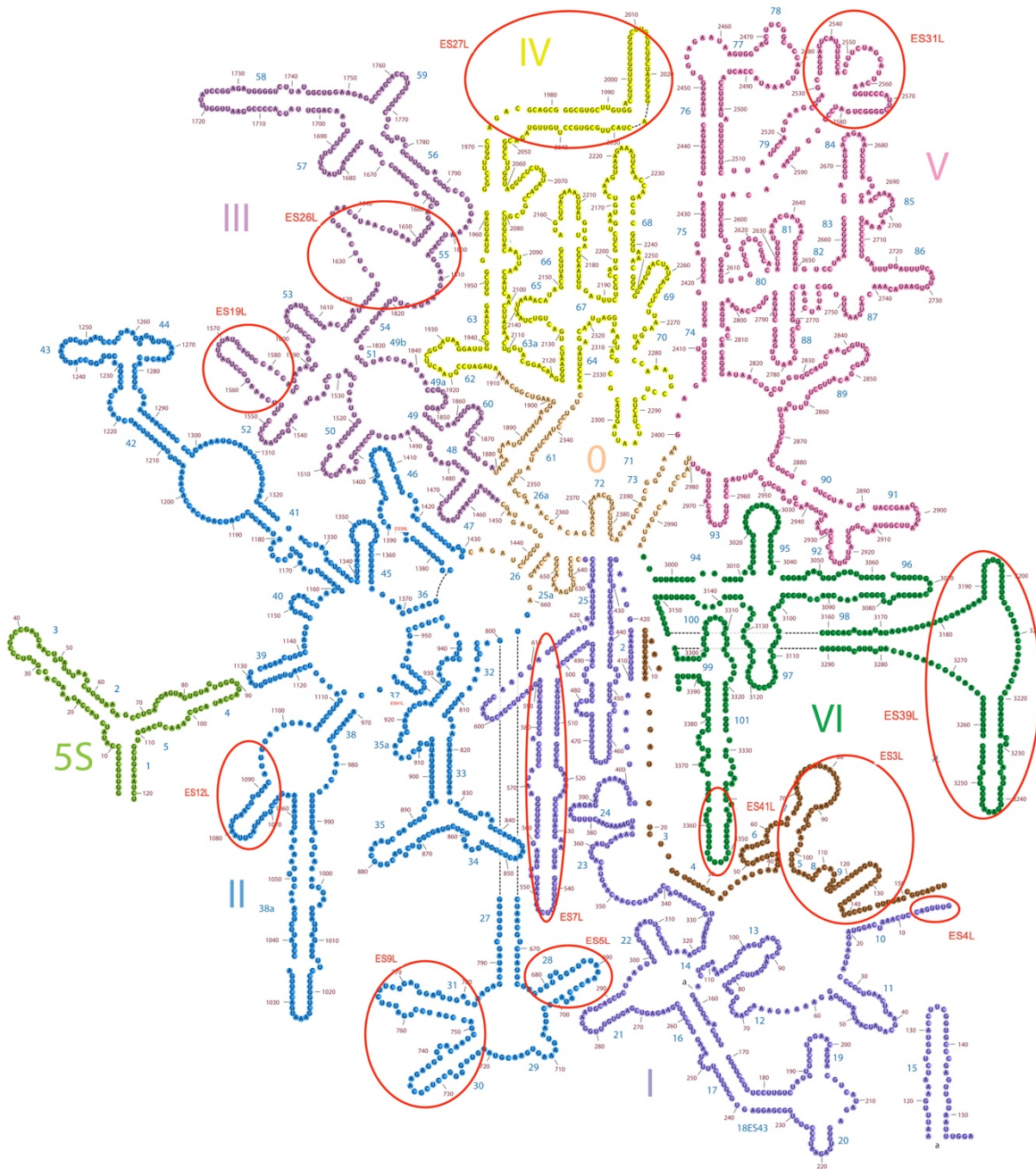


**Figure 6.** Sequence and secondary structure of rRNA of LSU from *S. cerevisiae*. Roman numerals denote different rRNA domains. Expansion segments are designated as the “ES”, where the first digit is the location of the segment, and the last means its name (from Ribovision website).

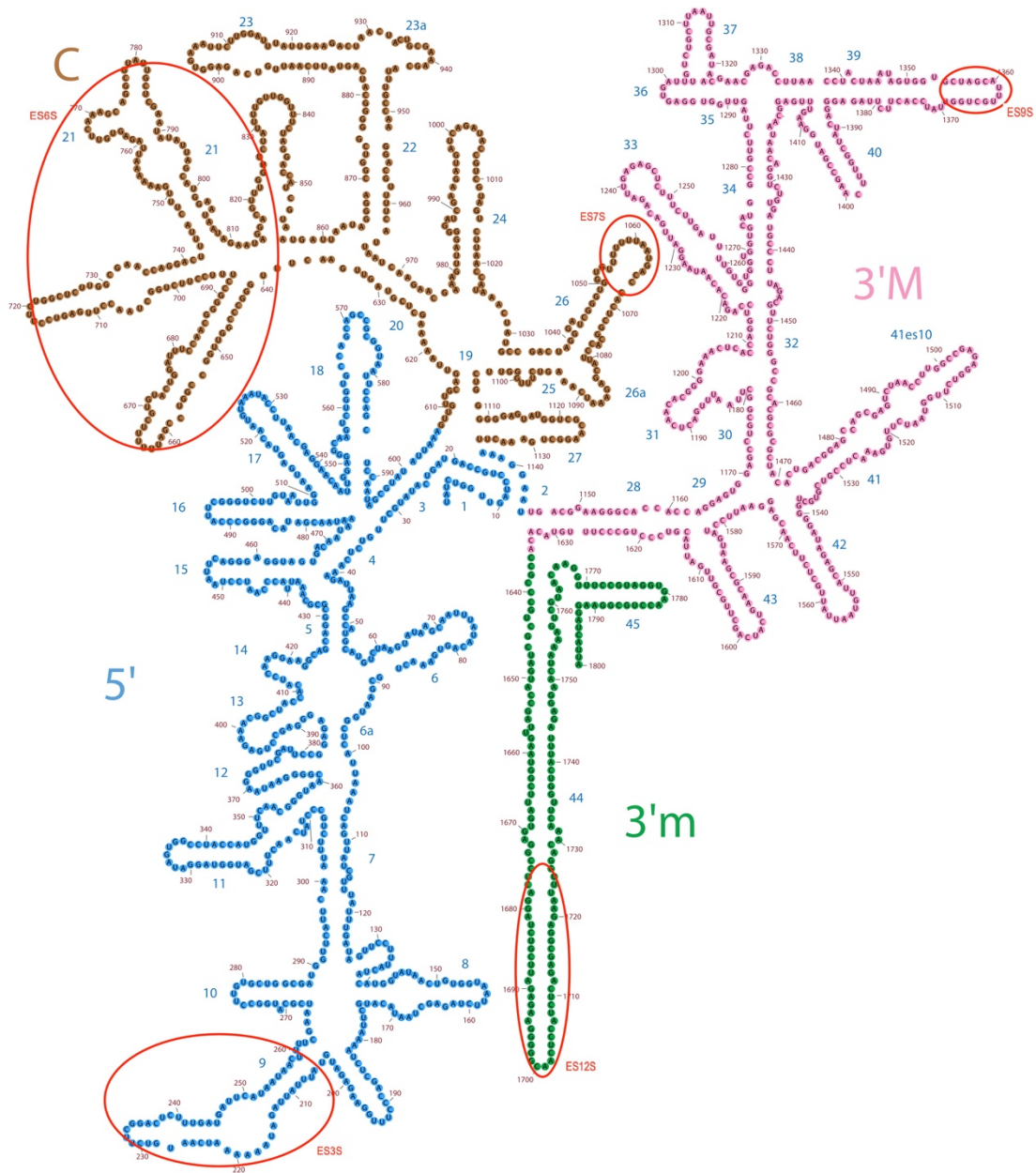


**Figure 7.** Sequence and secondary structure of 18S from *S. cerevisiae*. Expansion segments are designated as the “es”, where the first digit is the location of the segment, and the last means its name (from Ribovision website).

---

## Protein synthesis

---

Protein synthesis can be divided into 4 main steps: initiation, elongation, termination and recycling.

### Initiation

The initiation phase involves the formation of a first complex on the small ribosomal subunit that sets the position of the initiation codon of mRNA (AUG), as well as the initiator tRNA (fMet-tRNA<sup>fMet</sup>) at the SSU P-site. Bacterial translation initiation will be covered in the details later on during this introduction and will be briefly mentioned in this section.

In bacteria, this process is mainly controlled by three translation initiation factors: IF1, IF2 and IF3. Initiation is a very conserved step among bacteria. It involves the orderly binding of mRNA, IFs 3, 2 and 1 factor and the fMet-tRNA<sup>fMet</sup>. After the accommodation of the start codon, the IFs depart, followed by the formation of the ribosome (also called 70S) by the association of the large ribosomal subunit (50S) to the small (30S) (from review Rodnina, 2018, Fig. 8).

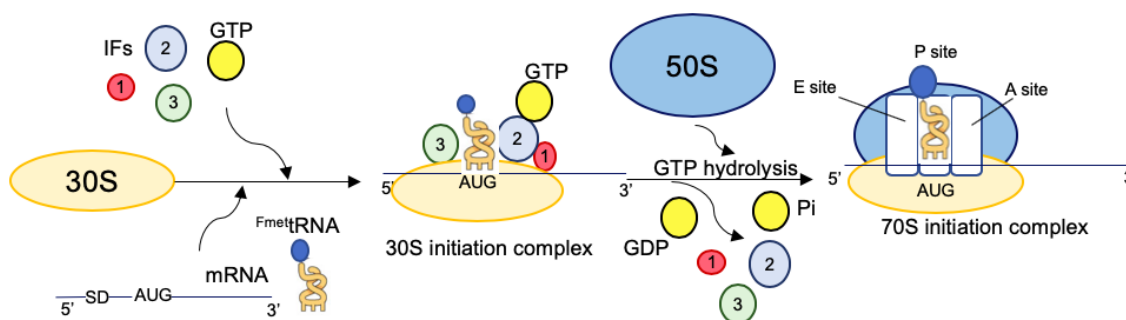


**Figure 8.** Scheme of the initiation process in bacteria. A detailed description is given in the text.

In eukaryotes, the initiation process is more complex and includes a dozen of eukaryotic initiation factors. It begins with the formation of the preinitiation complex (43S). Firstly, the ternary complex (TC) is formed from eukaryotic initiation factor 2 (eIF2), guanosine triphosphate (GTP) molecule and initiator tRNA (Met-tRNA<sup>Met</sup>). Subsequently, this complex binds to the post-recycled complex that consist of small ribosomal subunit, eukaryotic initiation factors 1, 1A and 3 (eIF1, eIF1A, eIF3) and the ATP binding cassette E1 (ABCE1).

Then the mRNA is recruited and after a series of large-scale conformational rearrangements the 48S complex is formed and scan for the start codon. After start codon recognition, almost of the initiation factors disassemble in sequentially and eukaryotic initiation factor (eIF5B) marks the last steps of the process with its binding to the GTPase center of the SSU, which stimulates the association of both ribosomal subunits, prior to it is released before the elongation process commences (from review Guca and Hashem, 2018, Fig. 9).

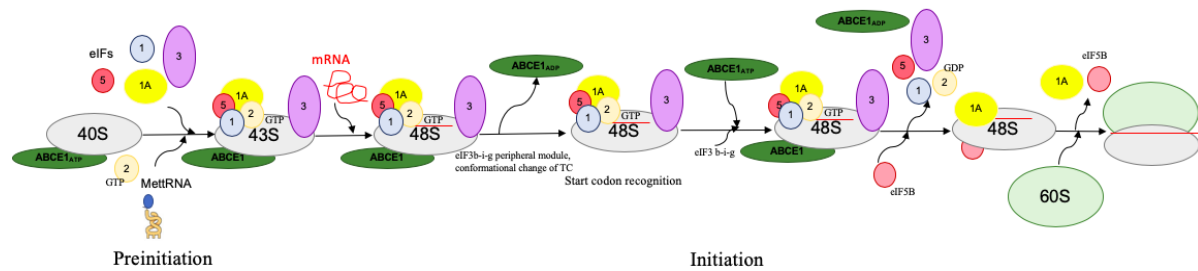


**Figure 9.** Translation initiation process in eukaryotes. A detailed description is given in the text.

## Elongation

The elongation process is better conserved compared to initiation among all species. It starts with the delivery of a new aminoacyl-tRNA (aa-tRNA) to the A-site through elongation factor Tu (EF-Tu) (eEF1A in eukaryotes) in complex with GTP (Schmeing and Ramakrishnan 2009; Voorhees and Ramakrishnan 2013). Only after the accommodation of the correct aa-tRNA, peptide bond formation takes place. Peptide-bond formation occurs by transferring the peptidyl chain from the P-site tRNA to the aa-tRNA A-site (Blanchard et al. 2004a; Sanbonmatsu et al. 2005). This is followed by the translocation process that involves the displacement of the incoming tRNA and moving the tRNAs from the A- and P- sites to the P- and E-sites. Translocation is catalyzed by EF-G (eEF2 in eukaryotes) in complex with GTP (Yamamoto et al. 2014, Fig. 10).

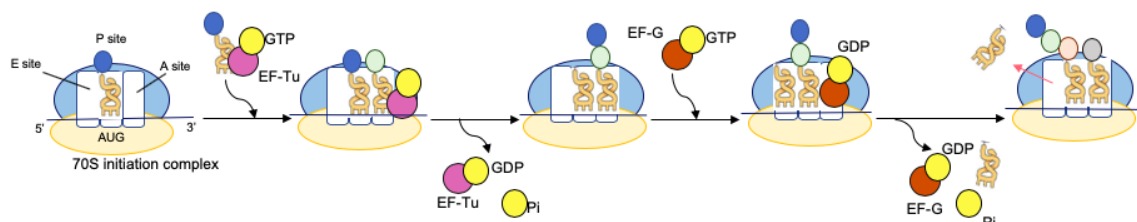


**Figure 10.** Conservative elongation process of protein synthesis in all kingdoms. Here is an example of this process for prokaryotes.

## Termination and recycling

The elongation phase continues until a stop codon is. The recognition of the stop codon is assured by ribosomal release factors (RF). Release factors 1 and 2 hydrolyze the peptidyl-tRNA bond and thereby dissociate the polypeptide chain and the ribosome (Klaholz 2011; Rodnina 2013). In turn, RF3 catalyzes the dissociation of RF1 and RF2 in the GTP-dependent manner. During the post-termination process, the complex is disassembled thanks to EF-G, ribosomal recycling factor (RRF) and IF3 (Freistroffer et al., 1997; Koutmou et al. 2014; Peske et al. 2014, Fig. 11). After the recycling phase a new round of translation initiation may begin.

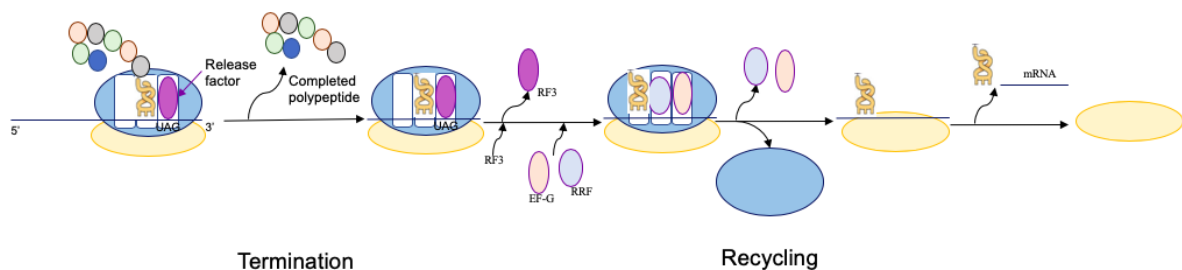


**Figure 11.** This diagram shows the last 2 steps of translation termination and recycling for prokaryotes.

In eukaryotes, termination and recycling processes are different. The termination process begins with the appearance of a stop codon (UGA, UGG and UAG) in the mRNA sequence. The eukaryotic termination factor 1 (eRF1) mimics tRNA and with eukaryotic termination factor 3 occupy the A-site of the ribosome. ABCE1 triggers ribosome disassembly into subunits by an ATP hydrolysis (Becker et al., 2012, Fig. 12).

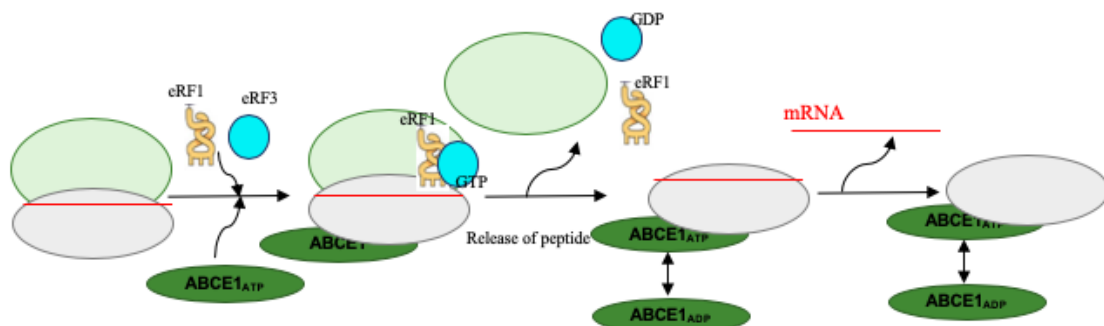


**Figure 12.** This diagram shows termination and recycling processes for eukaryotes that are different from prokaryotes.

Figures 13 and 14 summarize the translation process in both prokaryotes and eukaryotes.

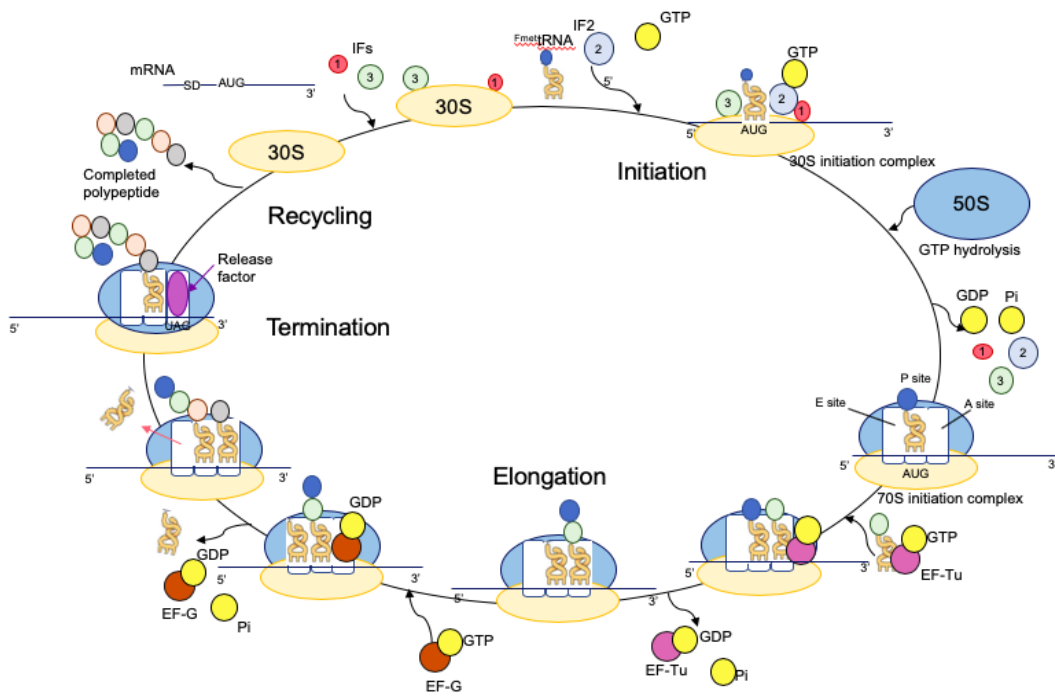


**Figure 13.** Schematic diagram of translation cycle in bacteria. The main steps of translation process are shown. Details regarding each step are provided in the main text.

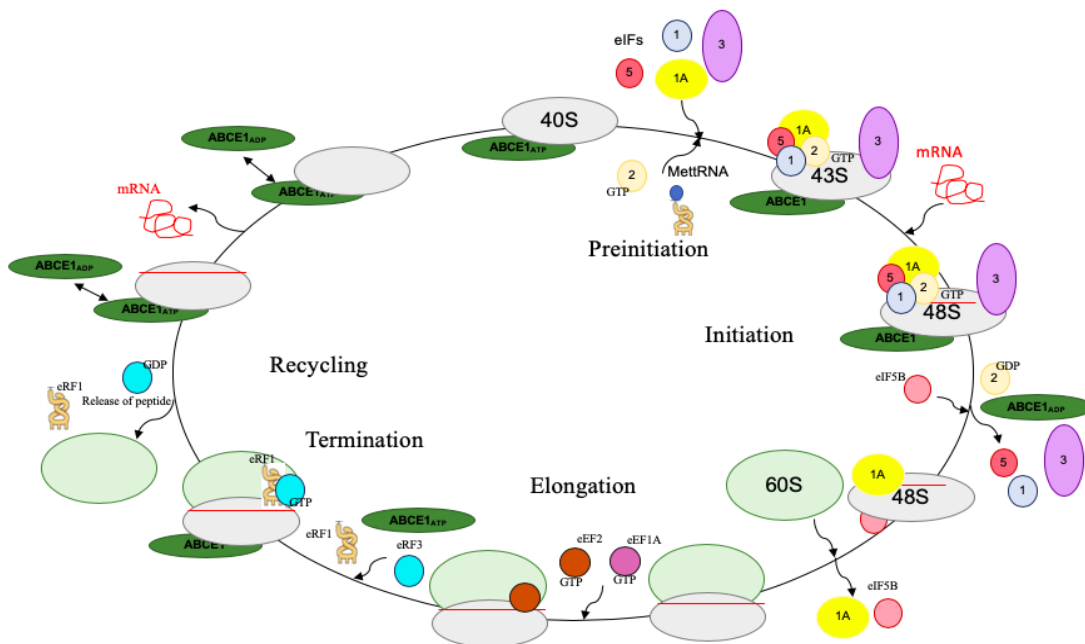


**Figure 14.** The translation cycle for eukaryotes which is divided into four main stages: initiation (including preinitiation), elongation, termination and recycling. Further details are also given in the text.

---

## Translation initiation in bacteria

---

As the project of the current thesis is focused on the initiation process, it will be detailed more exhaustively than the other phases of mRNA translation regulation. The process of translation initiation is a tightly controlled phase and is the target of many regulatory mechanisms important for cellular physiology, viral infections and other diseases. This process has been studied for many years by different groups, but yet still not fully understood. Two renowned research groups, Marina Rodnina and Venki Ramakrishnan, have set the pace in this domain and published highly significant results that I will briefly discuss. The group of Marina Rodnina studied the protein binding pathway using Förster resonance energy transfer (FRET) experiments. The results of their FRET studies have concluded a certain assembly sequence according to which it is the mRNA that binds first to the small ribosomal subunit, followed indifferently by IF2 and IF3, and only after IF1 then fMet-tRNA<sup>fMet</sup> can join (Milon et al., 2012, Fig. 15).

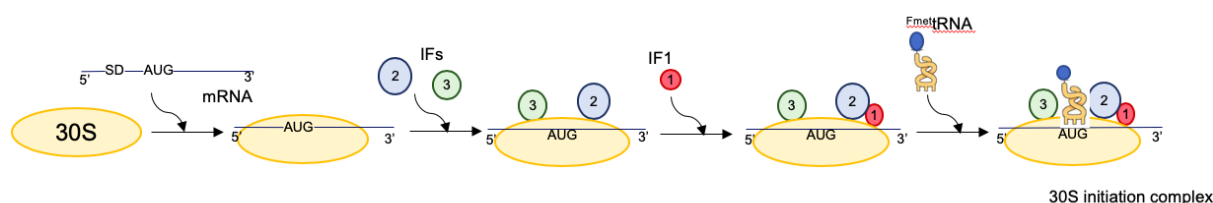


**Figure 15.** The process of the initiation complex formation based on FRET experiments (Milon et al., 2012).

Four years later, an article from the Venki Ramakrishnan's group presented significantly different conclusions from those described by the Rodnina group. Indeed, they find that the process commences similarly by the binding of the mRNA, after which IF1 and IF3 bind to the 30S-mRNA complex, followed by the simultaneous binding of IF2 and fMet-tRNA<sup>fMet</sup> to the initiation complex (Hussain et al., 2016, Fig. 16).

Such significant discrepancies highlights a lack of clear understanding of how the formation of the 30S IC occurs.

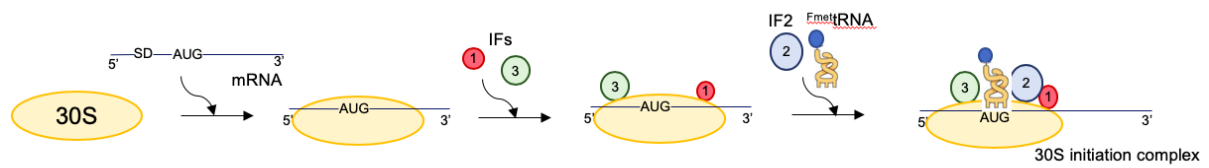


**Figure 16.** The assembly of the initiation complex, based on cryo-EM structures (Hussain et al., 2016).

## Components of initiation complex in bacteria

### IF1

Initiation factor 1 (IF1) is an 8 kDa protein that binds in the 30S A-site and is encoded by *infA* gene (Fig. 17). Its homologs are aIF1A in archaea and eIF1A in eukaryotes (Kyrpides and Woese 1998, Sørensen et al., 2001, Gaur et al., 2008). The structure of IF1 from *E. coli* was determined by NMR in 1997 (Sette et al., 1997). Four years later IF1 in complex with small ribosomal subunit was crystallized (Carter et al., 2001).

### IF1 functions

Several functions of IF1 have been shown during protein synthesis. IF1 appears to interact synergically with IF2, as both of these factors stimulate reciprocally their binding to the ribosome (Stringer et al., 1977, Weiel and Hershey, 1982, Celano et al., 1988, Gualerzi and Pon, 1990). IF1, together with IF2, is selective in recognizing fMet-tRNA<sup>fMet</sup> from deacylated and deformedylated tRNA (Antoun et al., 2006a). Moreover, these proteins play a role in increasing the binding of mRNA to the initiation complex (Studer and Joseph, 2006).

IF1 was characterized from three bacterial species, *E. coli*, *T. thermophilus* and *Bacillus stearothermophilus* (Hershey et al., 1977, Wolfrum et al., 2003, Kapralou et al., 2009). Interestingly, as thermophilic IF2 compare to *E. coli* has a shorter N-terminal domain, IF1 does not promote binding of IF2 to the 30S ribosomal subunit (Kapralou et al., 2008).

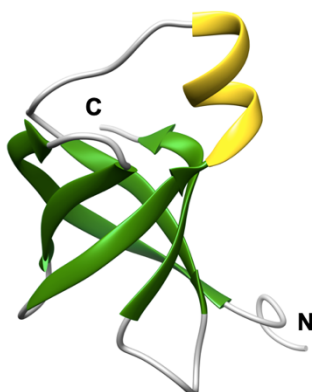


**Figure 17.** The structure of IF1 from *S. aureus* determined with multidimensional NMR spectroscopy, where helices are colored in yellow, strands in green and coils in grey (2N8N from Kim et al., 2016).

## IF2

Initiation factor 2 (IF2) is the largest bacterial initiation factor and it includes several domains. In *E. coli*, IF2 is 890 amino acids long and has a molecular weight of 97,35 kDa. However, in *S. aureus* IF2 is shorter 185 amino acids and is 77 kDa. IF2 is encoded by *infB* and was shown to be essential (Plumbridge et al., 1982, Laalami et al., 1991). Noteworthy, IF2 and the eukaryotic factor eIF5B are homologs that possess similar functions during the initiation step. (Choi et al., 1998, Pestova et al., 2000)

IF2 consists of 2 large domains divided into 6 subdomain: N-terminal domain (NTD) subdivided into N1 and N2 and the C-terminal domain (CTD) subdivided into G, III, C1 and C2. The NTD of IF2 interacts with IF1 and S12. (Boileau et al., 1983, Julián et al., 2011). It enhances the interaction of the factor with the 30S subunit (Caserta et al., 2006). In some species like *T. thermophilus*, N2 domain is inexistent (Simonetti et al., 2013). This factor has a GTP binding subdomain that is highly conserved among all species (Steffensen et al., 1997, Simonetti et al., 2013). The CTD recognizes and binds the fMet-tRNA<sup>fMet</sup> through C2. No particular function for C1 was shown yet (Guenneugues et al., 2000, Spurio et al., 2000, Szkaradkiewicz et al., 2000, Fig. 18)

### *The GTPase activity*

The GTPase activity of IF2 depends on the presence of an attached ribosome (Luchin et al., 1999). Guanosine triphosphate (GTP) hydrolysis is triggered by 50S subunit joining to the 30S initiation complex (Luchin et al., 1999, Tomsic et al., 2000).

### *IF2 functions*

IF2 is a protein that is associated with the ribosome throughout the entire initiation process, participating initially in the formation of the 30S initiation complex and subsequently in the assembly of the 70S initiation complex (Milon et al., 2006). It is responsible for recognition of the formyl group of fMet-tRNA<sup>fMet</sup> and in combination with GTP is able to recruit fMet-tRNA<sup>fMet</sup> to the small ribosomal subunit, ensuring the proper location of the initiator tRNA in the ribosomal P-site (Lockwood et al., 1971, Majumdar et al., 1976, Sundari et al., 1976, La Teana et al., 1996). It was shown that IF2 participates not only in translation initiation process. It also assists in protein folding and renaturation in the cytoplasm (Caldas et al., 2000).

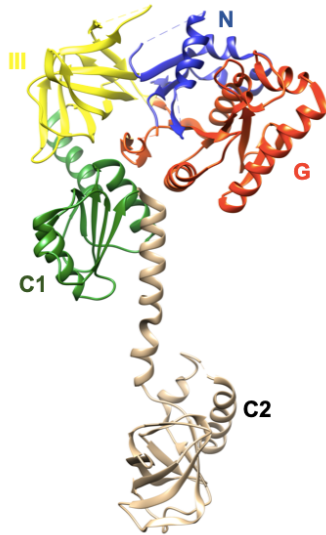


**Figure 18.** X-ray structure of translation IF2 from *Methanothermobacter thermautotrophicus*, where helices are colored in yellow, strands in green and coils in grey. Domains are indicated in the picture. More detailed information is provided in text (**1G7R** from Roll-Mecak et al., 2000).

### IF3

Initiation factor 3 (IF3) is a 20,4 kDa protein encoded by *infC* and has just one functional homolog, eIF1 (Olsson et al., 1996, Sabol et al., 1970, Lomakin et al., 2006).

The first structure of IF3 was solved by NMR in 1994 (Fortier et al., 1994). A year later the structure of this protein was elucidated by X-ray crystallography (Biou et al., 1995). It was shown that IF3 consists of 2 domains (N- and C-domains) connected by a flexible linker (Moreau et al., 1997). Most of the know functions of IF3 are performed by the C-domain, while the N-terminal part modulates the thermodynamic stability of the 30S-IF3 complex (Garcia et al., 1995, Petrelli et al., 2001) Moreover, the N-domain is involved in start codon recognition, initiator tRNA selection and inhibition of leaderless mRNA translation (Maar et al., 2008). The C-terminal domain (CTD) binds reversibly near the P-site, while the N-terminal domain (NTD) binds first to the platform and then to the elbow of fMet-tRNA<sup>fMet</sup> (Tapprich et al., 1989, McCutcheon et al., 1999, Dallas and Noller, 2001, Fabbretti et al., 2007, Julián et al., 2011, Fig 19).

#### *IF3 functions*

Initiation factor 3 prevents ribosomal subunits association by binding to the 30S subunit and does not dissociate from it before the arrival of the 50S subunit (Antoun et al., 2006, Debey et al., 1975, Grunberg-Manago et al., 1975). It was shown that 50S also has a non-canonical binding site for IF3 (Goyal et al., 2017). It catalyzes the formation of 30S initiation complexes (30S IC) (Wintermeyer and Gualerzi, 1983). IF3 selects the initiator tRNA against elongator tRNAs in 30S IC (Hartz et al., 1989). It stimulates dissociation of deacylated tRNA

or incorrectly bound tRNAs from the ribosomal P-site (Karimi et al., 1999, Peske et al., 2005, Antoun et al., 2006). It is also known that IF3 discriminates against initiation of leaderless mRNAs on the 30S subunit and non-initiator codon in the P-site (Sussman et al., 1996, Haggerty and Lovett, 1997, Meinnel et al., 1999, O'Donnell and Janssen, 2002). In addition, IF3 stimulates the dissociation of deacylated tRNA from post-termination complexes (Hirokawa et al., 2002, Karimi et al., 1999, Peske et al., 2005) and plays a role in recycling stalled ribosomal complexes (Singh et al., 2005, 2008). Finally, together with IF1 is involved in the reaction of the cell to cold shock conditions (Giuliodori et al., 2004, 2007).

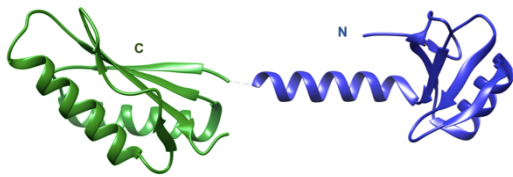


**Figure 19.** Cryo-EM structure of IF3 from *Thermus thermophilus*, where helices are colored in yellow, strands in green and coils in grey. Domains are indicated in the picture (5LMO from Hussain et al., 2016).

### **fMet-tRNA<sup>fMet</sup>**

#### *initiator tRNA*

There are 3 forms of tRNA in the cell: aminoacyl-tRNA, peptidyl-tRNA and deacylated tRNA, which differ depending on the acylation stage, where the amino acid or peptide is attached to the 3'-end of the tRNA or this group is missing. In bacteria, translation initiation involves a specific tRNA, the initiator tRNA (itRNA) that is capable of recognizing of alternative initiation codons (AUG, GUG, UUG) (RajBhandary, 1994, Blattner et al., 1997, Kozak, 1999; Mayer et al., 2003).

Initiator tRNA has a number of structural features:

- 1) The discrepancy between nucleotides 1 and 72 (C1 and A72 in *E. coli*) at the end of the acceptor stem which prevent binding of fMet-tRNA<sup>fMet</sup> to EF-Tu (RajBhandary, 1994).
- 2) Purine:pyrimidine base pairs 11:24 are replaced by pyrimidine:purine in elongation tRNA (Varshney et al., 1993).
- 3) The presence of three conserved G:C base pairs at the bottom of the anticodon stem that make the anticodon stem less flexible compared to the anticodon stem loops of elongator tRNAs which favors binding of the tRNA<sup>fMet</sup> to the P site on the ribosome (Cory et al., 1968, Dube et al., 1968, Rich and RajBhandary, 1976, Seong and RajBhandary, 1987, Schweisguth and Moore, 1997).

## Aminoacylation

Aminoacylation of tRNA is carried out by aminoacyl-tRNA synthetases. In the case of initiator tRNA<sup>fMet</sup>, this function is performed by methionyl-tRNA synthetase (MetRS). The anticodon plays a crucial role in the recognition of tRNA<sup>fMet</sup> by MetRS (Schulman 1991). Aminoacylation will not take place if the anticodon of initiator tRNA is mutated (Fourmy et al., 1991; Mechulam et al., 1999).

## Formylation

Formylation of Met-tRNA<sup>fMet</sup> in bacteria, chloroplasts and mitochondria is catalyzed by methionyl-tRNA formyltransferase (MTF) with the participation of the N10-formyltetrahydrofolate (formyl-N10-THF) as a donor of the formyl group (Schmitt et al., 1996a, 1996b, 1998). The marker by which MTF recognizes initiator tRNA is the non-Watson-Crick base pair 1:72 in tRNA<sup>fMet</sup>. (Schmitt et al., 1998) Initiator tRNA also differs from elongator by the presence of the formyl group that prevents binding to EF-Tu and facilitates the selection of fMet-tRNA<sup>fMet</sup> by IF2 (Sundari et al., 1976, Hansen et al., 1986, RajBhandary, 1994, Nissen et al., 1995, Kozak, 1999).

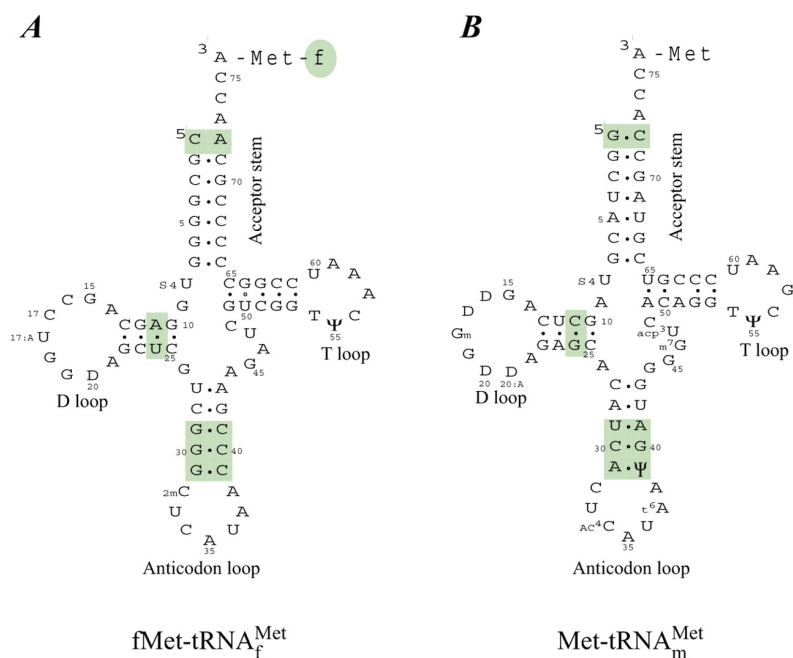


**Figure 20.** Comparison of initiator (A) and elongator (B) methionine-tRNAs. The regions important for initiator tRNA are highlighted. Details are given in the text (Søgaard, 2005).

## **mRNA**

Messenger RNA (mRNA) is an RNA containing information about the amino acid sequence of proteins, which is synthesized on the basis of DNA during transcription process, after which is used during translation stage as a matrix for protein synthesis.

Single-stranded RNAs can bind to 30S with high affinity even in the absence of initiation factors and fMet-tRNA<sup>fMet</sup> (Kozak, 1999, De Smit and van Duin, 2003). In *E. coli*, it has been shown that ribosomal protein S1 is involved in this process. It unfolds highly structured mRNAs, making binding between 30S and mRNA more stable (Duval et al., 2013). Also, mRNA has A/U-rich elements which are recognized by protein S1 (Steitz, 1969, Dreyfus, 1988, Jin et al., 2006).

### *Translation initiation region*

The mRNA contains a combination of several elements located in translation initiation region (TIR) affecting the efficiency of initiation process that are the start codon, the Shine-Dalgarno sequence and the spacer between the SD sequence and the start codon. The role of TIR is to proper position the mRNA on the 30S subunit for translation initiation (Dreyfus, 1988).

### *The Shine-Dalgarno sequence (SD)*

The Shine-Dalgarno sequence is a purine-rich sequence consisting of 4-8 nucleotides and separated from the start codon by a 5-13 spacer (Schneider et al., 1986). The SD complementary to the anti-Shine-Dalgarno sequence (aSD) located at the 3'-end of 16S rRNA (Shine and Dalgarno, 1974). In *E. coli*, a typical SD sequence is GGAGG and most common spacer length is 7-10 nucleotides long (Ma et al., 2002).

### *The start codon*

There are several types of start codons. In *E. coli*, 83% of the total is AUG codon (Ma et al., 2002). The remaining 14% is GUG and 3% is UUG codons. Rare non-canonical codons AUU, AUC and CUG have been reported (Schneider et al., 1986, Polard et al., 1991, McCarthy and Brimacombe, 1994, Binns and Masters, 2002, Baudet et al., 2010).

---

## Translation regulation in *S. aureus*

---

The primary project of the current thesis is to study mRNA translation initiation in *S. aureus*. Staphylococci are gram-positive cocci (~1 µm in diameter) that cause many forms of infections. They grow and together they form clusters, pairs and occasionally short chains. The configuration of the cocci helps to distinguish micrococci and staphylococci from streptococci, which usually form chains. One of the most significant representatives is *Staphylococcus aureus* that tends to localize in the nose, respiratory tract and on the skin upon transmission. One fifth of the human populations in the world suffer from diseases caused by *S. aureus*. These organisms can grow aerobically or anaerobically at temperatures between 18 °C and 40 °C and in a pH range from 4.2 to 9.3 (Le Loir et al., 2003, Taylor, 2019).

Pathogenic strains produce virulence factors, such as potent protein toxins that damage biological membranes, leading to cell death. Furthermore, *S. aureus* secretes many factors that inhibit the complement cascade or prevent recognition by host defenses. One of the most representative examples are enterotoxins causing food poisoning and when expressed systemically, can cause toxic shock syndrome (Lyon and Skurray 1987, Prevost et al., 1995).

In staphylococci, the ability to respond to cell density with genetic adaptations is due to one main system called “accessory gene regulator” (Agr) (Le and Otto, 2015). It is a key to the temporal regulation of adhesins and exotoxins and is consists of two divergent transcripts, RNAII encodes a quorum sensing cassette (AgrBD) and a two-component system (AgrAC) while RNAIII is the multifunctional RNA, which encodes a PSM δ-hemolysin (hld). (Novick, 2008). RNAIII is a 514-nt highly abundant and stable regulatory RNA. Its structure, but not its sequence, is well conserved among several staphylococcal species (Benito et al., 2000). The main function of RNAIII is regulating translation of both individual exoproteins and pleiotropic regulators (Novick, 2008). For example, RNAIII represses *spa* gene expression that codes for the surface protein A, one of the major virulence factors, interfering with Ig-mediated opsonization (Patel et al., 1987) and promoting collagen mediated adhesion to connective tissues by its interaction to the von Willebrand factor (Hartleib et al, 2000, Gomez et al., 2004). The 3' end of RNAIII is partially complementary to the 5' end of *spa* mRNA. Although this annealing is sufficient to inhibit *in vitro* the formation of the translation initiation complex, the coordinated action of RNase III is essential *in vivo* to degrade the mRNA and irreversibly arrest translation. (Huntzinger, 2005, Fig. 21)

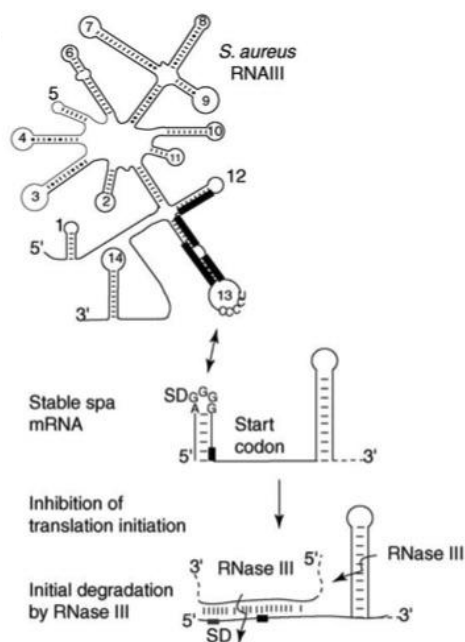


**Figure 21.** RNA-mediated mechanisms used in virulence gene regulation. The mechanism of action of *S. aureus* RNAIII on *spa* expression (Romby et al., 2006).

### Specific features of the protein synthesizing apparatus of *Staphylococcus aureus*

Despite the fact that ribosomes of different bacterial species are very similar, there are many species-specific peculiarities that can reflect on various vital processes, including the process of translation initiation. These unique species-specific differences are associated with structural variations, specific for each species. For example, uS9, uL3 and bL31 in *S. aureus*, uS14 in *E. coli* and uS8, bL19 and bL28 in *T. thermophilus* present extensions that protrude from the ribosome. Similarly, for the rRNA, the presence of short insertions and deletions in the 16S and 23S rRNA are also common species-specific features. For instance, helix 6, helix 10, helix 26 (h26) and helix 44 in the small subunit of the ribosome, and also Helix 28 and Helix 68 in the large subunit have different lengths or adopt different folds and orientations. h26 on the SSU participates in the ribosome's dimerization during the hibernation process in *S. aureus* by creating contacts between two SSU belonging to two different ribosomes. This helix is longer than in *S. aureus* when compared to other known bacterial species. In gram-negative bacteria like *T. thermophilus* this helix is shorter by 3 base pairs, making contact between the ribosomes impossible without additional rotation (Khusainov et al., 2017).

Another striking example of ribosome variability is protein bL31 that bridges two subunits where it interacts with uS13, uS19, uL5 and 5S rRNA. There are 2 types of this protein: type A and B. In *S. aureus*, only type B is present (type A is not encoded), which

contains an additional loop, instead of a zinc-binding motif. For the rest type B is absolutely analogous to type A, namely it includes a three-stranded beta sheet near the N-terminus and a C-terminal extension, which may contain an alpha helix. In general, bL31 can adapt to the large-scale movements of the ribosome important for tRNA proofreading (Jenner et al., 2010, Khusainov, 2016).

### *S1*

S1 is an essential and atypical ribosomal protein that plays a major role in unfolding highly structured mRNAs before binding to the ribosome. Depends on the organism S1 may have different functions and play a different role during the translation initiation process. In *E. coli* it consists from 6 domains: 1st and 2nd are involved in ribosome binding, the rest 4 have been shown to interact with mRNA (Subramanian, 1983).

Several studies have been conducted related to the replacement of S1 protein for the same protein from another organism. It was shown that the addition of S1 from *E. coli* or from *Micrococcus luteus* to depleted S1 ribosomes of *E. coli* restored 30S properties for translation of mRNA carrying weak SD, but these proteins did not affect the *B. subtilis* ribosomes. Since these proteins are similar in *B. subtilis* and *S. aureus* and have lost the N-terminal domain, which has been shown to promote specific binding to S2 in *E. coli* 30S, it may explain why this protein does not play a major role in the translation process (Farwell et al., 1992, Vellanoweth and Rabinowitz, 1992).

It was also shown that *B. subtilis* ribosomes have a higher tolerance to non-AUG initiation codons than *E. coli* ribosomes. The presence of mRNA with a strong SD sequence also significantly increases the ability to bind to the ribosome. In this regard, it was suggested that firmicutes eliminates the need for S1 protein acting on 30S due to the presence of a large amount of mRNA with a strong SD (Omotajo et al., 2015).

### *Initiation factors*

The amino acid sequences of initiation factors 1 and 3 from three bacterial species (*Thermus thermophilus*, *Staphylococcus aureus* and *Escherichia coli*) are similar. In initiation factor 1 the C-terminal region is very conserved, however, the N-terminal region in *S. aureus* is longer than in *T. thermophilus* and shorter than in *E. coli*. Already indicating species-specific structural differences (Fig 22).

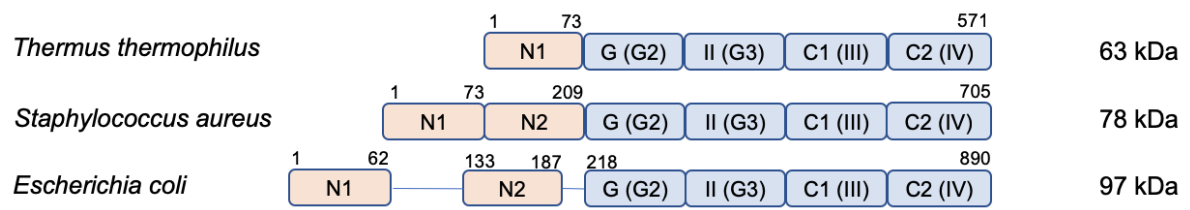


**Figure 22.** Scheme of the initiation factor 2 structure from *T. thermophilus*, *S. aureus* and *E. coli*.

---

## Antibiotics

---

Antibiotics may act on one or more different steps in bacterial metabolism. Most of known antibiotics act on cell wall synthesis (penicillins and cephalosporins), while others act on protein synthesis (Ghooi and Thatte, 1995). In turn, there are a number of mechanisms allowing bacteria to resist the action of antibiotics.

### *Selective membrane permeability*

The major antibiotics penicillins, cephalosporins, monobactams and glycopeptides (vancomycin and teicoplanin), also called  $\beta$ -lactams inhibit bacterial cell wall synthesis by preventing synthesis of peptidoglycan, which is an important constituent of the bacterial cell wall (Ghooi and Thatte, 1995, Trevor et al., 2015). This group of antibiotics combines the presence of a  $\beta$ -lactam ring that can be hydrolyzed by the action of enzymes ( $\beta$ -lactamase), making these drugs ineffective (Bondi and Dietz, 1945). Given the high clinical efficacy and low toxicity,  $\beta$ -lactam antibiotics form the basis of antimicrobial chemotherapy at the present stage, taking the leading place in treating most infections.

### *Protein synthesis inhibitors*

In recent years, interest in the ribosome as a target for the discovery of new antibacterial agents has increased and was caused by defining the structure of whole bacterial ribosomes, subunits, domains and antibiotic complexes (Hermann Review, 2005, Tenson and Mankin, 2006). The advent of three-dimensional structures confirmed early biochemical studies that antibiotics interact with the bacterial ribosome RNA. Resistance to this family of antibiotics are partly due to changes in the drug-binding sites (chemical modification and/or change in conformation). Mutations and/or deletions of ribosomal proteins can also cause resistance, but since ribosomal proteins usually do not interact directly with the drug, it is believed that resistance occurs indirectly, causing conformational changes in rRNA (Schlunzen et al., 2001, Tu et al., 2005, Davidovich et al., 2007).

Antibiotics targeting the translation apparatus may act on certain functional steps - some block the termination, others initiation but most of them inhibit elongation (Wilson, 2009, Sohmen et al., 2009).

For instance, the formation of 70S can be inhibited by pactamycin on the 30S subunit or by avilamycin on the 50S subunit. compounds specifically targeting the initiation phase are limited in terms of clinical application owing to problems with drug specificity (edeine), toxicity (evernimicin) and solubility (thiopeptides) (Dinos et al., 2004, Belova et al., 2001, Mikolajka et al., 2011). As for the inhibition of elongation, streptomycin and tetracyclines prevent the delivery of aminoacylated-tRNA (aa-tRNA) to the A-site of the ribosome (Day, 1966, Cox et al., 2012). Chloramphenicol, linezolid and puromycin interfere with the peptide-bond formation between the A- and P-site tRNAs (Cundliffe and McQuillen, 1967, Monroe, 1967, Kalpaxis et al., 1989 Skripkin et al., 2008). Translocation of the tRNAs is inhibited by aminoglycoside and elongation of the nascent chain is inhibited by the macrolides (Walsh, 2003). While all of the above-mentioned antibiotics bind on the 30S, some elongation inhibitors also target the 50S. Finally, the peptidyl-transferase inhibitors (chloramphenicol) prevent termination, whereas recycling is inhibited by translocation inhibitors (fusidic acid) (Caskey et al., 1971, Savelsbergh et al., 2009, Fig 23, Table 3).

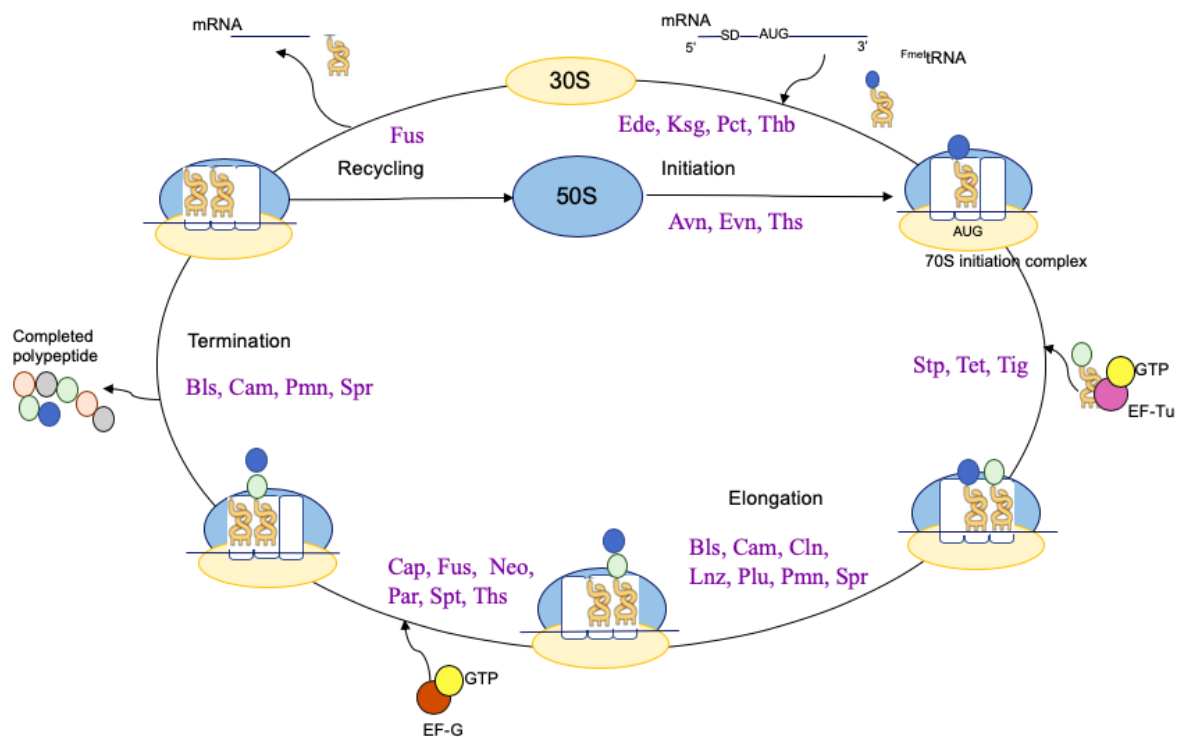


**Figure 23.** A scheme shows at which stage of protein synthesis different antibiotics bind to the ribosome (adapted from Wilson, 2014).

**Table 3.** Mechanisms of action and resistance mechanisms of selected ribosome-targeting antibiotics. DM - drug modification/ degradation, E efflux/membrane permeability, EF elongation factor, FP factor-assisted protection, ND not determined, PTC peptidyl-transferase center, TA target alteration via modification, TM target mutation (adapted from Wilson, 2014).

<b>Antibiotic</b>	<b>Molecular target</b>	<b>Inhibition mechanism</b>	<b>Resistance mechanisms</b>
Chloramphenicol	50S	PTC	DM, E, TA, TM
Clindamycin, lincomycin	50S	PTC	DM, E, TA, TM
Dalfopristin, quinupristin	50S	PTC	E, TA, TM
Doxycycline, tigecycline	30S	tRNA delivery	DM, E, Fp, TM
Edeine	30S	Initiation	DM, TM
Evernimicin, avilamycin	50S	Initiation	TA, TM
Kanamycin	30S	Initiation	DM
Kasugamycin	30S	Initiation	DM, TA, TM
Linezolid	50S	PTC	E, TA, TM
Puromycin	50S	PTC	DM
Sparsomycin	50S	PTC	E, TM
Spectinomycin	30S	Translocation	DM, E, TA, TM
Streptomycin	30S	Translocation	DM, E, TA, TM
Thermorubin	70S	Initiation	ND
Thiostrepton	50S	Factor binding	TA, TM
Tiamulin	50S	PTC	E, TA, TM
Tobramycin	30S	Initiation	DM, E
Viomycin, capreomycin	70S	Translocation	DM, TA, TM

#### *Antibiotics that inhibit the synthesis of nucleic acids*

Quinolones are synthetic antibiotics that target DNA gyrase as their site of action (Leshner et al., 1962). There are three mechanisms of action for these antibiotics: (1) by developing point mutations in the targets, (2) by decreasing the intracellular concentration of the

quinolone and (3) by acquisition of mobile elements carrying the *qnr* gene, which confers resistance to quinolones (Ruiz, 2012).

Antibiotics that inhibit RNA synthesis include rifamycin, which binds to RNA polymerase, an enzyme that catalyzes the process of transcription. It is a broad-spectrum antibiotic that inhibits both gram-negative and gram-positive. Rifamycin is often used in combination with other antibiotics, since bacteria quickly develop resistance to it by acquiring point mutations in RNA polymerase that prevent the binding of the antibiotic (Hartmann et al., 1967, Campbell et al., 2001).

#### *Fatty acid synthesis inhibitors*

Fab-001 (MUT056399; FAB Pharmaceuticals) and AFN-1252 (Affinium Pharmaceuticals) are molecules that are in clinical trials. It has already been shown that these molecules are highly effective against several strains of MRSA (Payne et al., 2002, Escaich et al., 2011).

#### **Current drugs against *S. aureus***

*Staphylococcus aureus* is an extremely adaptive pathogen with a proven ability to develop resistance. Despite the presence of a large number of antibiotics, there is a need to develop new compounds more effective and less toxic to fight against this organism (Chambers and DeLeo, 2009).

The first-line treatment against methicillin-susceptible strains (MSSA) are  $\beta$ -lactamase-resistant penicillins (methicillin, oxacillin, cloxacillin, and flucloxacillin) or non- $\beta$ -lactam antibiotics (clindamycin and co-trimoxazole) against methicillin-resistant strains (MRSA). To treat more serious invasive infections glycopeptide antibiotics are used (vancomycin and teicoplanin) that are administered intravenously. They are toxic and should be regularly monitored with a blood test. Some representative examples of antibiotics and their mechanism of resistance are shown in the Table 4 below.

**Table 4.** Antibiotics used against *S. aureus* and the mechanism of their resistance (Rayner and Munckhof, 2005, Johnson and Decker, 2008, Morgan, 2011).

Name	Mechanism of resistance
Penicillin	$\beta$ -lactamase, enzymatic inactivation of penicillin
Methicillin	Expression of new penicillin-binding protein
Tetracycline	Efflux from cell, modification of ribosome
Chloramphenicol	Enzymatic inactivation
Erythromycin	Enzymatic modification of ribosomal RNA. Prevents drug binding to ribosome
Streptomycin	Mutation in ribosomal protein, prevents drug binding, enzymatic inactivation
Kanamycin, Gentamicin	Enzymatic inactivation
Trimethoprim	Alternative dihydrofolate reductase
Mupirocin	Alternative isoleucyl-tRNA
Fluoroquinolones	Altered DNA gyrase, efflux
Antiseptics	Efflux

After having introduced the above-mentioned concepts, I will present now my two projects of this thesis.

---

## **Project 1: Assembly pathway of the *S. aureus* initiation complex**

---

While the ribosomal structures of gram-negative bacteria like *Thermus thermophilus* and *Escherichia coli* were solved a long time ago, the structure of gram-positive bacteria was published only 3 years ago, despite the practical significance of this group, since most pathogens to humans are gram-positive bacteria.

Pathogenic bacteria like *Staphylococcus aureus* produce an extremely high resistance to antibiotics, which mainly affect the process of protein synthesis. It is also known that the process of protein synthesis in gram-positive and gram-negative bacteria has significant differences. Therefore, for a better understanding of the mechanism of antibiotic resistance, it is necessary to study this process in detail.

Moreover, pathogenic bacteria have complex translation regulation mechanisms that allow them to survive under stressful conditions.

### **Aim of the project:**

The main goal of this project is to study the initiating process in *S. aureus*, a rate-limiting step that includes the action of many precisely regulated components.

It is necessary to obtain high-resolution structures in order to gain further insight on this finely regulated pathway and possible species-specific differences of this process.

---

## Project 2: Crystallogensis of *Candida albicans* 80S

---

One of the most common human fungal pathogen is a *Candida albicans*, causing from superficial, cutaneous-mucosal to deep-seated and disseminated infections (Segal, 2005). It has been found in at least 70% of the human population (Ruhnke and Maschmeyer, 2002). There is a definite correlation between the host and the microbes in normal conditions, with an equilibrium shift towards *C. albicans* leads to the emergence of various diseases and their aggravation in the presence of immunodeficiency (Sardi, 2016).

Treatment of diseases caused by this organism costs about 2-4 billion dollars in the United States (Perloth et al., 2007). The ineffectiveness of the treatment is due to the occurrence of serious side effects associated with the fact that the cellular targets in *C. albicans* are often shared with humans (Berman and Sudbery, 2002).

Thus, there is a need to study the physiological mechanisms of *C. albicans*, with the further use of the knowledge gained in the development of new drugs in the fight against this pathogen.

*Candida*'s cells can grow in a wide range of conditions that can affect cell shape. They grow at pH from 2 to 8 and from 20 to 40 °C. The optimum temperature is 37 degrees. At low pH (less than 6), the cells grow in an ovoid-shaped budding type, but when the pH>7, hyphal growth is induced (Odds, 1988). This organism is a facultative anaerobe that at least 4 times more resistant to antifungal treatments in anaerobic than in aerobic conditions (Dumitru et al., 2004).

### Specific features of *Candida albicans* ribosome

The molecular weight of *Candida albicans* ribosome is 3.2 MDaltons. This ribosome consist of 44 r-proteins in the large subunit and 35 in the small subunit. The ratio of rRNA to r-proteins is 1.27 (Annex) (Bruchlen D. thesis).

Using bioinformatics methods, it was shown that A- and P-sites between *C. albicans*, *Saccharomyces cerevisiae* (*S. cerevisiae*) and *Homo sapiens* are conserved (Bruchlen D. thesis). A significant difference was found in the E-site between *C. albicans* and *S. cerevisiae* that could explain the resistance of *C. albicans* to cycloheximide (CHX) (Goldway et al., 1995).

CHX is a known inhibitor of the eukaryotic translation that binds on the E-site of ribosome without any conformational modifications of the residues. It inhibits the mRNA translation mechanism by stalling translating ribosomes on mRNA. It also blocks the release of tRNA after their delivery of the new amino acids (Garreau de Loubresse et al., 2014).

The size of the E-site binding pocket is smaller due to a modification of 56 amino acid of the eL42 r-protein. The modification is associated with the replacement of proline in *S. cerevisiae* by glutamine in *C. albicans*, causing a steric clash that is certainly implicated in this CHX resistance (Bruchlen D. thesis).

Another feature of the species is connected with the eS26 protein, which is longer in fungi compared to protozoa and C-terminal region of this protein is different from the metazoan group (Bruchlen D. thesis).

### **Aim of the project:**

This project was started by David BRUCHLEN in 2012 in Marat Yusupov's laboratory (IGBMC, University of Strasbourg) when the ribosome structure from pathogens was not yet determined. Due to the similarity of *Candida albicans* and *Saccharomyces cerevisiae*, it was decided to start using the purification and crystallization protocols that have already been developed in the laboratory.

Despite the similarity of these yeasts, it was not possible to obtain crystals under these conditions. David spent 4 years to obtain crystals with high-resolution diffraction. Once, he managed to get the structure of 3.7 Å, which is not enough to study the effect of antibiotics against this organism. Moreover, these crystallization conditions were not reproducible.

My goal in this project was to optimize the protocols of purification and crystallization of the ribosome *C. albicans*, make them reproducible and further improve the resolution of the ribosome structure needed to study the effect of antibiotics. Now this project is still ongoing by my colleagues in Marat Yusupov's laboratory.

## RESEARCH PROJECT 1

---

### **Translation initiation complex from *S. aureus***

---

## ***In vitro* reconstruction of translation initiation complex**

---

### **MATERIALS AND METHODS**

#### **70S PURIFICATION**

Buffers were used during the experiment:

Buffer A:

20 mM Hepes-KOH pH 7.5

100 mM NH<sub>4</sub>Cl

21 mM Mg(OAc)<sub>2</sub>

1 mM DTT

Buffer B:

10 mM Hepes-KOH pH 7.5

500 mM KCl

25 mM Mg(OAc)<sub>2</sub>

1.1 M Sucrose

0.5 mM EDTA

1 mM DTT

Buffer E:

10 mM Hepes-KOH pH 7.5

100 mM KCl

10.5 mM Mg(OAc)<sub>2</sub>

0.5 mM EDTA

1 mM DTT

Buffer G:

10 mM Hepes-KOH pH 7.5

30 mM NH<sub>4</sub>Cl

1 mM Mg(OAc)<sub>2</sub>

1 mM DTT

## ***Staphylococcus aureus* cell growth**

*For our experiments we used the RN6390 strain for fast and efficient cell lysis. In this strain the production of RNAIII is increased and the biofilms formation is decreased.*

All experiments were carried out in a special laboratory with safety level 2. A brain heart infusion medium (BHI) was used for cell growth. Cells were grown at 37 °C and harvested in the early logarithmic phase ( $OD^{600} = 1$  OD/ml), when ribosomes are more active and be found in maximum concentration (Gourse et al., 1996). Cells were washed in buffer A and kept frozen at -80 °C, due to subsequent long-term experiments.

The protocol of full ribosome (70S) purification, which will be described below, was developed by Iskander Khusainov in the laboratory of Marat Yusupov (IGBMC, University of Strasbourg) (Khusainov et al., 2016).

## **Lysis**

*For cell lysis, we used the antibacterial enzyme lysostaphin, which is capable of cleaving pentaglycin cross-linking bridges found in Staphylococci. We could not use bulky equipment like French press and microfluidizer due to lack of space in a special laboratory with safety level 2.*

Frozen cells were resuspended in buffer A containing 1 mM EDTA, lysostaphin, DNase I and protease inhibitor cocktail (Roche) and then incubated at 37 °C for 45 minutes in a water bath. All subsequent procedures were performed at +4 °C or on ice. Cell debris was removed by centrifugation at 30000 g for 90 minutes.

## **PEG precipitation**

*This step was taken from the yeast ribosome purification protocol and is necessary for the gentle precipitation of ribosomes from the cell extract.*

PEG20K (stock 30% w/v from Hampton research) was added to the supernatant to final concentration 2.8% w/v (5 minutes, 4 °C). The resulting solution was centrifuged 20000 g for

5 minutes. The supernatant containing the ribosomes and light cellular components were collected and PEG 20K was added to it till the final concentration of 4.2% (10 minutes, 4 °C). The resulting solution was centrifuged at 20000 g for 10 minutes. At this stage, ribosomes are precipitated, while everything that is lighter remains in the supernatant.

### Sucrose cushion

*This is a common step for purification of the vacant ribosome. It includes to use the sucrose cushion with 0.5-1 M salt concentration. This step allows us to remove from the sample mRNA, tRNA, translation factors and other proteins bound to the ribosome.*

The ribosomal pellet obtained in the previous step was resuspended in 35 ml of buffer A containing 1 mM EDTA and layered to 25 ml cushion of buffer B. After this, the solution was centrifuged at 45000 rpm for 15 hours using the Beckman Type 45 Ti rotor.

### Sucrose density gradient centrifugation

*The idea of this step was to separate the full ribosomes (70S) from dimers (100S) and subunits, due to size and weight.*

The ribosomal pellet from sucrose cushion was resuspended in buffer E, loaded on 7% - 30% w/v sucrose gradients and centrifuged at 17100 rpm for 15.5 hours on swinging the rotor Beckman SW28, 3,5 mg of ribosomes per tube. (Fig. 24).

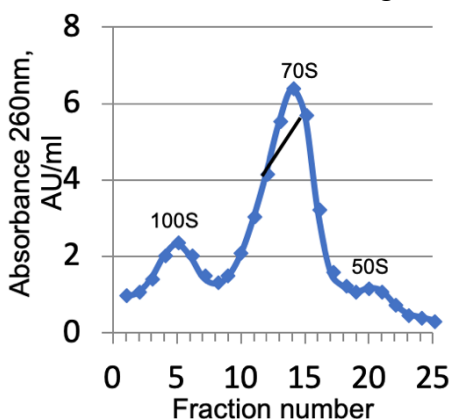


**Figure 24.** Sucrose gradient profile. The absorbance was measured by Nanodrop 2000c (Thermo Scientific). The black line indicates pooled 70S fractions.

## Last PEG precipitation

Selected fractions were pooled and the concentration of  $\text{Mg}(\text{OAc})_2$  was adjusted to 25 mM. Further, PEG20K was added to the final concentration 4.5% w/v to precipitate the ribosome (10 minutes, 4 °C) and the solution was centrifuged at 20000 g for 12 minutes. After this, the pellet was resuspended in buffer G and used later for small ribosomal subunit purification.

The purity and quality of the obtained sample were checked by several methods: protein PAGE, agarose gel in native and denaturing conditions, mass spectrometry and crystallization.

## One-dimensional polyacrylamide gel (PAGE)

*One-dimensional PAGE in SDS denaturing conditions separates proteins by molecular weight. Using this method, information about the presence of non-ribosomal proteins in the sample can be obtained.*

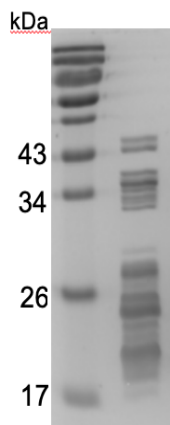


**Figure 25.** One-dimensional PAGE of *S. aureus* 70S ribosome.

The gel demonstrates the purity of the sample and the absence of high molecular weight contaminants like pyruvate dehydrogenase complex, usually co-purified with bacterial ribosome (Fig. 25).

## Agarose gel in native and denaturing conditions

The native agarose gel contains 0.8% agarose and TBE buffer (90 mM tris-HCl pH 8.3, 89 mM boric acid and 10 mM EDTA pH 8, pH was adjusted till 8.3 by HCl). Guanidine

thiocyanate was added to the sample till the final concentration of 10 mM to obtain denaturing conditions.

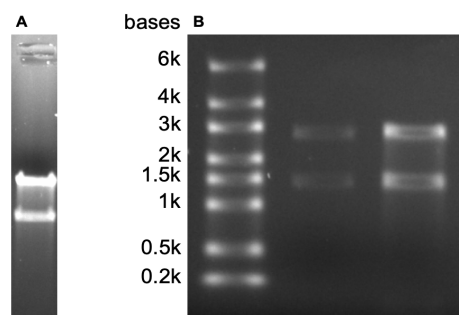


**Figure 26.** Agarose gels in native (A) and denaturing conditions (B). On native gel the upper and lower bands correspond to 50S and 30S. On denaturing gel of 70S (1 and 2  $\mu$ g) the upper and lower bands correspond to 23S and 16S rRNA respectively.

## Mass spectrometry

*Mass spectrometry is an analytical technique that used to identify molecules in the mixture. Biologists use this method to analyze a purified protein, detect impurities in the sample and to study the protein content of the sample of cells. In comparative proteomics studies, one or both of two parameters are generally used: a spectral count, which is the total number of spectra identified for the protein or some measure of ion abundance. LC-MS/MS analysis is a practical semi quantitative technique with which you can establish the presence or absence of proteins in extreme cases (Milac et al., 2012, Lundgren et al., 2010).*

Analysis of *S. aureus* ribosome sample shows the presence of all ribosomal proteins except S1 (Table 5) and a low amount of non-ribosomal proteins which indicates the purity of the sample (Table 6).

**Table 5.** List of ribosomal proteins found in *S. aureus* ribosome sample by LC-MS/MS analysis, where b - bacterial specific proteins, u - universal proteins.

Small ribosomal subunit proteins				Large ribosomal subunit proteins			
Protein	Spectral count	MW (kDa)	pI	Protein	Spectral count	MW (kDa)	pI
bS1	0	43,3	4,60	uL1	236	24,7	9,5
uS2	260	29,1	5,3	uL2	380	30,1	11,3

uS3	190	24,1	10,2	uL3	295	23,7	10,2
uS4	219	23,0	10,4	uL4	156	22,5	10,4
uS5	155	17,7	10,3	uL5	227	20,3	9,32
bS6	143	11,6	4,9	uL6	242	19,8	9,9
uS7	154	17,8	10,4	bL7/L12	201	12,7	4,5
uS8	146	14,8	9,8	uL10	113	17,7	4,6
uS9	129	14,8	11,0	uL11	48	14,9	9,7
uS10	91	11,6	10,2	uL13	186	16,3	9,7
uS11	111	13,9	11,9	uL14	94	13,1	10,7
uS12	115	15,3	11,9	uL15	282	15,6	10,8
uS13	240	13,7	10,8	uL16	189	16,2	11,1
uS14	4	7,3	11,6	bL17	228	13,7	10,3
uS15	57	10,6	10,9	uL18	95	13,1	10,4
bS16	82	10,2	10,4	bL19	168	13,4	12,0
uS17	159	10,2	10,2	bL20	132	13,7	11,7
bS18	35	9,3	11,7	bL21	235	11,4	10,3
uS19	139	10,6	10,4	uL22	186	12,8	10,4
bS20	50	9,0	11,0	uL23	287	10,6	10,3
bS21	31	7,0	11,6	uL24	88	11,5	10,3
				bL25	95	23,8	4,2
				bL27	175	10,3	10,6
				bL28	16	7,0	13,0
				uL29	108	8,1	10,1
				uL30	81	6,5	10,6
				bL31	51	9,7	9,1
				bL32	6,5	11,3	13
				bL33	27	5,9	10,7
				bL35	33	7,7	12,8

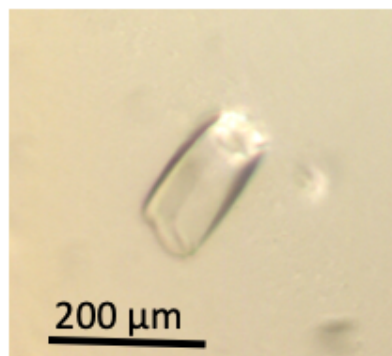
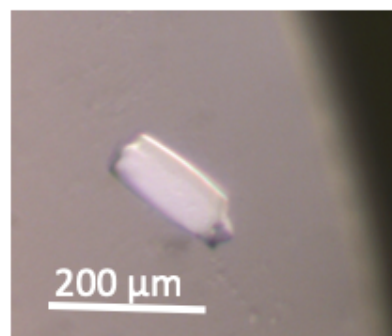
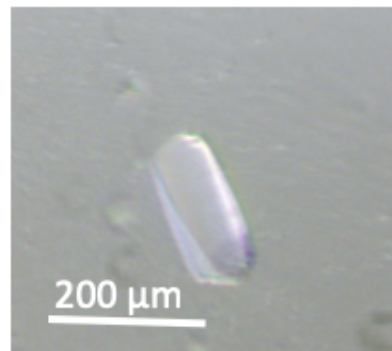
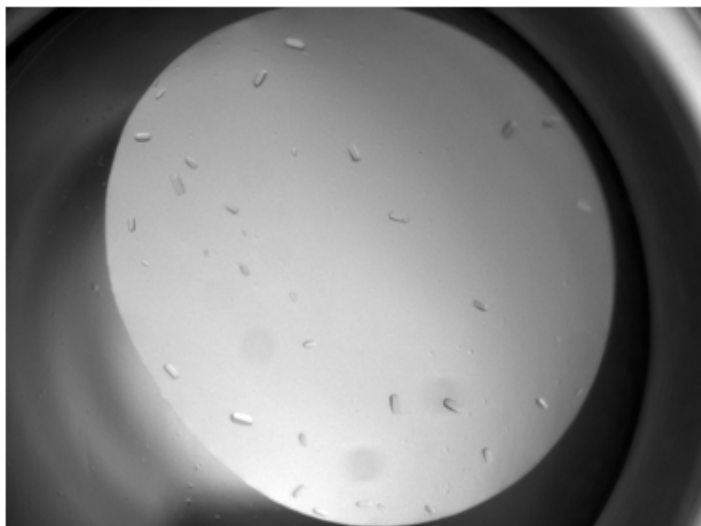
				bL36	28	4,3	11,8
--	--	--	--	------	----	-----	------

**Table 6.** List of non-ribosomal proteins found in *S. aureus* ribosome sample by LS-MS/MS analysis.

Protein	Spectral count	MW (kDa)	pI
Dehydrogenase E1 component subunit beta	30	35,2	4,5
Protein HU	24	9,6	10,0
Dehydrogenase E1 component subunit alpha	19	41,4	4,8
Protein YhbY	9	11,0	5,5
SsrA-binding protein	5	17,7	10,5
Acetyltransferase component of pyruvate dehydrogenase complex	4	46,3	4,8
Stress protein 13	1	14,8	10,1

## Crystallization

The purity of the sample was also checked by crystallization. The protocol was taken from Marat Yusupov's laboratory.



### 2 + 2 $\mu$ l CrysChem plate

#### **Reservoir:**

100	<u>mM</u>	<u>bis-Tris propane pH 7.0</u>
15	<u>mM</u>	<u>Mg-acetate</u>
325	<u>mM</u>	<u>NH<sub>4</sub>SCN</u>
4.6	<u>%</u>	<u>PEG 8000</u>
10	<u>mM</u>	<u>Spermidine</u>

#### **Sample:**

8	<u>mg/ml</u>	<u>Ribosomes</u>
2.8	<u>mM</u>	<u>Deoxy BigChap</u>

Figure 27. Crystals of 70S ribosome from *S. aureus*.

As a result, around 200  $\mu$ m crystals were obtained which is an indicator of the purity of the sample (Fig. 27).

## 30S PURIFICATION

Buffers were used during the experiment:

Buffer G:

10 mM HEPES-KOH pH 7.5

30 mM NH<sub>4</sub>Cl

1 mM Mg(OAc)<sub>2</sub>

1 mM DTT

Buffer D:

10 mM HEPES-KOH pH 7.5

30 mM NH<sub>4</sub>Cl

1 mM Mg(OAc)<sub>2</sub>

2.5 mM Spermidine

1 mM DTT

### Sucrose density gradient centrifugation

After obtaining 70S, the sample in buffer G was loaded on 0-30% w/v sucrose gradients centrifuged at 21600 rpm for 14.5 hours using a Beckman SW28 rotor (Fig. 28).

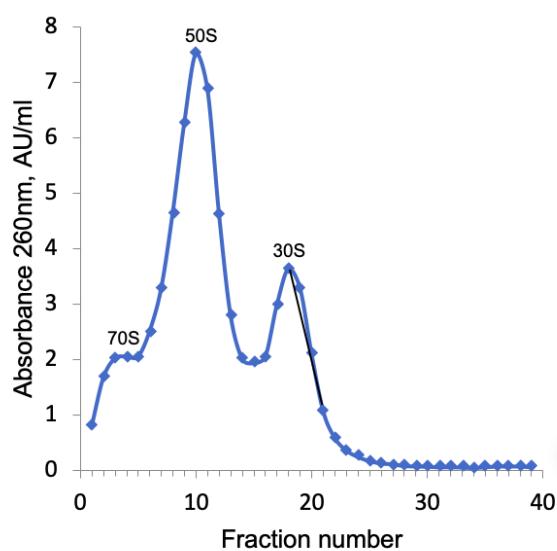


**Figure 28.** Sucrose gradient profile. The absorbance was measured by Nanodrop 2000c (Thermo Scientific). The black line indicates pooled 30S fractions.

## Concentration and storage of the sample

Selected fractions were pooled and the concentration of  $\text{Mg}(\text{OAc})_2$  was adjusted to 10 mM. In addition, spermidine was added to a final concentration of 2.5 mM. The sample was concentrated using centricons 100K simultaneously changing buffer G to buffer D. The sample was frozen in liquid nitrogen and stored at  $-80\text{ }^\circ\text{C}$ .

## One-dimensional PAGE in denaturing conditions

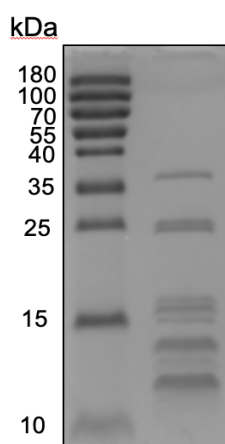


**Figure 29.** One-dimensional PAGE of *S. aureus* 30S.

The gel shows the absence of contaminants with the high molecular weight (Fig. 29).

## Agarose gel in denaturing conditions

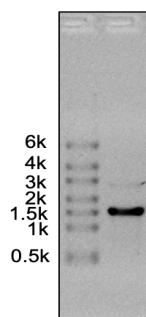


**Figure 30.** Agarose gel of 30S ribosome. The band correspond to 16S rRNA.

The gel shows the absence of rRNA (16S) degradation (Fig. 30).

## Toeprinting assay

*Toe-printing assay is a method that allows us to examine the interactions between mRNA and ribosome. This method requires reverse transcriptase, which in the absence of a ribosome, would simply create a complete cDNA copy of mRNA. However, when the reverse transcriptase will be blocked by the ribosome, synthesized short cDNA fragments called toeprints. The mRNA that was used for this experiment was 225 nt in length, UUG start codon and open Shine-Dalgarno (SD) sequence. This mRNA has the ability to easily bind to the ribosome, due to the strong SD sequence.*

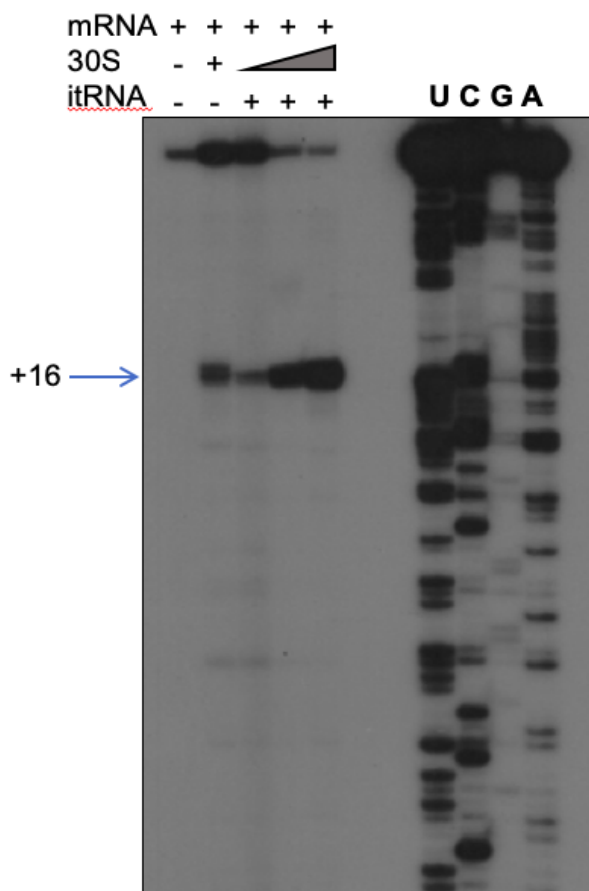


**Figure 31.** Formation of simplified translation initiation complex by toeprinting assays. Lanes U, C, G, A are sequencing ladders. The toeprint at position +16 is shown by an arrow. Experimental conditions were described in Fechter et al., 2009.

The toeprint signal is increasing with the increasing ribosome concentration, which proves the ability of mRNA bind to the ribosome (Fig. 31).

## INITIATION FACTORS PURIFICATION

### *IF1 and IF3 purifications*

Buffers for IF1 purification:

Buffer A:

20 mM Tris-HCl, pH 7.5

2 mM MgCl<sub>2</sub>

60 mM KCl

40 mM NH<sub>4</sub>Cl

1 mM EDTA pH 7.5

1 mM DTT

Buffer E:

20 mM Tris-HCl, pH 7.5

2 mM MgCl<sub>2</sub>

60 mM KCl

1 M NH<sub>4</sub>Cl

10 mM Imidazole

1 mM DTT

Buffer Q:

20 mM Tris-HCl, pH 7.5

2 mM MgCl<sub>2</sub>

40 mM NH<sub>4</sub>Cl

1 mM DTT

Buffer QB:

20 mM Tris-HCl, pH 7.5

2 mM MgCl<sub>2</sub>

1 M NH<sub>4</sub>Cl

1 mM DTT

Buffers for IF3 purification:

Buffer A:

50 mM Tris-HCl, pH 7.5

2 mM MgCl<sub>2</sub>

500 mM KCl

5% glycerol

Buffer E:

50 mM Tris-HCl, pH 7.5  
2 mM MgCl<sub>2</sub>  
500 mM KCl

Buffer Q:

50 mM Tris-HCl, pH 7.5  
2 mM MgCl<sub>2</sub>  
100 mM NH<sub>4</sub>Cl

## **Cell growth**

The vector pNEAvH containing *infA/infC* gene from *S. aureus* was transformed into *E. coli* BL21(DE3). Cells were grown in LB medium with 100 µg/ml of ampicillin. The expression was induced during 3 hours with 1 mM isopropyl β-d-1-thiogalactopyranoside (IPTG). After cells were centrifuged and resuspended in 10 mM tris-HCl pH 7.5 buffer. Cells were stored at -80 °C.

## **Lysis**

Cells were thawed for 40 minutes and then resuspended in buffer A with DNase I and protease inhibitor cocktail (without EDTA). After, the cells were destroyed using emulsiflex and centrifuged at 20000 g for 1 hour.

## **Affinity chromatography**

The principle of affinity chromatography is the ability of a his-tag protein to bind to nickel beads due to the affinity of polyhistidine tag to metal ions, followed by elution of the protein of interest with a competitive molecule like imidazole.

## **Dialysis**

The decrease salt and imidazole concentrations was performed using dialysis method overnight at +4 °C. Also, during dialysis, the his-tag of IF1 was cleaved with tev protease. For IF3, we skipped this step because of its low efficiency.

## **Ion exchange chromatography**

To obtain the sample with high purity, an ion exchange chromatography step was added. Since IF1 has an isoelectric point (pI) of 6.72 and IF3 9.7 a cation-exchange chromatography

column monoS was used. The sample was eluted gradually by increasing the salt concentration from 100 mM till 1 M. After several purifications of IF3, cation exchange chromatography was replaced by gel filtration (Superdex 75 16/600) to get more sample.

### **Storage**

The final sample was frozen in liquid nitrogen with 10% glycerol and stored at -80 °C.

## *IF2 purification*

Buffers were used during the experiment:

Buffer A:

20 mM Tris-HCl, pH 7.5

2 mM MgCl<sub>2</sub>

60 mM KCl

40 mM NH<sub>4</sub>Cl

1 mM EDTA pH 7.5

1 mM DTT

Buffer E:

20 mM Tris-HCl, pH 7.5

2 mM MgCl<sub>2</sub>

60 mM KCl

1 M NH<sub>4</sub>Cl

10 mM Imidazole

1 mM DTT

Buffer Q:

20 mM Tris-HCl, pH 7.5

2 mM MgCl<sub>2</sub>

40 mM NH<sub>4</sub>Cl

1 mM EDTA pH 7.5

1 mM DTT

Buffer QB:

20 mM Tris-HCl, pH 7.5

2 mM MgCl<sub>2</sub>

1 M NH<sub>4</sub>Cl

1 mM EDTA pH 7.5

1 mM DTT

## **Cell growth**

The vector pNEAvH containing *infB* gene from *S. aureus* was transformed into *E. coli* BL21(DE3). Cells were grown in LB medium with 100 µg/ml of ampicillin. The expression of IF2 was induced with 1 mM IPTG. Cells from 3 L culture were centrifuged and the pellet

was resuspended in 10 mM tris-HCl pH 7.5 buffer. Cells were stored at -80 °C until further use.

## **Lysis**

Thawed cells were resuspended in buffer A that contains also lysozyme, DNase I and protease inhibitor cocktail (without EDTA), sonicated and centrifuged at 15000 g for 30 min. Ammonium chloride was added to the collected supernatant till 1 M to precipitate ribosomes and centrifuged at 60000 rpm for 45 minutes using a Beckman Ti 70.1 rotor.

## **Affinity chromatography**

The protein his-tag due to the affinity binds to nickel agarose beads (Qiagen). Further, the sample was eluted with a competitive molecule imidazole (100 mM).

## **Dialysis**

The buffer change from E to Q was performed using dialysis method overnight at +4 °C. Tev cleavage was not performed due to ability of protein without his-tag also to bind with nickel beads.

## **Ion exchange chromatography**

An anion exchange chromatography step was added to obtain a pure sample (pI = 5.09). The sample was eluted gradually by increasing the salt concentration from 100 mM till 1 M.

## **Storage**

The final sample was frozen in liquid nitrogen with 10% glycerol and stored at -80 °C.

The purity of the obtained samples was checked on polyacrylamide gels.

## One-dimensional PAGE

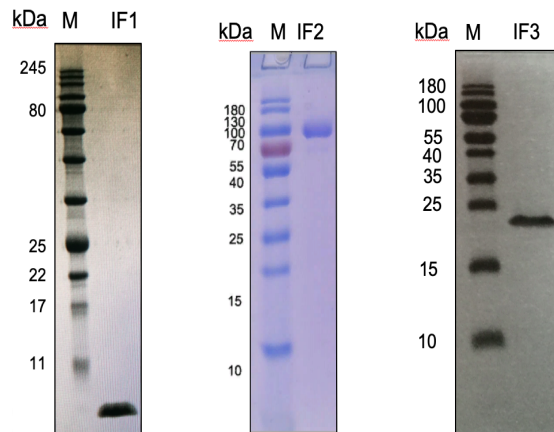


**Figure 32.** One-dimensional PAGE of initiation factors. The first factor (IF1) has a molecular weight of 8 kDa, second factor (IF2) – 79 kDa and third factor (IF3) – 23,1 kDa.

## mRNA PURIFICATION

For our experiments, we used staphylococcus specific *spa* mRNA which encodes major virulence factor protein A. The mRNA length is 225 nucleotides with the UUG start codon and a strong Shine-Dalgarno sequence (Fig. 33).

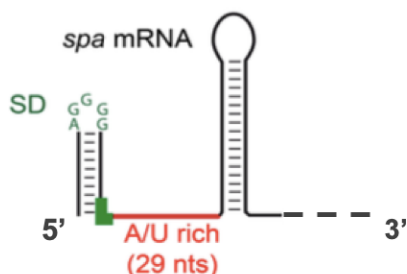


Figure 33. Structure of *spa* mRNA.

### Cell growth

The vector pUT7 containing *spa* gene from *S. aureus* was transformed into *E. coli* XL1 (from Pascale Romby's laboratory). Cells were grown in LB medium with 100 µg/ml of ampicillin.

### Plasmid purification

Plasmid purification was done using NucleoBond Xtra miniprep kit (Macherey nagel).

### Linearization

Linearization of plasmid was performed restriction enzyme BamHI. The resulting DNA was extracted with phenol-chloroform and precipitated in absolute ethanol. Further, the sample was loaded on agarose gel to separate linearized DNA from the plasmid, with subsequent use of NucleoSpin Gel and PCR Clean-up kit (Macherey nagel) to purify the DNA from the gel.

### “In vitro” transcription

The transcription was performed using T7 MEGAscript kit (Ambion). For 1 µg of DNA used:

- 7,5 mM ATP solution,
- 7,5 mM CTP solution,
- 7,5 mM GTP solution,
- 7,5 mM UTP solution,
- 1 U/µl RNasin
- 1X reaction buffer,
- 7,5 U/µl T7 RNA polymerase

10x reaction buffer:  
44.1 M Tris-HCl pH 7.5  
1 M NaCl  
1 mM EDTA pH 7.5  
1 mM DTT  
0,1 mM Spermidine

Incubated at 37 °C for 4 hours.

After 4 hours incubation, DNase TURBO was added till final concentration 2 U/ $\mu$ l and incubated additional 15 minutes at 37 °C. DNase TURBO is a specifically engineered hyperactive DNase that exhibits up to 350% greater catalytic efficiency than wild type DNase I (from T7 MEGAscript kit, Ambion). Then the obtained RNA was extracted with phenol-chloroform and precipitated with isopropanol.

### Midi-size gel

An additional purification step is required to obtain a high purity sample. For this, a 6% polyacrylamide gel was used which was run for 3.5 hours at 300 V. The resulting RNA was eluted in a buffer with 500 mM NH<sub>4</sub>Cl, 1 mM EDTA pH 8 and 16% phenol.

### Storage

The sample was stored at -20 °C until further use.

Purified mRNA was checked on a 6% polyacrylamide gel (Fig. 34).

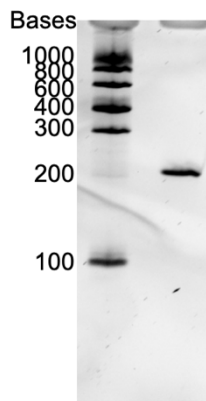


**Figure 34.** 6% PAGE of spa mRNA (225nts).

## **fMet-tRNA<sup>fMet</sup> PREPARATION**

### *Methionyl-tRNA<sup>fmet</sup> synthetase (MetRS)*

MetRS is a 74 kDa synthetase that catalyzes the formation of methionyl-tRNA<sup>fMet</sup>.

Buffers were used during the experiment:

Buffer A:

20 mM Tris-HCl, pH 7.5

30 mM KCl

1 mM EDTA pH 7.5

1 mM DTT

Buffer E:

20 mM Tris-HCl, pH 7.5

1 M NH<sub>4</sub>Cl

10 mM Imidazole

1 mM DTT

Buffer Q:

20 mM Tris-HCl, pH 7.5

30 mM KCl

50% glycerol

1 mM DTT

### **Cell growth**

The plasmid pET15b overexpressing MetRS from *E. coli* was provided by Cheemeng Tan (Addgene plasmid #111464). Cells were grown in terrific broth medium with 100 µg/ml of ampicillin and 0,4 mM IPTG grown overnight. Then cells were centrifuged and resuspended in 10 mM tris-HCl pH 7,5 buffer.

### **Lysis**

Thawed cells were resuspended in buffer A with DNase I and protease inhibitor cocktail and lysed using the emulsiflex. Then the sample was centrifuged at 20000 g for 1 h to precipitate cell debris.

### **Affinity chromatography**

A sufficiently pure sample was obtained using affinity chromatography. After the his-tag protein bound to nickel beads, it was eluted with 300 mM Imidazole.

## Dialysis

The sample was dialyzed into buffer Q in order to remove imidazole from the sample.

## Storage

The sample was kept at -20 °C in 50% glycerol.

Purified MetRS was checked on 15% PAGE (Fig. 35).

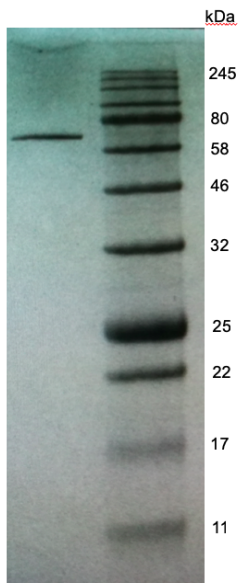


**Figure 35.** One-dimensional PAGE of MetRS (74 kDa).

### *Methionyl-tRNA<sup>fMet</sup> formyltransferase (MTF)*

MTF is a 30 kDa enzyme that catalyzes the attachment of the formyl group to methionyl-tRNA<sup>fMet</sup>.

Buffers were used during the experiment are the same as for MetRS.

#### **Cell growth**

The plasmid pSC101 overexpressing MTF from *E. coli* was provided by Cheemeng Tan (Addgene plasmid #111492). Cells were grown in LB medium with 50 µg/ml of kanamycin and 1 mM IPTG grown for 3 hours. Then cells were centrifuged and resuspended in 10 mM tris-HCl pH 7,5 buffer.

The lysis, affinity chromatography, dialysis and storage stages are the same as described previously for MetRS.

Purified MTF was checked on 15% PAGE (Fig. 36).

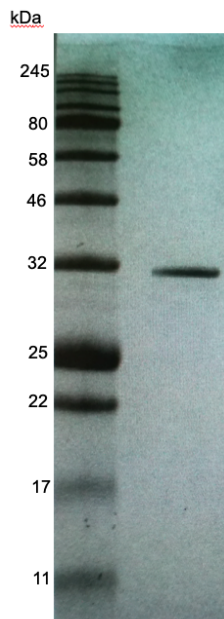


**Figure 36.** One-dimensional PAGE of MTF (30 kDa).

## *tRNA<sup>Met</sup>*

The protocols that will be described below have been adapted from protocols that were published in “Methods in Enzymology” (Mechulam et al., 2007).

Buffers were used during the experiment:

Buffer A:

50 mM tris-HCl pH 7.2

150 mM NaCl

Buffer B:

20 mM tris-HCl pH 7

20 mM Mg(Oac)<sub>2</sub>

Buffer Q:

20 mM HEPES-KOH pH 7

Buffer QB:

20 mM HEPES-KOH pH 7

1M NaCl

Buffer P:

50 mM K<sub>3</sub>PO<sub>4</sub> pH 7

1,7 M (NH<sub>4</sub>)<sub>2</sub>SO<sub>4</sub>

Buffer PB:

20mM MOPS pH 8

### **Cell growth**

The plasmid pBS used for overexpression of *tRNA* from *E. coli* was provided from A. Innis's laboratory already transformed into HB101 strain. Cells were grown in LB medium overnight and after centrifugation were resuspended in buffer A.

### **Phenol-chloroform extraction, DNA and tRNA precipitation**

After thawing cells, nucleic acids were extracted with phenol-chloroform. Sodium acetate and isopropanol were added to the obtained sample to precipitate DNA. After that, *tRNA* was precipitated by adding more isopropanol.

## Deacetylation of tRNA

The pellet was resuspended in 200 mM tris-Ac pH 9 buffer and incubated for 1 hour at 37 °C. Then it was precipitated in absolute ethanol and resuspended in 10 mM ammonium acetate pH 5. The quality of purification of initiator tRNA was checked on a 6% polyacrylamide gel (Fig. 37).

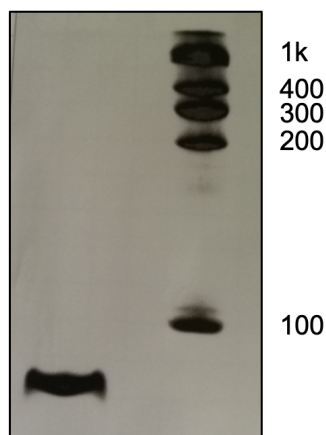


Figure 37. 6% PAGE of itRNA (75 n).

## Ion exchange and hydrophobic interaction chromatography

The first purification step was performed using anion chromatography (Q sepharose column). Then the sample was precipitated with isopropanol and was applied to phenyl column. Finally, the sample was concentrated using centricon tubes 10K and was kept at -20 °C.

## Preparation of formyl donor

10-Formyltetrahydrofolate (f-THF) is a donor of formyl group for formyltransferase reactions usually derived from folinic acid (Sigma-Aldrich). Folinic acid were dissolved in 50 mM  $\beta$ -mercaptoethanol and 1 N HCl and incubated at room temperature for 4 hours. The amount of formyl donor was measured at 350 nm every hour. After 4 hours the sample was diluted 6 times with water and pH was adjusted to 7.5 with 2 M tris-base pH 11. The sample was kept at -20 °C.

## Aminoacylation and formylation of tRNA<sup>fMet</sup>

The reaction was performed 2 times: first with S100 (Rajbhandary and Ghosh, 1969) supernatant after centrifugation at 100000 g) and then with enzymes.

### *1<sup>st</sup> reaction*

2X buffer:  
200 mM HEPES-KOH pH 7

40 mM MgCl<sub>2</sub>  
60 mM KCl  
8,3 mM ATP  
0,83 mM L-Met

Reaction mix:  
100 nmoles itRNA  
1x buffer  
200 nmoles f-THF  
1,7 mg/ml S100

The sample was incubated at 37 °C for 45 minutes, then extracted with phenol and precipitated in absolute ethanol. After that, the sample was run on phenyl column in order to remove non-aminoacylated and non-formylated tRNAs.

*2<sup>nd</sup> reaction*

10X buffer:  
102 mM Mg(OAc)<sub>2</sub>  
307 mM imidazole pH 7.6  
54 mM β-mercaptoethanol  
1025 mM KCl

Reaction mix:  
100 nmoles of itRNA from previous reaction  
1X buffer  
4 mM ATP  
200 nmoles f-THF  
0,4 mM L-Met  
0,04 mg/ml MetRS  
0,04 mg/ml MTF  
0,15 mg/ml BSA

The sample was incubated at 37 °C for 45 minutes, precipitated in absolute ethanol and run one more time on phenyl column. Finally, the sample was concentrated with centricon tubes and stored at -80 °C.

## CRYO-ELECTRON MICROSCOPY

The main method used during this thesis project is cryo-electron microscopy (cryo-EM). In the following I will introduce briefly this technique. Cryo-EM is a powerful structural biology technique used to solve the structures of macromolecular complexes very often at atomic resolutions. Jacques Dubochet, Joachim Frank and Richard Henderson set the bases of the technique and subsequently received the Nobel Prize in Chemistry in 2017. Today, cryo-EM can handle even small molecules (~30 kDa (Liu et al., 2019)). Its major advantages are the ability of analyzing heterogeneous complexes with a large number of conformations (Serna, 2019) without the need of forming crystals, which can be extremely challenging for large and/or hydrophobic molecular assemblies.

### **The remarkable progress in cryo-EM**

Initial results in this area were achieved with highly symmetric viral particles and large stable multicomponent complexes, such as ribosomes. At the same time, barriers related to resolution limits, the size of macromolecular targets, the lack of internal symmetry and the solubility of the sample began to appear which were subsequently overcome in many cases. Some important improvements were achieved using higher accelerating voltages (200 - 300 kV) and an electron source with a field emission gun, others using a stable lens system (Glaeser et al., 2011), an improved vacuum system, and stable cryo-stages that minimize sample drift. But the major improvement was the advent of direct electron detector device (DDD) cameras which a superior detective quantum efficiency, a measure of the combined effects of the signal and noise performance of an imaging system. Along with improving the hardware of the technique (DDD, transmission electron microscopes, vitrification devices) the softwares have also made a revolutionary leap ahead. Before image processing involved many independent and time-consuming steps while now all processes are quite automated and take a small amount of time (McMullan et al, 2009, Faruqi and McMullan, 2011, Li et al., 2013, Milazzo et al., 2011).

### **The transmission electron microscope**

The structure and principle of a transmission electron microscopy (TEM) is similar to a light microscope, but electromagnetic lenses instead of glass lenses and electrons instead of light are used. In the TEM high-energy electrons pass through a thin sample and form a projected image on a screen or image sensor, similar to the way a projector forms a magnified image of a frame of photographic film.

Due to the small size of the electrons, which are easily deflected under the action of hydrocarbons or gas molecules, it is necessary to use the electron beam in a vacuum environment (Dubochet et al., 1982). Moreover, by the reason of the incompatibility between the requirements for

vacuum and the natural hydrated state of biological samples, it was decided to keep the sample frozen at the temperature of liquid nitrogen or helium throughout the experiment.

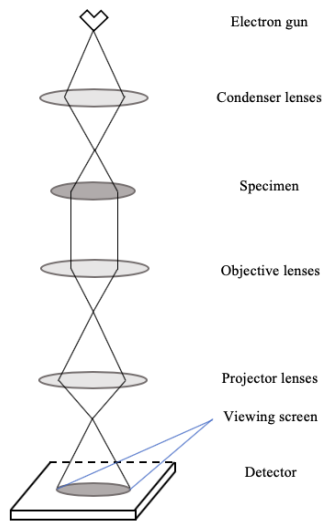


**Figure 38.** Schematic representation of basic composition of electron microscope.

An electron gun emits the electrons that pass through a vacuum and get focused into a thin beam by condenser lenses. Then the beam passes through the objective lens and the projector lens that after project the image onto a viewing screen or detector. In addition, there are several intermediate lenses along the column that magnify the image (Fig 38).

### Sample preparation and data acquisition

The first steps concern of course the sample purification, dilution to the appropriate concentration in a chosen buffer. The sample must then be deposited on an EM grid (copper and more rarely gold) that is often covered by a carbon layer (Fig. 39). The next step is to freeze the sample in liquid ethane using a device referred to as the “vitrobot”. A drop of sample is usually applied on the grid under high humidity and low temperature conditions, blotted to remove the excess of liquid to get monolayer of sample and immediately plunged into liquid ethane cooled down to the temperature of liquid nitrogen. Then the sample is transferred to liquid nitrogen. The point being to freeze the sample in vitreous (non-crystalline) ice.

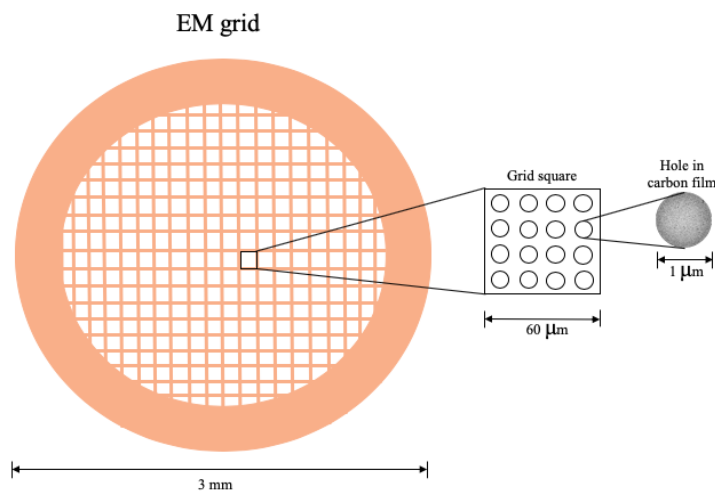


**Figure 39.** Representation of the cryo-EM grid at different scales (adapted from Wang and Sigworth, 2006).

After that, the sample is visualized and collected on a cryo-electron microscope to obtain 2D projections. During data collection and irradiating a sample with electrons, the protein being denser than ice, appears darker on the image, mainly due to phase contrast. At the end, the sample is analyzed using certain programs and an atomic model is built (Fig. 40).

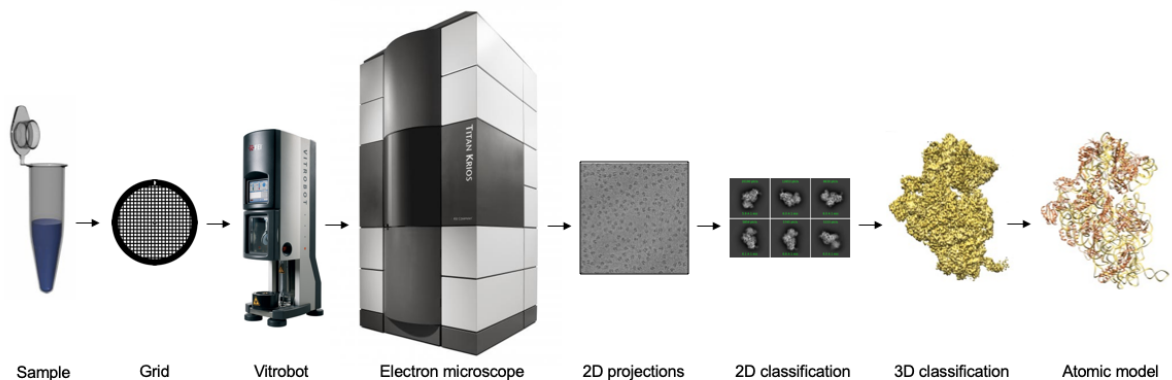


**Figure 40.** Scheme of sample analysis by cryo-electron microscopy.

## Cryo-electron microscopes

### *Titan Krios*

Titan Krios is the latest generation electron microscope with capacities for high-resolution data collection. The electron source is a Field Emission Gun (FEG) that can be operated at 80keV, 100keV, 200keV or 300keV. The advantages of this microscope are an autoloader mechanism allows mounting

twelve grids at a time and 2<sup>nd</sup> objective lens. The first data acquisition was performed in Netherlands Center for Electron Nanoscopy (NeCEN, Leiden) on Titan microscope equipped with Falcon II detector.

#### *Tecnai F30 Polara*

The Tecnai F30 Polara cryo-electron microscope allows to collect the data for both cryo-electron tomography and single particle analysis experiments. Its FEG is usually tuned to 100keV, 200keV or 300keV. The grids are manually mounted six at a time. Several data acquisitions were performed on this microscope located in the Centre de Biologie Intégrative (CBI, Illkirch, France).

#### *Talos Arctica*

The Talos Arctica is a fully automated 200 kV FEG electron microscope. This microscope is also used for cryo-electron tomography and single particle cryo-electron microscopy. It is equipped with an autoloader system that permits loading of up to twelve specimens. The latest data acquisitions were performed on the Talos Arctica microscope located in European Institute of Chemistry and Biology (IECB, Pessac, France).

Table 7 shows the characteristics of the Titan Krios, Tecnai F30 Polara and Talos Arctica microscopes.

**Table 7.** Characteristics of microscopes used for data acquisition.

	Titan Krios	Tecnai F30 Polara	Talos Arctica
Voltage (kV)	300	300	200
Defocus range (µm)	-0,6 — -4,0	-1,5 — -4,5	-0,5 — -3,0
Pixel size	1,04	1,81	1,24
Magnification	134000x	59000x	120000x

### **Image processing**

Can be subdivided to several sequential tasks:

### *Frame re-alignment*

With the advent of direct detector device (DDD) cameras, it became possible to collect a cryo-EM image as “movie”, i.e.; multiple frames covering few seconds of exposure, which allows potentially for the correction of movement of the specimen, due both to instabilities in the microscope specimen stage and electron beam-induced movements, simply by realigning corresponding areas of the grid from the same movie. Subsequently, the quality of the integrated images improves significantly and can potentially go to atomic resolutions (Baker, 2010, Scheres, 2014).

### *Contrast transfer function*

It is a mathematical function that describes how aberrations in a TEM modify the image of a sample, expressed in Fourier space. The correction is necessary because the CTF causes resolution-dependent amplitude modulations (Thon rings; Thon, 1966) and phase reversals in the image. Without any CTF correction, reconstructed model may contain significant local density displacements. Some parameters, such as the wavelength and the coefficient of spherical aberration, are given by the microscope settings, while others (defocusing and astigmatism) are established experimentally. After mathematical calculation of the CTF, images should be assessed qualitatively for drift, astigmatism, and overall resolution. The CTF is an oscillating function which crosses zero several times. When the function values are 0, information is lost, therefore, it is necessary to collect data at different defocus settings, which leads to averaged values with the CTF correction (Penczek, 2010).

### *Particle picking and extraction*

After selection of good micrographs based partly on the Thon rings, particles are picked manually or semi-automatically and then extracted from the micrographs for further manipulations.

### *Particle sorting (classification)*

Classification is needed in order to obtain homogeneous sets of particle that represent different ensembles of conformations. Classification can be in two or three dimensions (2D or 3D). The 2D classification is often deployed without a prior reference (reference-free) simply by cross-matching all images to each other's, which gives an initial idea of the heterogeneity in the data set. 3D classification on the other hand allows to sort different particle images after reconstruction them in several different 3D volumes (cryo-EM reconstructions). The accuracy of the classification depends largely on the quality of the sample. The image processing algorithms are still limited by the amount of structural heterogeneity that can be tolerated. Classifying small, asymmetric and/or extremely dynamic samples remains significantly challenging.

## Refinement

After classification, the stage of optimized refinement begins, which reduces the tendency of the model to correlate noise in one image, thereby increasing the accuracy and quality of the resulting map. This process is iterative and can potentially yield cryo-EM reconstructions at atomic resolutions.

The image processing steps are summarized in the figure 41 below.

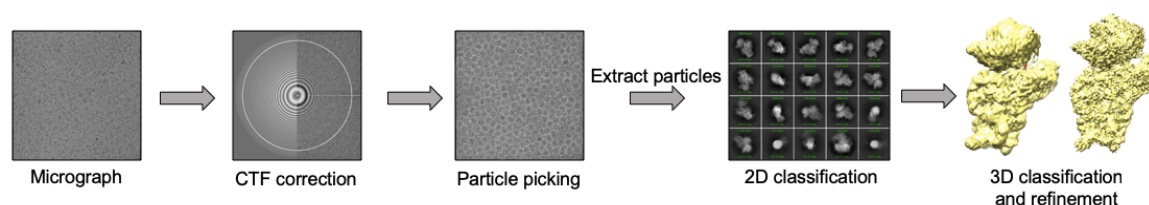


**Figure 41.** Principle steps of image processing in CryoSparc.

## Resolution in cryo-EM

Resolution is probably the most important parameter in assessing the quality of an electron density map determined by cryo-EM. The most common metric for estimation global resolution is the Fourier shell correlation (FSC) that is calculating the resolution by comparing the structure form divided datasets with the obtained structure, but this approach cannot account for variance in the local resolution of difference areas of the cryo-EM map. For local resolution estimation ResMap, MonoRes or other tools are used. All these approaches require a considerable amount of processing time and in some cases their estimates are significantly different from one another.

## RESULTS

### Functional tests of initiation factors

To check the initiation factors activity and the best ratio between factors and ribosome for the complex formation we used toeprinting assay. There are many methods that could be used but most of them either require a large amount of material or use the *E. coli* system. In the 90s, Larry Gold showed the possibility of checking the activity of initiation factors by toeprinting method.

### IF1 activity

As IF1 promotes the binding of the IF2 to the 30S ribosomal subunit (Stringer et al., 1977, Weiel and Hershey, 1982, Celano et al., 1988), it is possible to check the concentration of IF1 with fixed concentration of IF2.

On the first lane on the figure 42, due to the adding mRNA only a signal of full-length extension appeared. On the second lane, mRNA was blocked by 30S that is demonstrated by appearing of several bands more or less at the right position. On the next lanes, adding a different concentration of IF1, the concentrations of mRNA, 30S, fMet-tRNA<sup>fMet</sup> and IF2 were left the same.

The quantification of the complex formation was done by estimation of amount of signal at position +16 in relation to the sum of +16 signal and the signal of full length in the ImageQuant TL software (Fig. 43).



## IF2 activity

IF2 promotes the binding of the fMet-tRNA<sup>fMet</sup> to the 30S (Lockwood et al., 1971, Majumdar et al., 1976, Sundari et al., 1976, La Teana et al., 1996). The IF2 activity was checked with the fixed concentration of fMet-tRNA<sup>fMet</sup>.

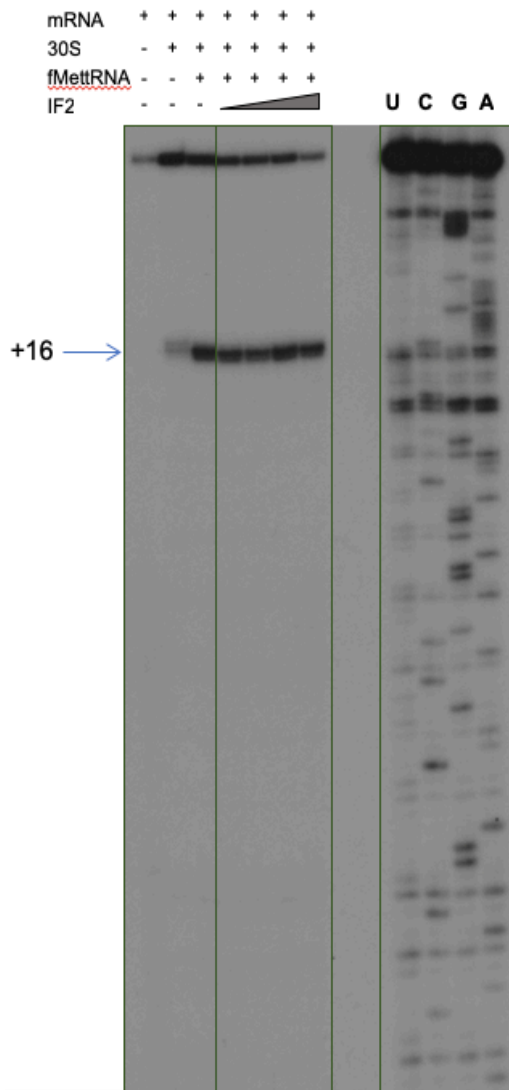


**Figure 44.** Formation of simplified initiation complex with IF2 by toeprinting assays. Lanes U, C, G, A are sequencing ladders. The toeprint at position +16 is shown by an arrow.

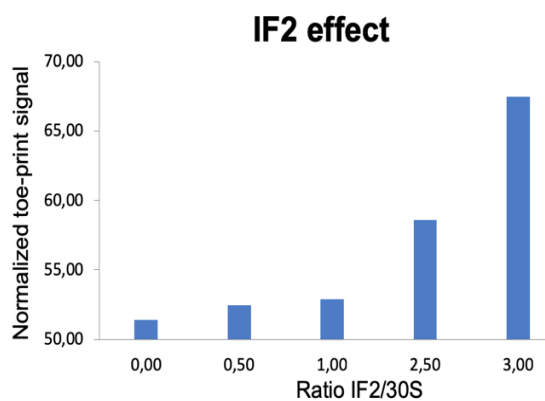


**Figure 45.** The quantification of the toeprint (given in %) was first normalized according to the full-length extension product bands using the ImageQuant TL software.



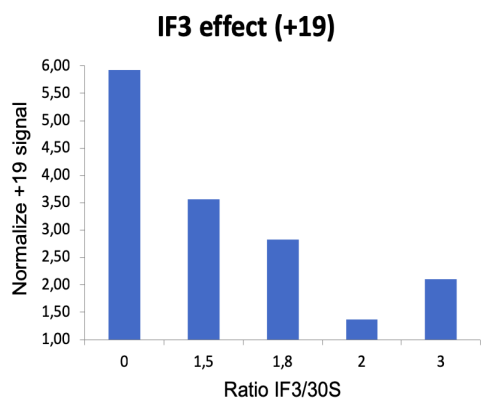


**Figure 47.** The quantification of the toeprint (given in %) was first normalized according to the full-length extension product bands using the ImageQuant TL software.

In the presence of not fully active IF3 there are signals of different tRNAs but when the IF3 is active, the band that was correspond to Lys-tRNA disappeared. The best concentration of IF3 selected for further experiments was 2 times more that the concentration of 30S (Fig. 46, 47).

The ratio used in the work:

IF1	3:1
IF2	3:1
IF3	2:1
mRNA	3:1
fMet-tRNA <sup>fMet</sup>	3:1

The first purification of 30S was done from 70S by separation of two subunits in sucrose gradients with low magnesium (1 mM Mg(OAc)<sub>2</sub>) and high salt (200 mM KCl) buffer concentrations. The 30S preparation was checked on agarose gel in denaturing conditions. No degradation was observed (Fig. 48). The ratio of the components was taken from the literature.

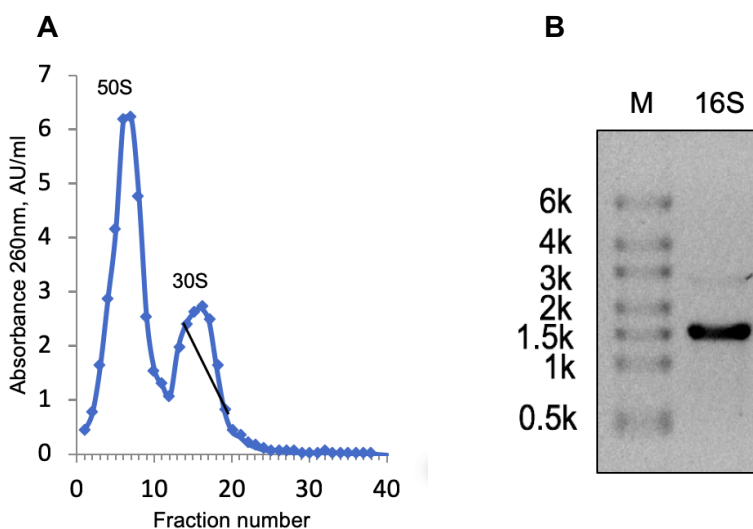


**Figure 48.** Sucrose gradient profile (A). The black line on gradient indicates pooled 30S fractions. No 16S degradation was observed on agarose gel (B).

## Mass spectrometry

Analysis of the small ribosomal subunit shows the presence of all proteins, including S1 protein with a low number of spectra count. This result in combination with other studies of S1 protein probably indicates that S1 from *S. aureus* is not a ribosomal protein. Only one non-ribosomal protein was found in the sample with 1 spectra count (Table 8).

**Table 8.** List of proteins found in *S. aureus* 30S ribosome sample by LC-MS/MS analysis, where b – bacterial specific proteins, u – universal proteins.

Protein	Spectral count	MW (kDa)	pI
bS1	4	43,3	4,60
uS2	258	29,1	5,3
uS3	280	24,1	10,2
uS4	328	23,0	10,4
uS5	184	17,7	10,3
bS6	139	11,6	4,9
uS7	243	17,8	10,4
uS8	120	14,8	9,8
uS9	102	14,8	11,0
uS10	128	11,6	10,2
uS11	105	13,9	11,9
uS12	194	15,3	11,9
uS13	278	13,7	10,8
uS14	71	7,3	11,6
uS15	112	10,6	10,9
bS16	75	10,2	10,4
uS17	150	10,2	10,2
bS18	96	9,3	11,7
uS19	298	10,6	10,4
bS20	266	9,0	11,0

bS21	19	7,0	11,6
non-ribosomal protein			
RNA-binding protein YhbY	1	11,0	5,57

### Negative stain electron microscopy

Negative stain electron microscopy (EM) is the best method for rapid sample assessment using the contrast enhancing stain reagent. This technique is useful for a variety of biological problems and also provides a rapid means of assessing samples for cryo-electron microscopy. The disadvantage of negative stain EM is the limited resolution up to 18 - 20 Å.

This approach can be used to verify the sample concentration required to the grids preparation for cryo-EM. The process itself consists in adsorbing the sample on a substrate, then a stain is applied, blotted and dried to obtain a thin layer of electron dense stain in which the particles are embedded (Fig. 49). All procedures were performed by Dr. Yaser Hashem.



**Figure 49.** Micrograph of SSU from *S. aureus*.

All procedures related to data collection or image processing were performed in Dr. Yaser Hashem laboratory by engineer Dr. Heddy Soufari. 4 µl of 90 nM *S. aureus* initiation complex was applied to the cryo-EM grid, blotted with filter paper from both sides for 3 seconds on Vitrobot apparatus (FEI, T = 4 °C, humidity 100%, blot force 5, blot waiting time 30 seconds) and vitrified in liquid ethane pre-cooled in liquid nitrogen. Data were collected on the Krios microscope (Titan, K2 Camera) and processed with Scipion package:

CTF estimation: ctffind4,

Particle extraction: XMIPP3,

3D classification: Relion,

Refinement: Relion.

One class was obtained with a moving head and an unstable structure. Also, there were several classes with flexible helix 44 (Fig. 50).

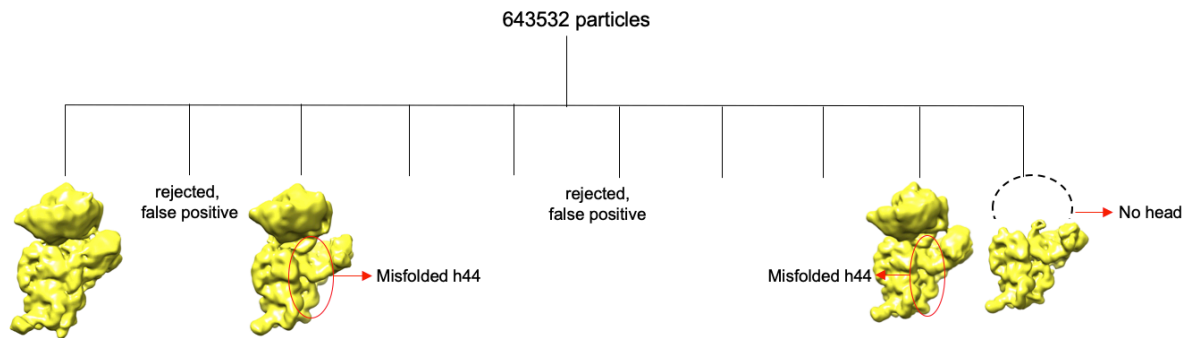


**Figure 50.** 3D classification of 643532 particles divided into 10 classes. Particles were rejected because they were artifacts due to automatic picking during image processing.

The effect of salt concentration on the 30S purification was checked by the sucrose gradient and then all samples were loaded on the 15% PAAG (Fig. 51, 52).

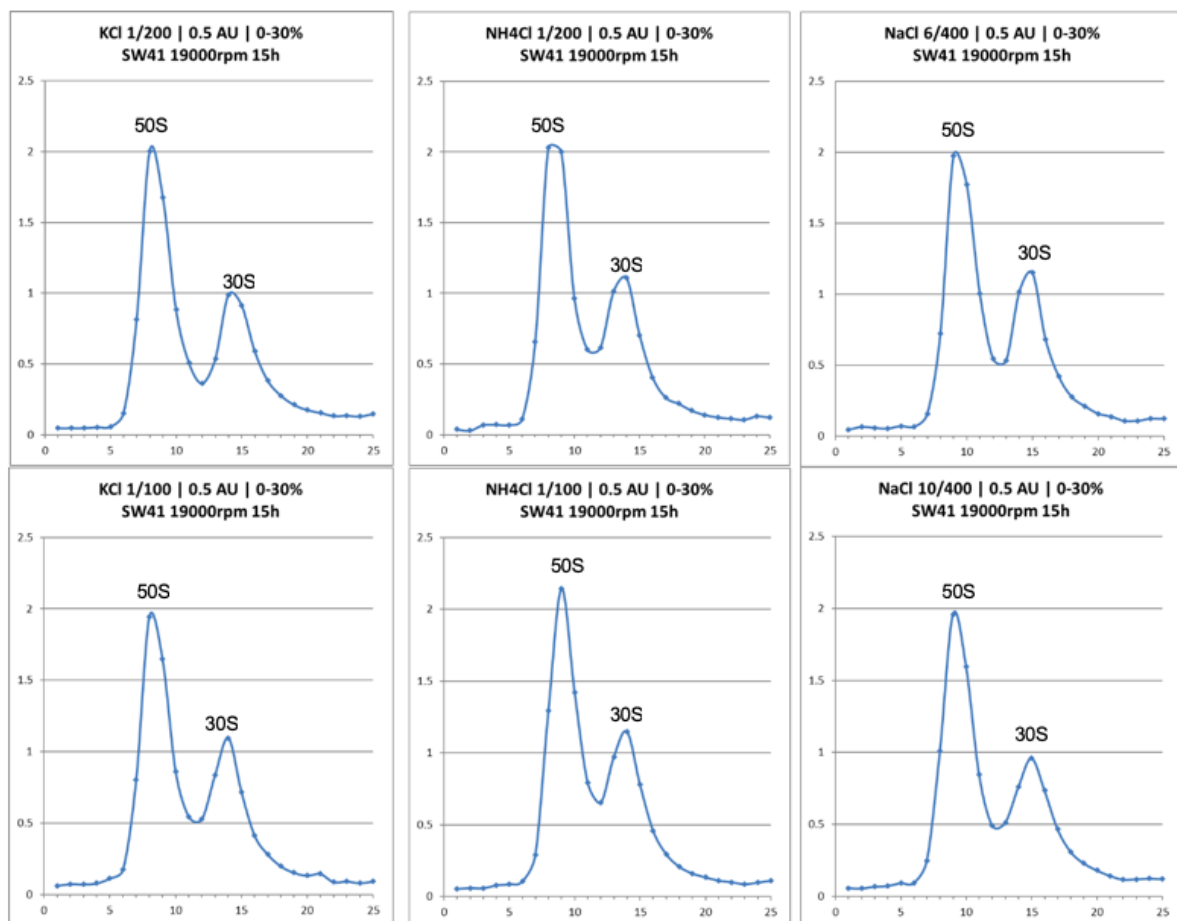


**Figure 51.** Sucrose gradient profiles. 100 mM and 200 mM of NH<sub>4</sub>Cl and KCl and 400 mM of NaCl have been checked.

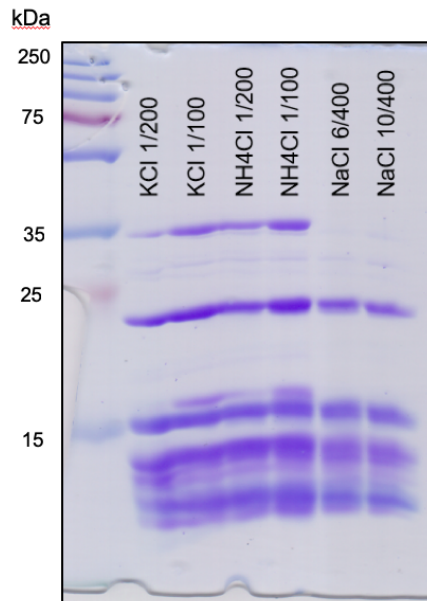


**Figure 52.** 15% polyacrylamide gel. The detailed information is in the text.

Results reveal that under high salt conditions (namely 200 mM KCl or 400 mM NaCl) some of the proteins of small ribosomal subunit dissociate from the ribosome. We suggest that it is bs2 (upper band) and another unidentified protein (lower band) (Fig. 52).

For large-scale purification conditions 100 mM NH<sub>4</sub>Cl were chosen as the most optimal.

Also, an additional gradient was added to completely remove 50S from the sample. Then, 30S preparation was checked on agarose gel in denaturing conditions to detect rRNA degradation (Fig. 53).

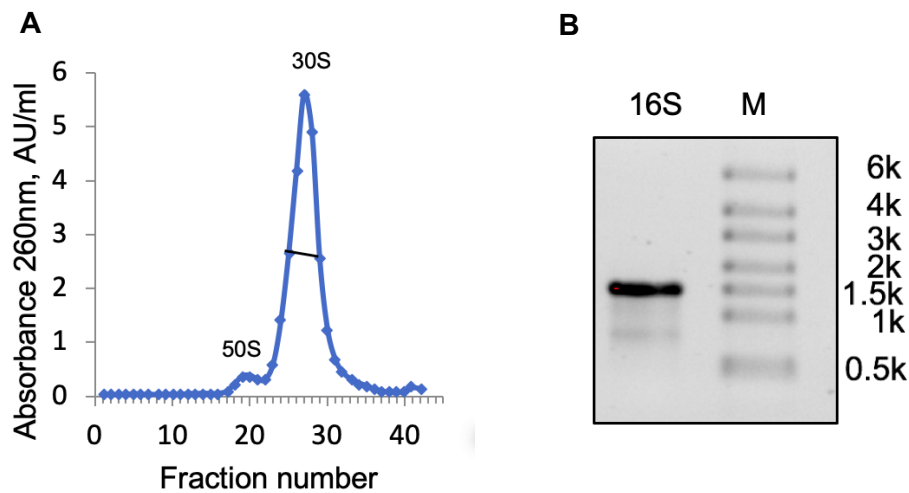


**Figure 53.** Sucrose gradient profile (A) and agarose gel of 16S rRNA. No ribosomal RNA degradation was observed (B).

## 2<sup>nd</sup> data acquisition

The sample with the correct ratio in low salt conditions was prepared for data collection on Polara microscope followed by data processing on Scipion.

The structure of 30S with mRNA, fMet-tRNA<sup>fMet</sup> and IF2 was obtained at 10 Å. The head of the 30S was not so flexible, at the same time the helix 44 was still in two positions in around 86% of the particles (Fig. 54).

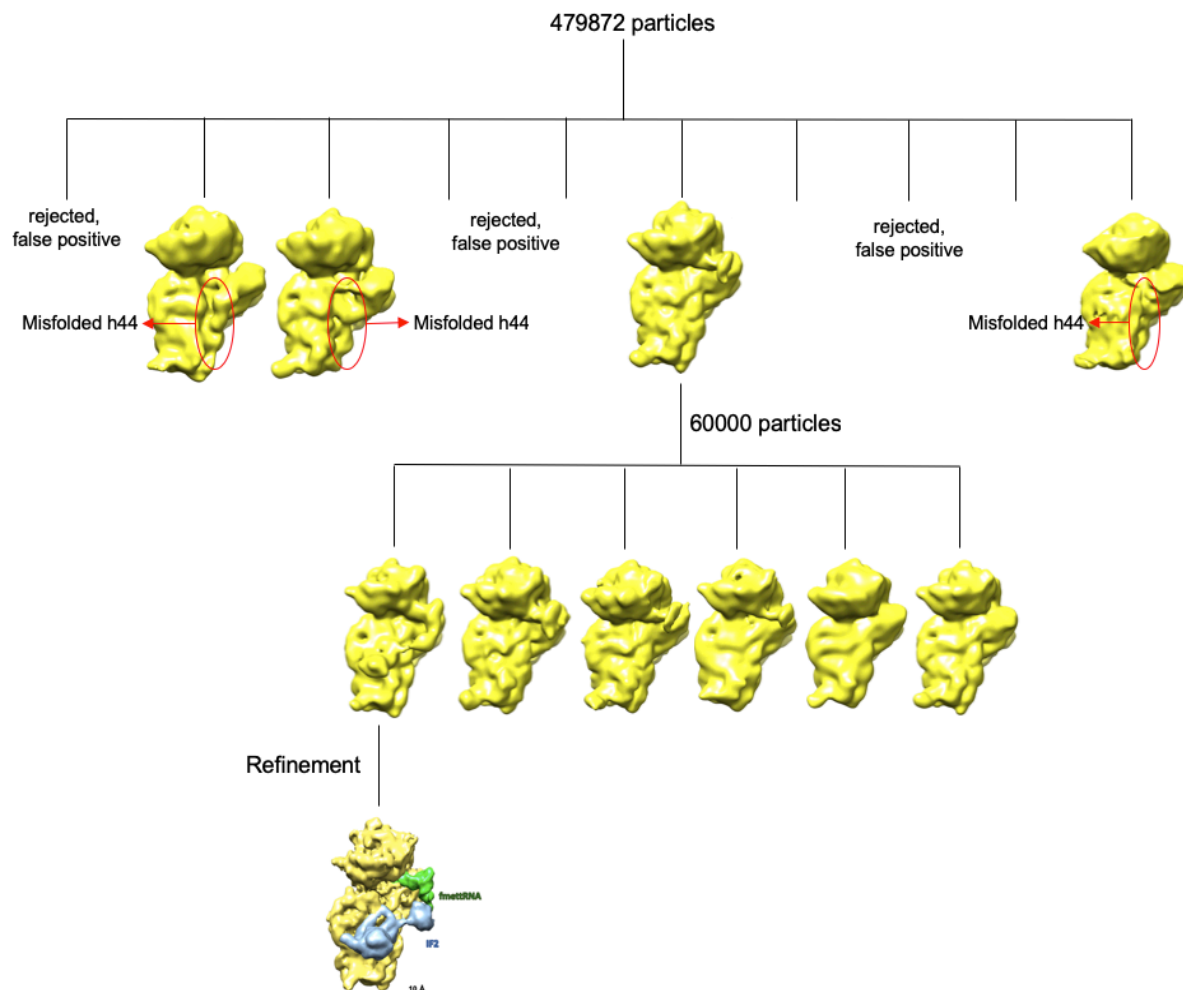


**Figure 54.** 3D classification of 479872 particles divided into 10 classes. Obtained 1 class with 60000 particles was reclassified into 6 classes. The final class was obtained at 10 Å after refinement step. Particles were rejected because they were artifacts due to automatic picking during image processing.

Perhaps the stage of ribosome purification was too long, it was decided to purify the small ribosomal subunit without additional sucrose gradient and do not freeze the sample before loading on the grids. The 30S preparation was checked on agarose gel in denaturing conditions (Fig. 55).

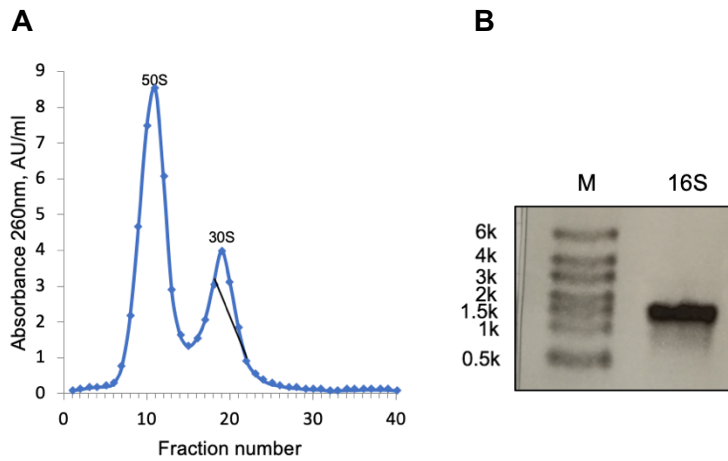


**Figure 55.** Sucrose gradient profile (A). The black line on gradient indicates pooled 30S fractions. No 16S degradation was observed on agarose gel (B).

### 3<sup>rd</sup> data acquisition

Two 30S with tRNA and IF3 structures in two conformations and one structure with IF2 were obtained, but still the helix 44 was flexible in around 60% of particles (Fig. 56).

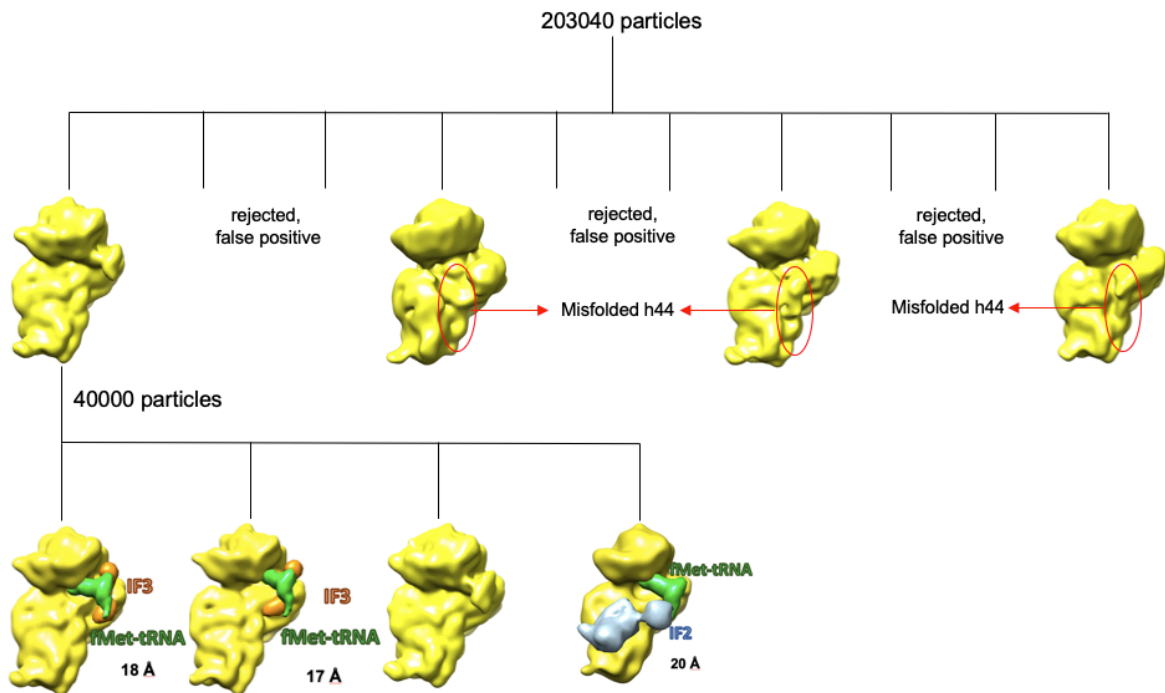


**Figure 56.** During 3D classification 1 class with 40000 particles was obtained and reclassified into 4 classes. Low resolution structures with IF3 in different conformations and IF2 were obtained. Particles were rejected because they were artifacts due to automatic picking during image processing.

Further, it was decided to optimize the ribosome purification step again. In 1977, it was shown the ribosomal subunits separation in 30 mM NH<sub>4</sub>Cl buffer (Fahnestock, 1977). Further

experiments were performed in low salt buffer conditions. In 10 mM Mg(OAc)<sub>2</sub> and low salt conditions the 70S was stable. In 1 mM Mg(OAc)<sub>2</sub> subunits separation became possible while in 2 mM Mg(OAc)<sub>2</sub> only partial separation was observed (Fig. 57).

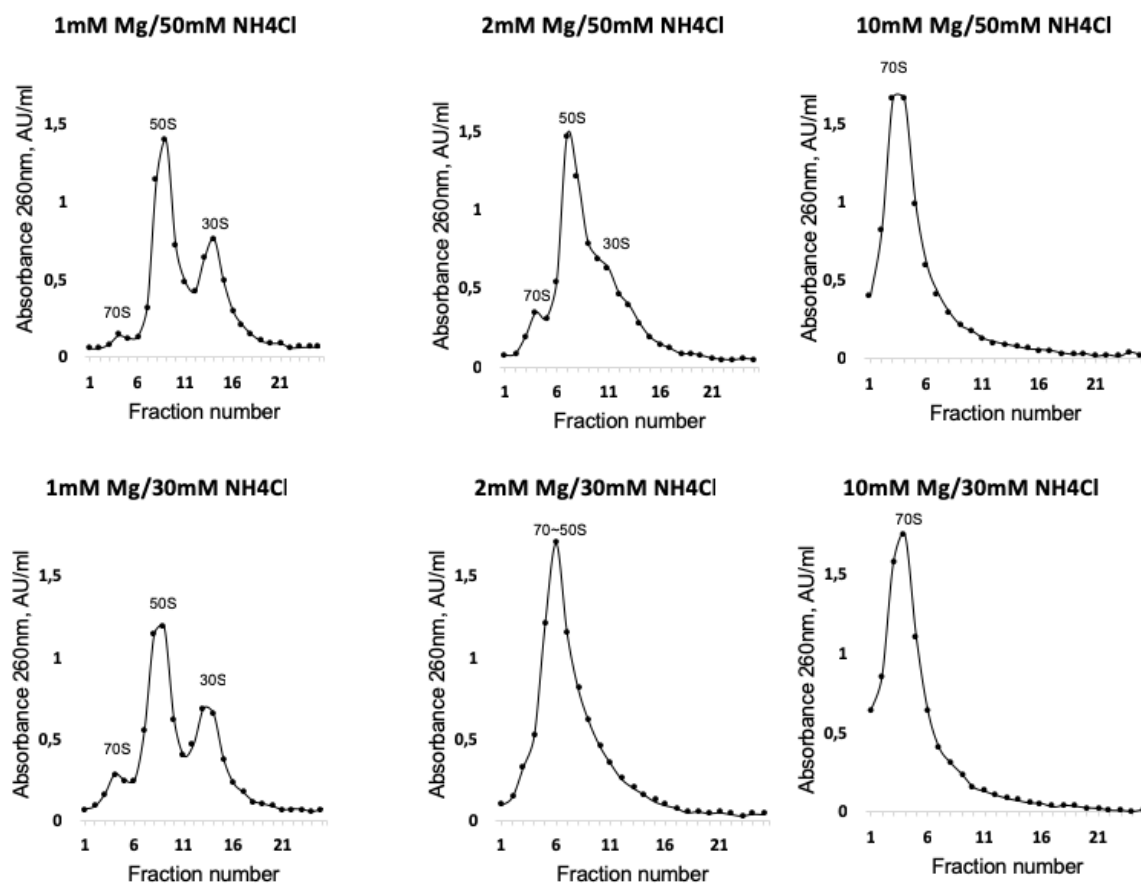


**Figure 57.** Sucrose gradient profiles. 30 mM and 50 mM NH<sub>4</sub>Cl have been checked.

For large-scale purification conditions 30 mM NH<sub>4</sub>Cl and 1 mM Mg(OAc)<sub>2</sub> were chosen as the most optimal.

### Stepwise initiation complex assembling

According to Marina Rodnina's and Venki Ramakrishnan's articles we designed the experiments progression that is summarized in the scheme below.

Inspired by crystallography it was decided to add spermidine to stabilize rRNA.

All planned experiments presented in Scheme 58 below.

Scheme of stepwise assembling of initiation complex

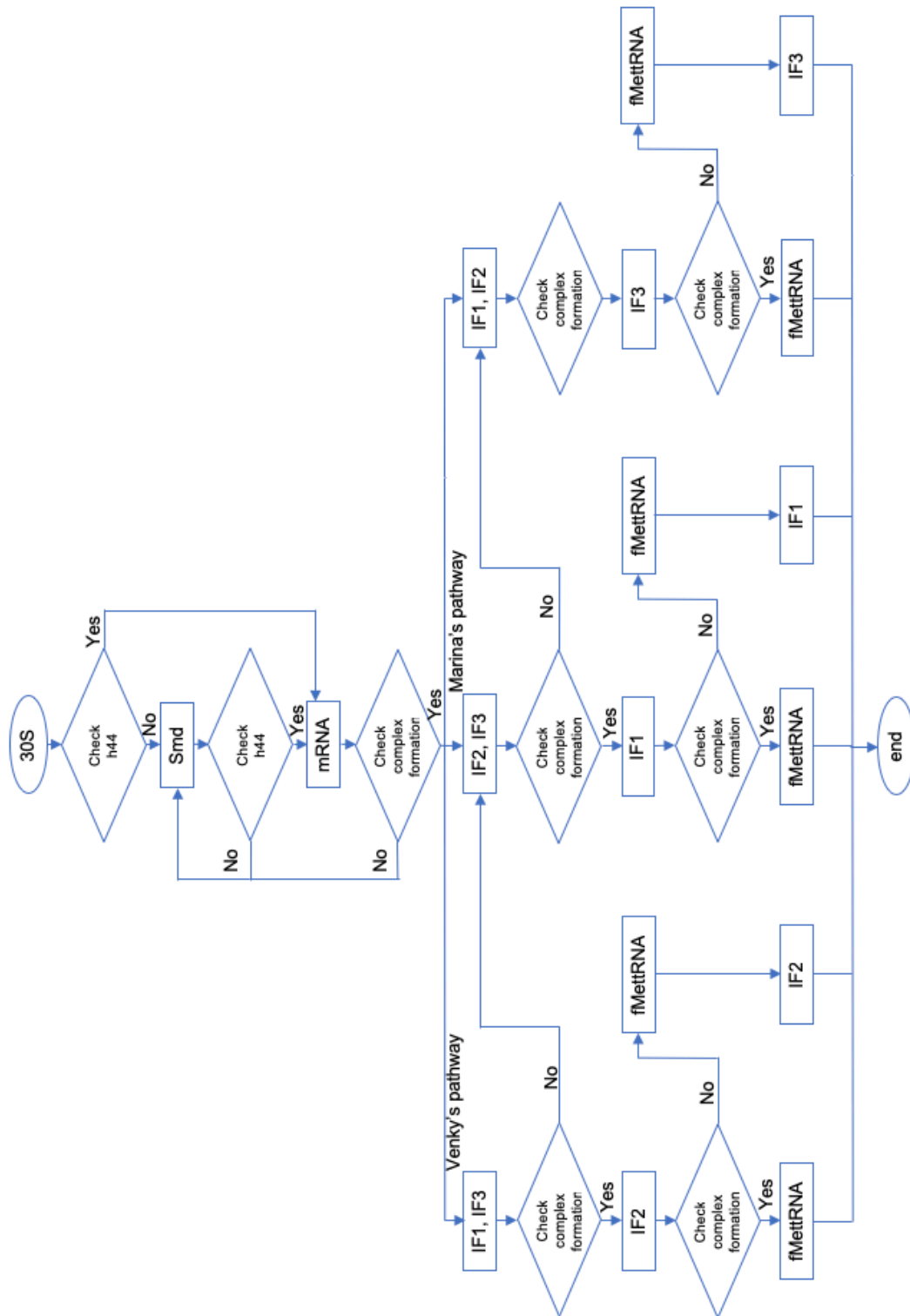
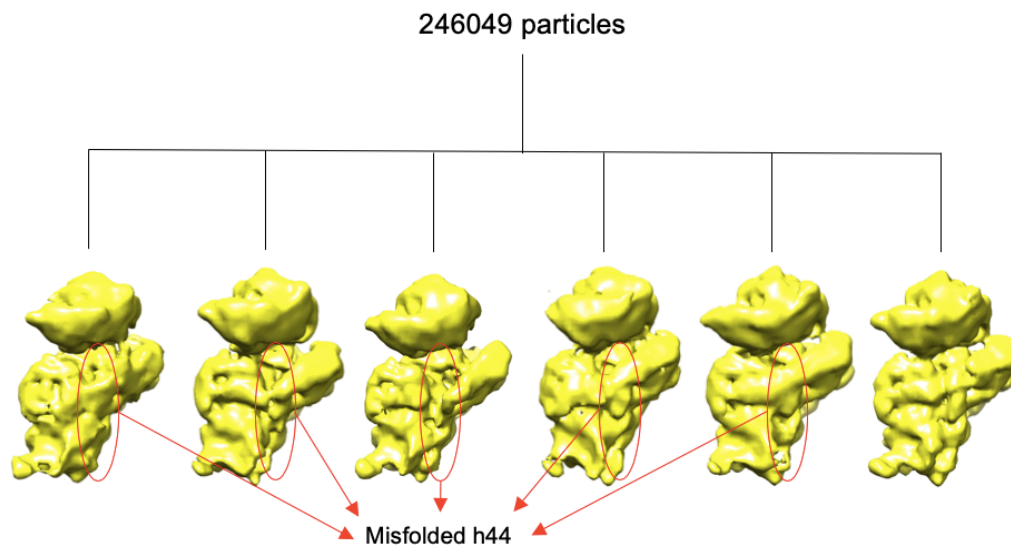


Figure 58. Scheme of stepwise assembling of initiation complex.

#### 4<sup>th</sup> data acquisition

After several hours of data collection on Talos microscope, the preliminary structure of the small ribosomal subunit (30S) was obtained at 10 Å. In five classes the flexibility of helix 44 was still observed (Fig. 59).



**Figure 59.** Structures obtained after 4th data collection: 30S without spermidine.

The flexible h44 was stabilized by adding spermidine at 2,5 mM concentration. The structure was processed in one class, no rRNA flexibility was observed (Fig. 60).

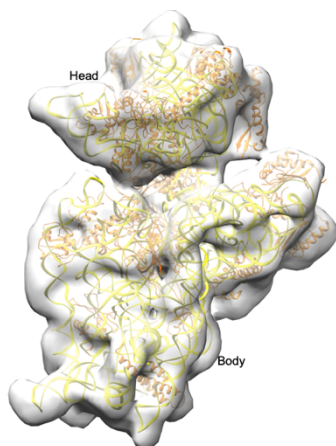


**Figure 60.** Structure obtained after 4th data collection: 30S with spermidine (35146 particles). The atomic model was taken from Khusainov et al., 2016 (5LI0, rRNA is in yellow color, r-proteins are in orange).

## 5<sup>th</sup> data acquisition

The next step was the addition of spa mRNA to the previous conditions. Different head positions were observed with (Fig. 62) and without spermidine (Fig. 61). The 30S structure with spermidine in closed conformation was obtained at 4.39 Å after 2 hours of data collection on Talos microscope. Data was processed in one class with the CryoSparr software.

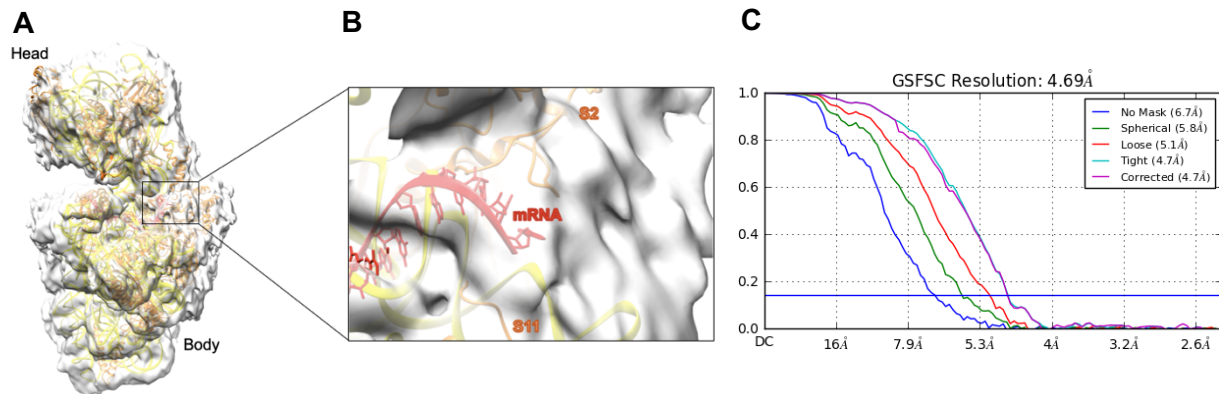


**Figure 61.** Structure obtained after 5th data collection (246049 particles):

- (A) cryo-EM reconstruction of 30S with mRNA without spermidine,
- (B) close-up view on the mRNA,
- (C) estimated resolution in CryoSparr software.

rRNA is highlighted in yellow, r-proteins are in orange, mRNA is in red colors (Khusainov et al., 2016, 5LI0).

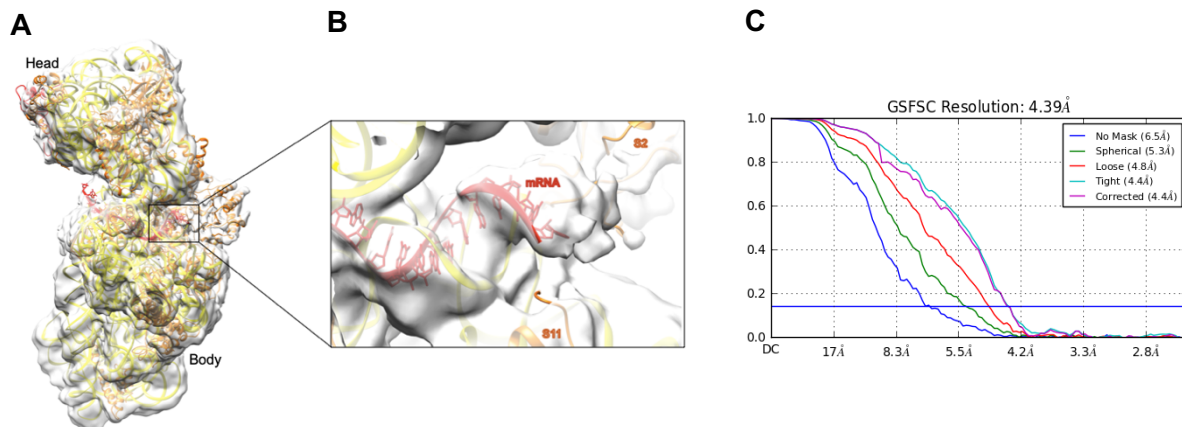


**Figure 62.** Cryo-EM reconstruction of 30S, mRNA and spermidine complex (A) with close-up view on the mRNA (B). The resolution was calculated in CryoSparr software (C). rRNA is highlighted in yellow, r-proteins are in orange, mRNA is in red colors (5LI0).

## 6<sup>th</sup> data acquisition

2 ways of sample incubation was checked: 1<sup>st</sup> sample was prepared by mixing 30S, mRNA, IF1 and IF3 at the same time and incubated at 37°C for 15 minutes (90131 particles)

(Fig. 63), 2<sup>nd</sup> sample was prepared by incubating 30S with mRNA at 37°C for 10 minutes and then with IF1 and IF3 for additional 5 minutes (340416 particles) (Fig. 64).

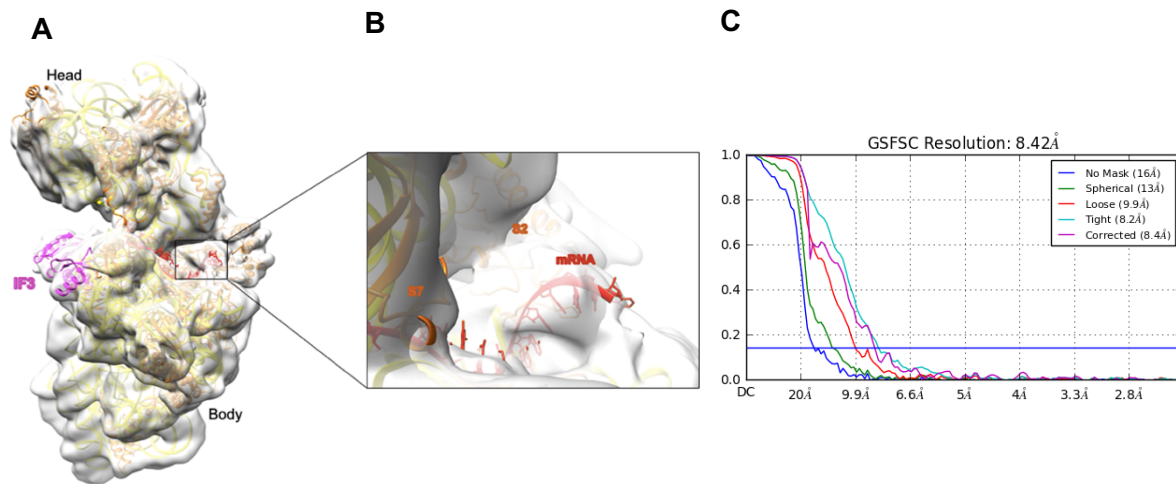


**Figure 63.** Structure obtained after 6<sup>th</sup> data acquisition:

(A) 30S with mRNA, IF1 and IF3 complex reconstruction (15 min incubation),

(B) close-up view on mRNA,

(C) the estimated resolution in CryoSparc software.

rRNA is highlighted in yellow, r-proteins are in orange, mRNA is in red and IF3 is in pink color (5LI0). IF1 was not detected.

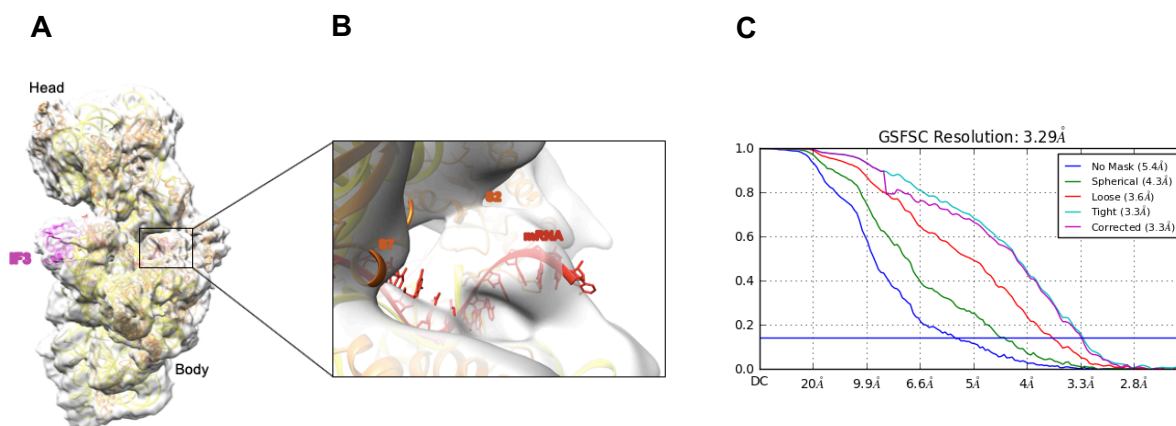


**Figure 64.** Structure obtained after 6<sup>th</sup> data acquisition:

(A) 30S with mRNA, IF1 and IF3 complex reconstruction (stepwise incubation),

(B) close-up view on mRNA,

(C) the estimated resolution in CryoSparc software.

rRNA is highlighted in yellow, r-proteins are in orange, mRNA is in red and IF3 is in pink color (5LI0). IF1 was not detected.

## 7<sup>th</sup> data acquisition

Next, it was decided to add stepwise the remaining components of the initiation complex. Variations of the prepared complexes are described below in the Table 9. Initially, 30S with mRNA was incubated at 37 °C for 5 min and then the rest components were added without incubation as described in Hussain *et al* and Milon *et al* articles.

**Table 9.** Variations of prepared complexes collected on Talos microscope and processed with Cryosparc software.

	1 complex	2 complex	3 complex	4 complex	5 complex
30S	+	+	+	+	+
mRNA	+	+	+	+	+
IF1	+			+	+
IF2		+	+	+	+
IF3	+	+	+	+	+
fMet-tRNA <sup>fMet</sup>	+		+		+

Unfortunately, the presence of 1 and 2 factors was not detected in any complex while IF3 was found in each complex (Fig. 65, 66, 67, 68 and 69).

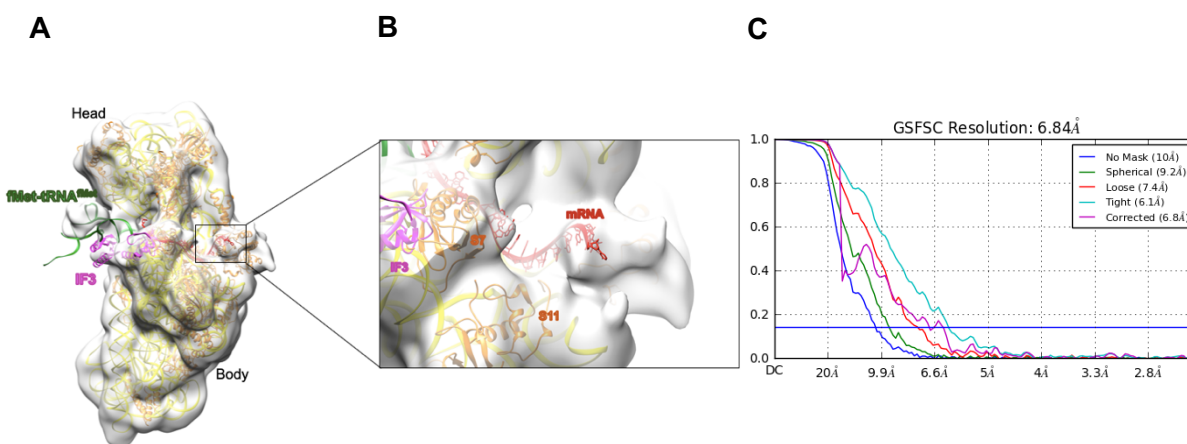


**Figure 65.** Structure obtained after 6th data collection: 30S with mRNA, fMet-tRNA<sup>fMet</sup> and IF3 complex reconstruction (A) with the close-up view on mRNA (B). IF1 was not detected (complex 1). rRNA is highlighted in yellow, r-proteins are in orange, mRNA is in red, IF3 is in pink and fMet-tRNA<sup>fMet</sup> is in green colors (5LI0, 124344 particles). The estimated resolution in CryoSparc was 6.8 Å (C).

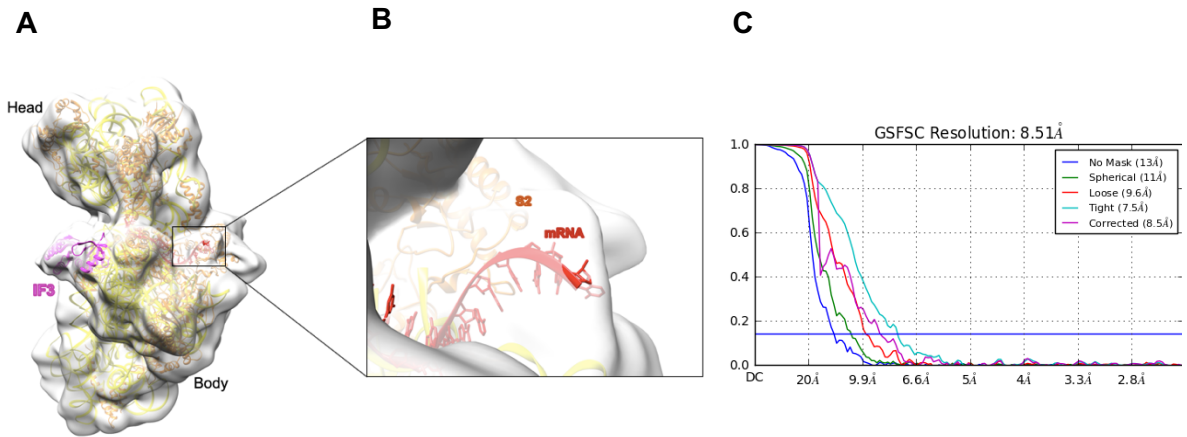


**Figure 66.** Cryo-EM reconstruction of 30S with mRNA and IF3 complex (A) with a close-up view on mRNA (B) at 8.5 Å (C). IF2 was not detected (complex 2). rRNA is highlighted in yellow, r-proteins are in orange, mRNA is in red and IF3 is in pink colors (5LI0, 107292 particles).

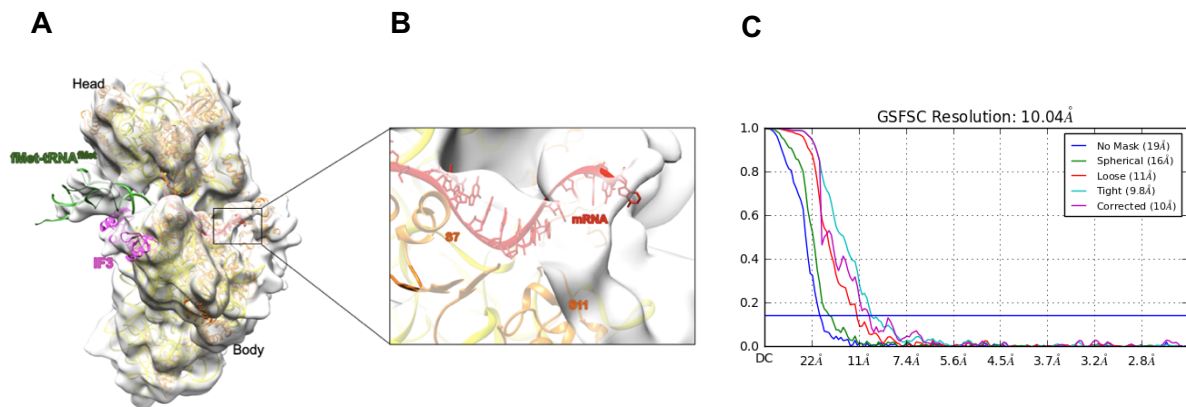


**Figure 67.** Structure obtained after 6th data collection: 30S with mRNA, fMet-tRNA<sup>fMet</sup> and IF3 (A) with close-up view on mRNA (B). IF2 was not detected (complex 3). rRNA is highlighted in yellow, r-proteins are in orange, mRNA is in red, IF3 is in pink and fMet-tRNA<sup>fMet</sup> is in green colors (5LI0, 90598 particles). The resolution was calculated in CryoSPARC software (C).

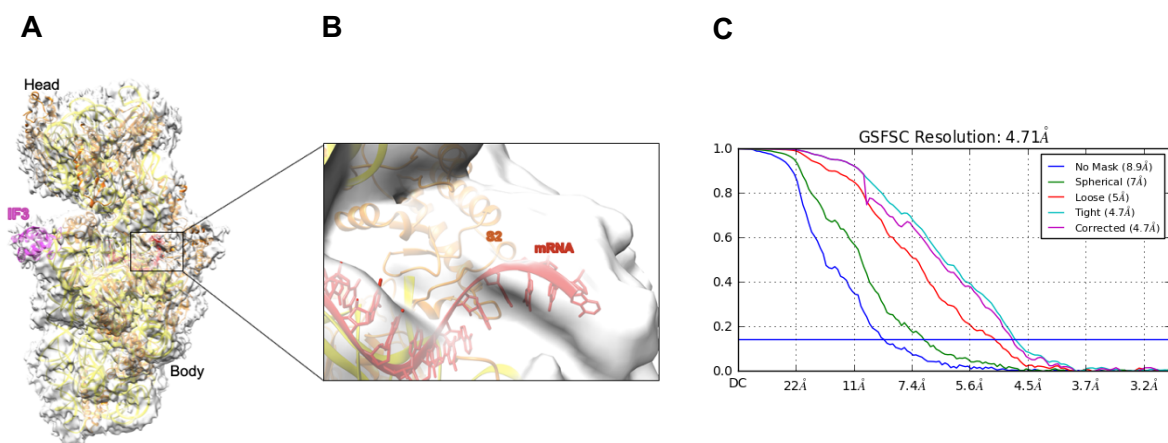


**Figure 68.** Structure obtained after 6th data collection: 30S with mRNA and IF3 (A) with close-up view on mRNA (B) at 4.7 Å (C). IF1 and IF2 were not detected (complex 4). rRNA is highlighted in yellow, r-proteins are in orange, mRNA is in red and IF3 is in pink colors (5LI0, 136627 particles).

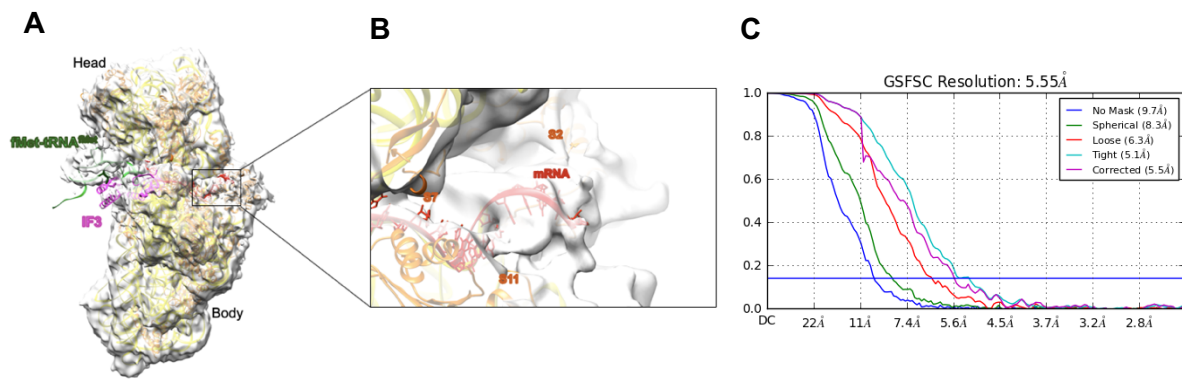


**Figure 69.** Structure obtained after 6th data collection: 30S with mRNA, fMet-tRNA<sup>fMet</sup> and IF3 (A) with close-up view on mRNA (B). IF1 and IF2 were not detected (complex 5). rRNA is highlighted in yellow, r-proteins are in orange, mRNA is in red, IF3 is in pink and fMet-tRNA<sup>fMet</sup> is in green colors (5LI0, 279232 particles). The resolution was estimated in CryoSparc software (C).

All obtained results are summarized and presented in Scheme 70.

Scheme of stepwise assembling of initiation complex

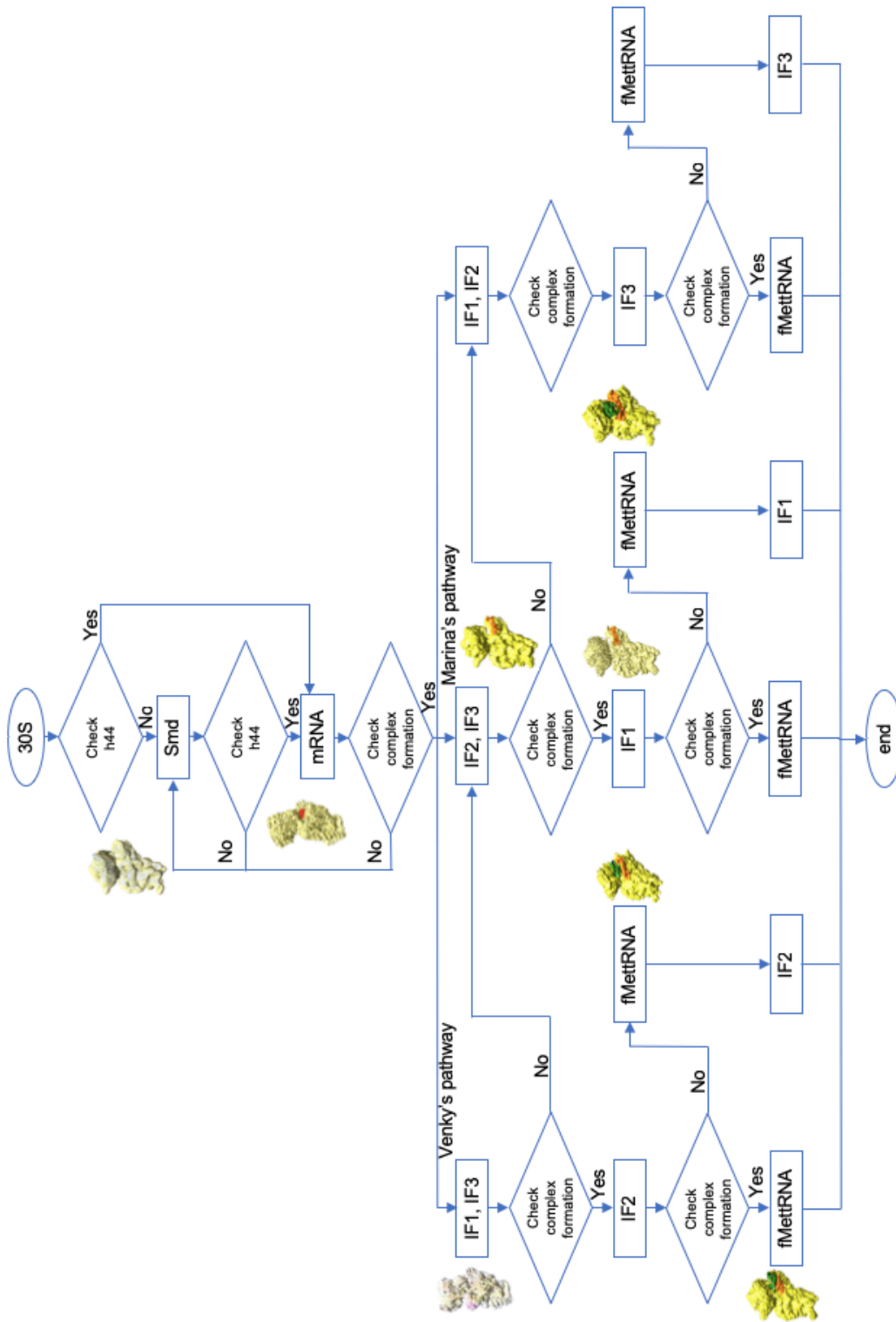


Figure 70. Scheme of stepwise assembling of initiation complex

---

## Ex vivo experiments

---

To obtain the initiation complex close to natural conditions, there is a method whose idea is to prevent the binding of subunits by decreasing the magnesium concentration with a non-hydrolysable GTP analog. Non-hydrolysable analogues of GTP, that irreversibly activates G proteins, are guanyl-5'-imidodiphosphate (GMPPNP) and 5'-guanosine-methylene-triphosphate (GMPPCP). GMPPNP and GMPPCP are synthetically prepared analogs where one of the oxygen atoms is replaced with amine or methylene groups. These components perform the functions of preventing GTP hydrolysis and large subunit joining to the initiation complex, as well as stalling of GTP-dependent complexes. This method has been used on mammalian cells and on kinetoplastids (Anthony and Merrick, 1992, Hershey and Monro, 1966, Gray and Hentze, 1994, Simonetti et al., 2016). A similar experiment with some adaptations for *S. aureus* is described below.

The *S. aureus* cell extract treated or not with GMP-PNP were fractionated by sucrose density gradients (Fig. 71) and then the obtained fractions were centrifuged in order to concentrate the sample. In order to do not inhibit the dissociation by spermidine (Umekage and Ueda, 2006) its concentration was reduced to 0.25 mM. Further, the sample was resuspended in buffer with 30 mM NH<sub>4</sub>Cl, 5 mM Mg(OAc)<sub>2</sub> and 10 mM Hepes-KOH pH 7.5 and then analyzed on SDS-PAGE (Fig. 72) and on native agarose gel (Fig. 73).

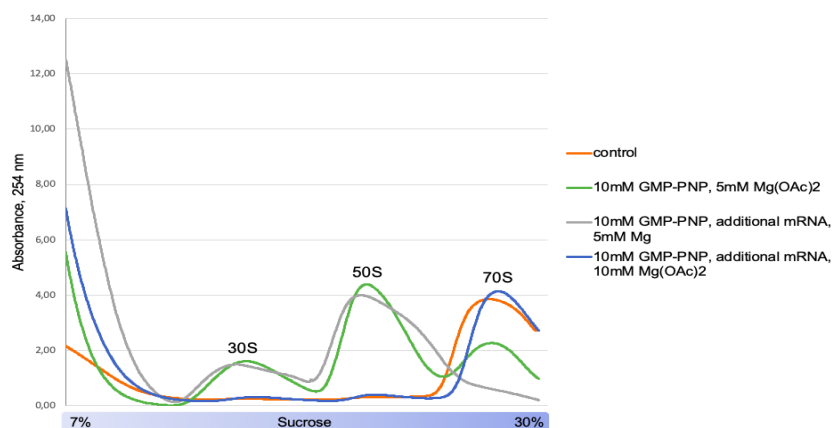


**Figure 71.** Sucrose gradient profile. The control (without GMP-PNP and mRNA, with 5 mM Mg(OAc)<sub>2</sub>) is shown by the orange line (I gradient). The sample with 10 mM GMP-PNP and 5 mM Mg(OAc)<sub>2</sub> is shown in green line (II gradient). The sample with previous conditions and additional mRNA is shown in grey line (III gradient). The sample with 10 mM GMP-PNP, additional mRNA and 10 mM Mg(OAc)<sub>2</sub> is shown in blue line (IV gradient).

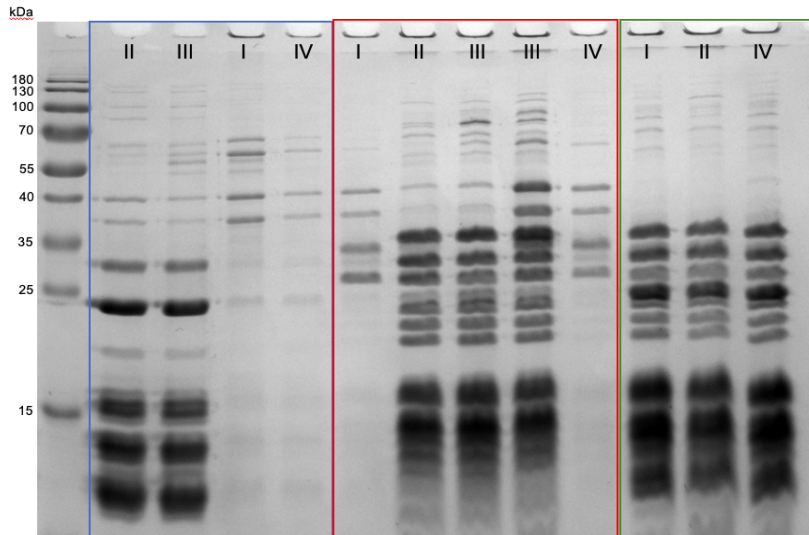


**Figure 72.** 15% polyacrylamide gel: 30S colored in blue, 50S - in red, 70S - in green. Roman numerals indicate the gradient number from Figure 58. On some lines, the sample is almost absent due to the low initial concentration. Some samples were concentrated with acetone that explains the waviness of some bands.

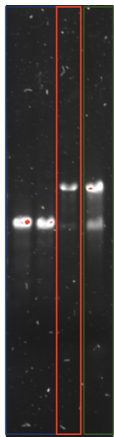


**Figure 73.** Agarose gel in native conditions of samples from III gradient (with 10 mM GMP-PNP, 5 mM  $Mg(OAc)_2$  and additional mRNA). First 2 lanes correspond to the 1<sup>st</sup> peak (blue), third lane – to the second peak (red) and the last lane – to the third peak (blue). The upper and lower bands correspond to 50S and 30S subunits respectively.

## 7<sup>th</sup> data acquisition

Then the sample was collected on Talos microscope and processed with Relion software. Unfortunately, all the particles had a flexible helix 44 (Fig. 74).

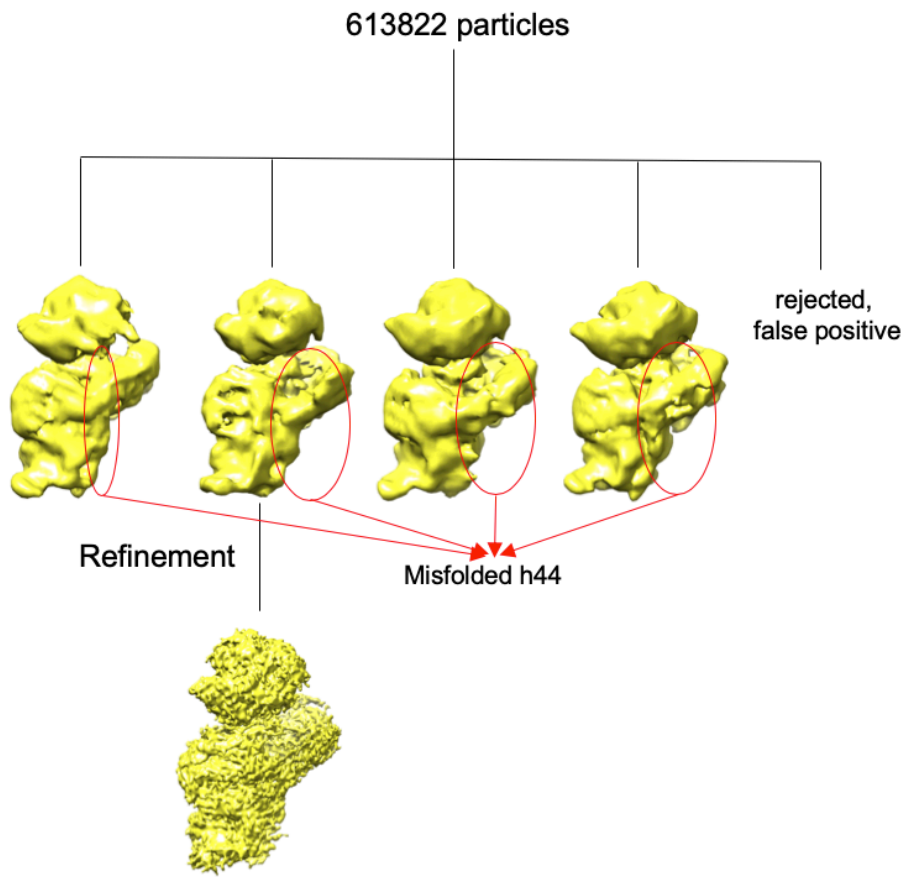


**Figure 74.** Structure obtained after 7th data collection. The ribosome was purified from cell extract with addition of GMP-PNP.

## DISCUSSION

Protein synthesis is a fundamental process found in all living cells. Despite very high conservation of these processes within bacteria, many species-specific features in the structures of ribosomes and translation factors in different species exist. In our studies, we focused on the initiation step as it is a fundamental rate-limiting and tightly controlled stage and is a target of various regulatory mechanisms.

According to recent studies, significant differences between gram-positive (*S. aureus* and *B. subtilis*) and gram-negative (*T. thermophilus* and *E. coli*) bacteria were observed. These peculiarities are primarily related to the ribosome structure. One of the most interesting examples is the *S. aureus* ribosome and its extension of helix 26 that binds close to the Shine-Dalgarno (SD) region and its involvement in forming 100S inactive dimers. Dimers are formed in response to stressful conditions for the protection and storage state. The process itself is called the ribosome hibernation. In *S. aureus*, it was shown that only one long HPF (long hibernation promoting factor) protein is involved in this process, while in *E. coli* bacteria three proteins are involved in this process: YfiA, RMF (ribosome modulation factor) and short HPF (Khusainov et al., 2017, Polikanov et al., 2012). Another feature of *S. aureus* ribosomes is the absence of S1 protein, which in gram-negative bacteria unfolds the highly structured mRNA for the proper accommodation on the 30S ribosomal subunit during the translation initiation stage (Khusainov et al., 2016, Duval et al., 2013). S1 protein is the largest and the most acidic ribosomal protein. In *S. aureus*, S1 loses the domains responsible for binding to the ribosome. Using different protocols of ribosome purification in high and low salt conditions, S1 protein was not detected in any case. In addition, this protein was also absent in the structure of *S. aureus* 100S dimers, in contrast to gram-negative bacteria (Beckert et al. 2018).

Toeprinting assay was performed in order to obtain the maximum amount of initiation complex and to choose more accurately the IF3 concentration, which causes dissociation of fMet-tRNA<sup>fMet</sup> from the initiation complex (Milon et al., 2007). Toeprinting method was chosen because it requires a very small amount of sample obtained from *S. aureus*. Due to the need to use *E. coli* components, “in vitro translation” method was less preferred. The other methods like isothermal titration calorimetry and filter-binding assay require a lot of material and in the case of the second one require also radioactive tRNAs. Initiation factor 1 activity was checked together with initiation factor 2 (IF2) as it promotes the binding of IF2 to the 30S (Stringer et al., 1977, Weiel and Hershey, 1982, Celano et al., 1988). It was shown that IF2

promotes the binding of fMet-tRNA<sup>fmet</sup> to the 30S (Lockwood et al., 1971, Majumdar et al., 1976, Sundari et al., 1976, La Teana et al., 1996). Its activity was tested by increasing IF2 concentration with fixed concentration of fMet-tRNA<sup>fmet</sup>. The optimal ratio of IF1 and IF2 to the 30S was found and corresponds to 3:1 proteins concentration to the ribosome concentration. The idea of checking the initiation factor 3 (IF3) activity by toe-printing assay was taken from the article Hartz et al., that was published in 1990. For their experiments, they used 3 types of tRNAs (methionine, cysteine and phenylalanine). They observed that IF3 has a specific function in the recognition of the methionine tRNA. It was shown that with the fully active IF3 the toe-print signals of other tRNAs disappeared. The same kind of experiment was performed and the best concentration of IF3 was found to be twice the ribosome concentration. The obtained results correspond to the literature data used for the initiation complex formation (Simonetti et al., 2008).

The negative stain electron microscopy (EM) was performed to find the optimal sample concentration for cryo-EM. Then the initiation complex was prepared and applied to the cryo-EM grids. The data was collected on the Titan microscope and processed in Scipion software package that includes Relion application for the 2D and 3D classification. As a result of data processing, one class with invisible 30S head was observed and in other classes the helix 44 was very flexible. After the salt conditions screening, it was possible to slightly increase the number of particles with proper conformation of the helix 44. The complex of the 30S with mRNA, fMet-tRNA<sup>fmet</sup> and IF2 was also obtained at 10 Å. However, in most cases the structure was unstable. The next data acquisition was performed with the fresh 30S preparation, which again slightly improved the number of good particles. Three low-resolution structures were obtained with IF2 and IF3 in two different conformations. Further changes in the protocol such as low salt concentration and addition of polyamines led us to obtain the ribosome with a stable conformation of the helix 44. It is known that polyamines or Mg<sup>2+</sup> ions are neutralizing the negative charge of the phosphate-sugar backbone, thus increasing the structural stability (Tabor, 1962, Sakai and Cohen, 1976). The binding sites of putrescine with a small ribosomal subunit were shown close to helix 44 (Noeske et al., 2015, Fig. 75). It can be assumed that spermidine may replace it and bind on the same place.

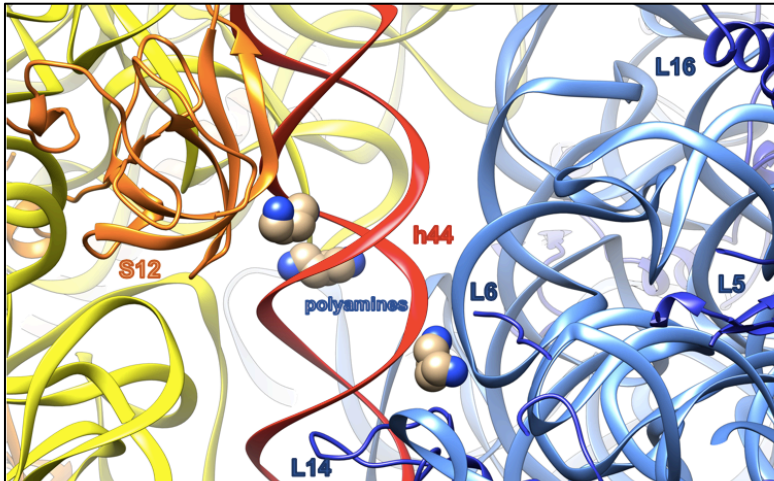


**Figure 75.** Atomic model of *E. coli* ribosome (Noeske et al., 2015, 4YBB): rRNA is in light grey, 30S proteins are in blue, 50S proteins are in red. Helix 44 highlighted in yellow, putrescine compound is shown in sphere shape.

Another interesting result is associated with 30S head conformation. It was observed that without adding spermidine during the ribosome or complex preparation the head conformation was open, while with spermidine it was closed allowing mRNA to properly accommodate inside the channel. This may also prove the need to add polyamines to the sample for the rRNA stabilization. The comparison of structures is shown in figures 76 and 77.

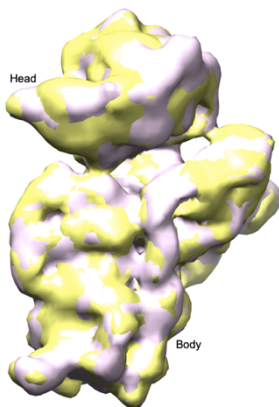


**Figure 76.** Comparison of two 30S structures: without spermidine in yellow and with spermidine in light magenta colors.

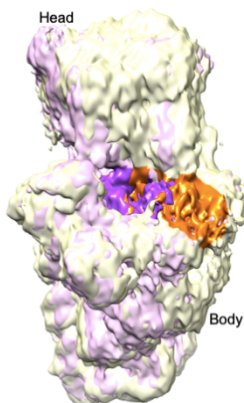


**Figure 77.** Comparison of two 30S with mRNA structures: without spermidine in yellow and with spermidine in light magenta colors. The mRNA region is stained darker than 30S.

In our later attempts, after we have started supplementing our complexes with spermidine in order to stabilize the rRNA, only the structure with the IF3 was obtained, IF1 and IF2 were absent in the structure. This can be explained by the addition of spermidine that may impact the IFs binding. Another hypothesis is the requirement of an additional factor/component for the proper complex formation. For this purpose, the experimental strategy was changed to the method closer to natural conditions. It was found that the effect of the ribosome separation into subunits by GMP-PNP depends on the magnesium concentration. By doubling the concentration of magnesium, the reaction was completely inhibited. Also, by adding additional mRNA double peak occurs, which may indicate the appearance of 30S complexes. This effect is still not clear. Additional experiments are required.

At high concentrations of spermidine, like 2 mM, the separation of ribosomal subunits can be inhibited (Umekage and Ueda, 2006). Thus, for the aforementioned *ex vivo* experiments, the spermidine concentration was 10 times less than was used before. Unfortunately, the obtained structures of 30S demonstrate the need to select concentration of polyamines more accurately.

The effect of the incubation time of the complex on its formation was also investigated. It was found that the stepwise complex assembly with the minimal incubation of factors is more preferable (Fig. 78).

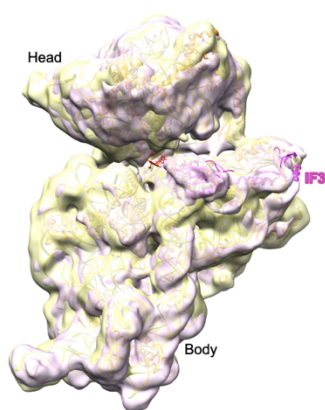


**Figure 78.** Comparison of two 30S with mRNA and IF3 structures: 15 minutes incubation of all components at once is in yellow and stepwise complex assembling in light magenta colors.

Comparing the two structures of 30S-mRNA with and without IF3, no difference in 30S-head conformation were observed (Fig. 79).

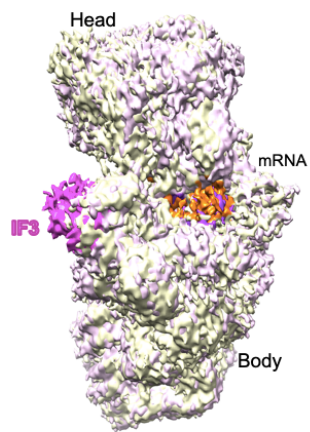


**Figure 79.** Comparison of two 30S-mRNA structures: without IF3 is in yellow and with IF3 in light magenta colors.

## PERSPECTIVES

The work described in this manuscript is only the first step in understanding how the initiation process in *Staphylococcus aureus* occurs.

Two pathways of stepwise assembling of initiation complex described in the literature may be related to species-specific features (Hussain et al., 2016, Milon et al., 2012). It can be assumed that in some bacterial species (*E. coli*) with long N-domain of IF2, the binding of IF1 or IF2 depends on their mutual presence, while in other species (*Th. thermophilus*) initiation factors can bind independently. This can lead to different species-specific pathways of protein binding to the ribosome. Further research is required in order to confirm or refute this hypothesis.

It is absolutely imperative to complete *ex vivo* experiments that could clarify the mechanism of the initiation process in *S. aureus*. Also, using this method, it is possible that additional factor/component could be found for the proper initiation complex formation.

Another interesting feature of *S. aureus* is the presence of virulent RNAs, which can affect the initiation stage. The study of this process can have not only theoretical, but also practical significance, because virulent RNAs participate in the biofilm's formation, which complicates the treatment of diseases caused by this bacterium.

All the results obtained in this work will help to describe the initiation process in *S. aureus* and the gained knowledge will be used to develop compounds against pathogenic bacterium.

## CONCLUDING REMARKS

Nowadays, studies of translation process in pathogenic bacteria have not only theoretical, but also practical significance. One example of pathogenic bacterium is *Staphylococcus aureus* that is responsible for severe nosocomial and community-acquired infections. The diseases caused by this bacterium include pneumonia, meningitis, endocarditis, osteomyelitis, septic arthritis and infections of bones and organs. Certain strains of *S. aureus* produce the superantigen TSST-1, which is responsible for the toxic shock syndrome (TSS). As a result, mortality rates are very high; death can occur within two hours. (Chen et al., 2007).

Also, this bacterium is highly resistant to most commonly used antibiotics. In 2014, a report came out from the World Health Organization that the antibiotic resistance is no longer a prediction for the future, the disease may appear now in every region of the world and has the potential to affect anyone, of any age, in any country. Antibiotic resistance is now a major threat to public health.

At the moment, study of protein synthesis from human pathogen *S. aureus* is a hot topic. The first ribosome structure from *S. aureus* was published only three years ago (Khusainov et al., 2016). Moreover, not only the ribosome is an interesting object to study. The initiation process as a rate limiting stage is also necessary to study. Despite all the difficulties that I have encountered, significant progress in the investigation of the initiation process was achieved.

The work described in this manuscript is only the initial step of studying the initiation process in *S. aureus*. The knowledge gained during my work will be used for further research. The obtained results may also be used in the future to fight against this bacterium.

## RESEARCH PROJECT 2

---

### **Structure determination of *Candida albicans* ribosome**

# MATERIALS AND METHODS

## 80S PURIFICATION

Purification, crystallization and post crystallization treatment of 80S from *C. albicans* were performed according to a similar protocol described for *S. cerevisiae* with some adaptations (Ben-Shem *et al.*, 2010).

Buffers were used during the experiment:

Buffer M:

30 mM Hepes-KOH pH 7,5

50 mM KCl

10 mM MgCl<sub>2</sub>

8,5% Mannitol w/v

0,5 mM EDTA

2 mM DTT

Buffer G:

10 mM Hepes-KOH pH 7,5

50 mM KOAc

10 mM NH<sub>4</sub>Cl

5mM Mg(OAc)<sub>2</sub>

2 mM DTT

### Cell growth

*The C. albicans SC5314 strain is a wild type strain isolated from a patient with a generalized infection. It was provided by Dr. Sadri Znaidi (Institut Pasteur, Paris, France) (Gillum et al., 1984).*

All manipulations with the cells were performed in a specially equipped laboratory with a safety level of 2. Cells were grown in a standard Yeast Extract Peptone Dextrose Agar (YPD) medium at 30 °C till OD<sub>600</sub> = 1 and further subjected to glucose starvation. This step is needed to homogenize the ribosomes and reversibly induce translation inhibition. After cells centrifugation, the pellet was resuspended in buffer M.

## Lysis

5 grams of cells obtained from 4 liters of culture were resuspended in buffer M with protease inhibitor cocktail (Roche), RNasin (Promega), Pefabloc (Roche), heparin (Sigma-Aldrich) and DTT. Heparin acts on the solubility of ribosomes which affects the amount of PEG used in subsequent steps. The cells were lysed by vortexing with glass beads and were centrifuged at 13000 rpm for 2 min and then 16000 rpm for 9 min using JA 25.50 rotor.

## PEG precipitation

PEG20K 30% w/v (Hampton research) was added to the supernatant to final concentration 4.5% w/v and then was centrifuged at 20000 g for 5 minutes to precipitate anything heavier than the ribosome. The concentration of KCl was adjusted till 130 mM. The PEG concentration was increased till 8.5% w/v and was centrifuged at 20000 g for 10 minutes to precipitate ribosomes. Then, the concentration of KCl in buffer M was changed to 150 mM and protease inhibitors, DTT and heparin were additionally added.

## Sucrose density gradient centrifugation

The ribosomes were loaded on a 10-30% w/v sucrose gradients and was centrifuged at 18000 rpm for 15 hours using Beckman SW28 swinging rotor (Fig. 80). The appropriate fractions were pooled and concentrations of MgCl<sub>2</sub> and KCl were adjusted to 10 mM and 150 mM respectively.

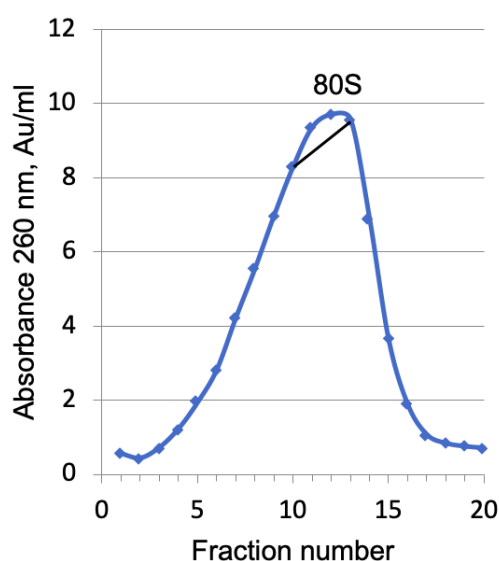


**Figure 80.** Sucrose gradient profile of *C. albicans* ribosome. The black line indicates pooled 80S fractions.

## Last PEG precipitation

The PEG20K was added till the final concentration 6.9% w/v to precipitate ribosomes and the sample was centrifuged at 20000 g for 10 min. The pellet was gently resuspended in buffer G to obtain the final concentration 23 mg/ml. The sample was frozen in liquid nitrogen and stored at -80 °C.

## X-RAY CRYSTALLOGRAPHY

The other technique I would like to present is X-ray crystallography, because of its relevance to a part of my thesis work. X-ray crystallography is a method that allows the structural determination of macromolecular complexes.

Wilhelm Röntgen discovered the X-ray in 1895. In 1912, Paul Peter Ewald and Max von Laue had the idea that crystals could be used as a diffraction grating for X-rays. Later, Max von Laue proposed a law that relates the scattering angles and the size and orientation of the distances between unit cells in a crystal, for which he was awarded the Nobel Prize in Physics in 1914.

In the 1980s, the large ribosomal subunit (LSU) was first crystallized by the Ada Yonath's in collaboration with Gunter Witmann (Yonath et al., 1980). The high-resolution structure of 50S was obtained by Nenad Ban in Thomas Steiz laboratory (Ban et al., 2000). The first structures of the complete ribosome, small ribosomal subunit (SSU) and its functional complexes from *Thermus thermophilus* were obtained by Marat Yusupov and Gulnara Yusupova in the laboratory of Harry Noller and in the laboratory of Venkatraman Ramakrishnan (Clemons et al., 1999, Yusupov et al., 2001, Yusupova et al., 2001). The structure of the ribosome with a resolution of 3.5 Å from *Escherichia coli* was determined in the laboratory of Jamie Cate (Schuwirth et al., 2005).

### Crystallization

The process of transition from liquid to solid crystalline state is called crystallization. The solid materials obtained during this process are called crystals. The crystallization process is characterized by the nucleation of the crystallite with its subsequent growth to a diffraction-quality crystal. The conditions under which the crystal(s) appeared did not always coincide with the conditions for their growth. The crystallographer's goal is to find those conditions under which one crystal with maximum size grows, since such crystals better diffract.

Figure 81 illustrates a phase diagram where solubility varies depending on the concentration of precipitant (e.g., polyethylene glycol (PEG) or salt). In the undersaturated region the crystals dissolve, while in the supersaturated region (metastable zone and labile zone) they grow. In practice, for the crystal formation, the protein concentration should exceed the solubility by at least three times. This is necessary to overcome the energy barrier that exists during crystal formation and represents the free energy needed to create a small cluster of proteins. In the “metastable zone”, the supersaturation is too small, the nucleation rate is low, and the crystals formation takes a sufficiently long period of time. In the adjacent “labile zone”, the supersaturation is large enough and spontaneous nucleation is observed. In the "precipitation zone" due to excessive supersaturation occurs aggregate formation and precipitation (Asherie, 2004).

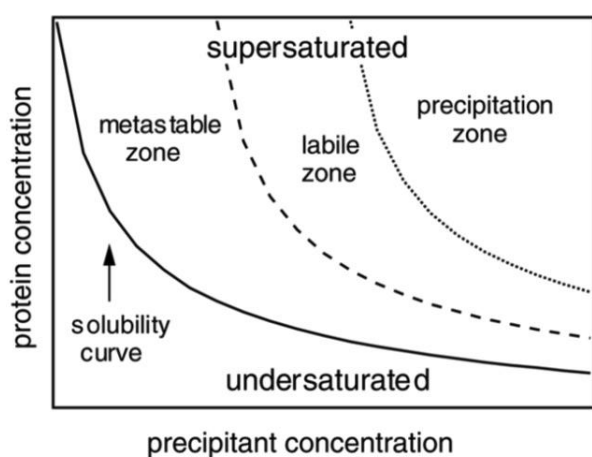


**Figure 81.** A schematic phase diagram showing the solubility of a protein in solution as a function of the concentration of the precipitant present (Asherie, 2004).

Many factors can influence the appearance and growth of crystals. Initially, a large search is carried out for optimal conditions with changes in physical and chemical parameters like changes in sample concentration, buffer components, pH, concentration of the precipitant and temperature conditions. All these manipulations can be carried out both manually and on specially designed robots.

### Overview of single-crystal X-ray diffraction

This technique has three main steps. The first step is to obtain sufficiently large crystals that are pure in composition and regular in structure. The second step is to place the crystal in an X-ray beam, producing a regular pattern of reflections. The intensities and directions of the diffracted X-rays are simultaneously recorded by the diffractometer. At the third stage, special algorithms are used to produce and refine the model of the arrangement of atoms within the

crystal. The refined structure is called the crystal structure and is usually stored in a public database (Fig. 82).

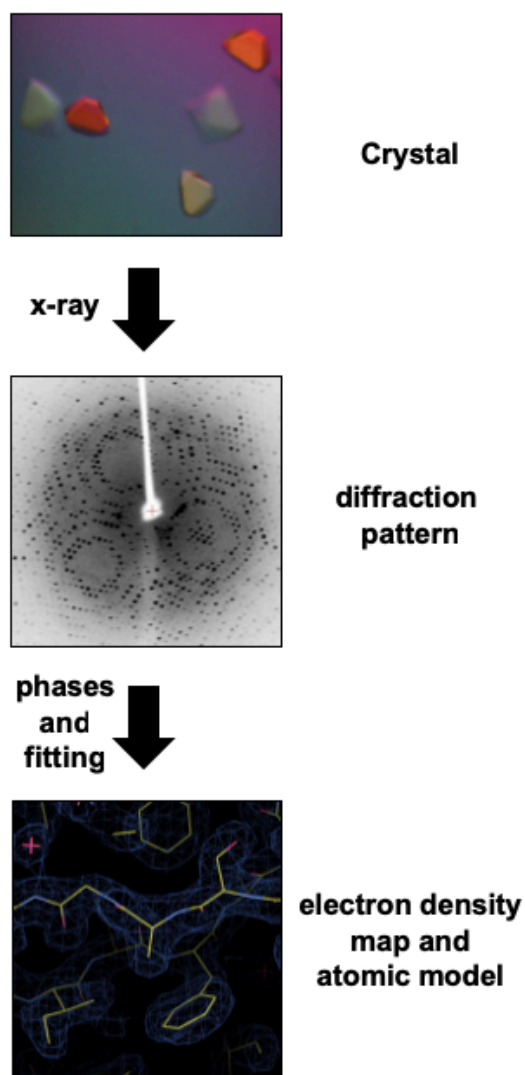


**Figure 82.** Schematic representation of diffraction experiment (From [www.imperial.ac.uk/x-ray-crystallography](http://www.imperial.ac.uk/x-ray-crystallography)).

### Resolution in X-ray crystallography

Resolution in X-ray crystallography is a physical parameter and is the distance from the center till the spot on the diffraction pattern. It is a more accurate parameter compared to electron microscopy.

## RESULTS

### One-dimensional PAGE

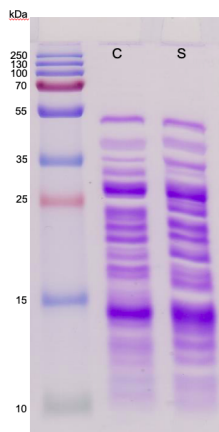


**Figure 83.** One-dimensional 15% PAGE of 80S from *C. albicans*(C) and *S. cerevisiae* (S).

Gel demonstrates the absence of high molecular weight non-ribosomal proteins (Fig. 83).

### Agarose gel in denaturing conditions

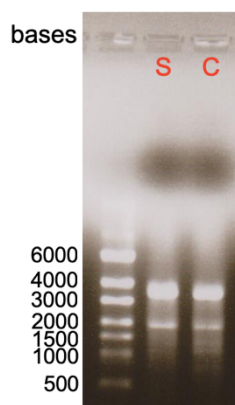


**Figure 84.** Agarose gel of 80S from *C. albicans*(C) and *S. cerevisiae* (S). The bands correspond to 25S (upper) and 18S (lower) rRNA.

Agarose gel demonstrates the absence of degradation of rRNA from *C. albicans* (Fig. 84).

### Mass spectrometry

The results from mass spectrometry analysis of 80S from *C. albicans* are summarized below (Table 10).

**Table 10.** List of proteins found in *C. albicans* 80S ribosome sample by LC-MS/MS analysis, where b - eukaryotic specific proteins, u - universal proteins.

Small ribosomal subunit				Large ribosomal subunit			
Protein	Score	MW	pI	Protein	Score	MW	pI
eS1_RPS1	240	29,0	10,04	uL1_RPL1	151	24,4	9,76
uS2-RPS0	180,5	28,7	4,91	uL2_RPL2	470	27,3	10,71
uS3_RPS3	331	27,3	9,23	uL3_RPL3	879	43,9	10,26
uS4_RPS9	148	21,7	10,20	uL4_RPL4	733	39,2	10,74
eS4_RPS4	190	29,4	10,15	uL5_RPL11	213	19,8	9,95
uS5_RPS2	156	26,9	10,24	uL6_RPL9	161	21,7	9,51
eS6_RPS6	233	27,1	10,15	eL6_RPL6	230	19,8	10,21
eS7_RPS7	283	21,2	9,92	eL8_RPL8	284	28,5	10,05
uS7_RPS5	285	25,2	8,7	uL10_RPP0	229	33,3	4,83
eS8_RPS8	332	22,7	11,09	uL11_RPL12	140	17,8	9,51
uS8_RPS22	201,5	14,8	9,88	uL13-RPL16	74	22,6	10,32
uS9_RPS16	137	15,7	10,29	eL13-RPL13	437	23,0	10,61
eS10_RPS10	94	13,8	9,83	eL14_RPL14	136	14,7	10,90

uS10_RPS20	123	13,3	9,94	uL14_RPL23	161	13,3	10,07
uS11_RPS14	168	14,0	10,90	eL15_RPL15	155	24,3	11,34
uS12_RPS23	183	16,0	10,81	uL15_RPL28	52	16,7	10,42
eS12_RPS12	105	15,7	4,70	uL16_RPL10	303	25,1	10,08
uS13_RPS18	162	17,0	10,35	eL18_RPL18	142	20,8	11,8
uS14_RPS29	13,8	6,6	9,76	uL18_RPL5	523	34,4	7,64
uS15_RPS13	118	16,9	10,23	eL19_RPL19	143	21,6	11,12
uS17_RPS11	81,44	17,6	10,43	eL20_RPL20	163	20,3	10,24
eS17_RPS17	163	15,7	10,46	eL21_RPL21	71	18,0	10,33
uS19_RPS15	154,5	15,9	10,32	eL22_RPL22	195	14,1	5,36
eS19_RPS19	229	16,1	9,42	uL22_RPL17	167	21,0	10,77
eS21_RPS21	140	9,6	8,15	uL23_RPL25	129	15,8	10,15
eS24_RPS24	129	15,5	10,87	eL24_RPL24	85	17,4	11,37
eS25_RPS25	74	11,6	10,15	uL24_RPL26	81	14,2	10,48
eS26_RPS26	52	13,6	10,89	eL27_RPL27	123	15,5	10,18
eS27_RPS27	11	9,0	8,73	uL29_RPL35	94	14,1	11,24

eS28_RPS28	51	7,5	10,36	eL30_RPL30	139	11,5	9,70
eS30_RPS30	52	7,1	11,47	uL30_RPL7	206	27,4	10,24
eS31_RPS31	29	16,8	10,48	eL31_RPL31	108	13,0	9,82
P1	22	10,7	4,02	eL32_RPL32	69	14,9	10,54
P2	98	10,9	3,93	eL33_RPL33	89	12,1	10,78
				eL34_RPL24	13	13,7	10,74
				eL36_RPL36	64	11,1	11,4
				eL37_RPL37	20	9,9	11,63
				eL38_RPL38	62,6	8,9	10,46
				eL40_RPL40	57	17,3	9,85
				eL42_RPL41	13	12,2	10,37
				eL43_RPL43	167	10,1	10,68

### **Analytical ultracentrifugation**

*Analytical ultracentrifugation is a method for the quantitative analysis of macromolecules in solution. The optical systems (absorbance and fluorescence) permit precise and selective observation of sedimentation in real time (Cole et al., 2008).*

The experiments were performed at 4 °C using Beckman XL-I analytical ultracentrifuge and Beckman An-50Ti rotor. Thawed ribosomes were diluted to 1 OD/ml (260 nm) and was

loaded into quartz cuvette. Scans were made every 4 min at 260 nm and 280 nm. The data analysis was done in Sednterp and Sedfit software.

After freezing the major part of the sample stays in 80S form. Also, a small amount of dimers is present in the sample (Fig. 85).

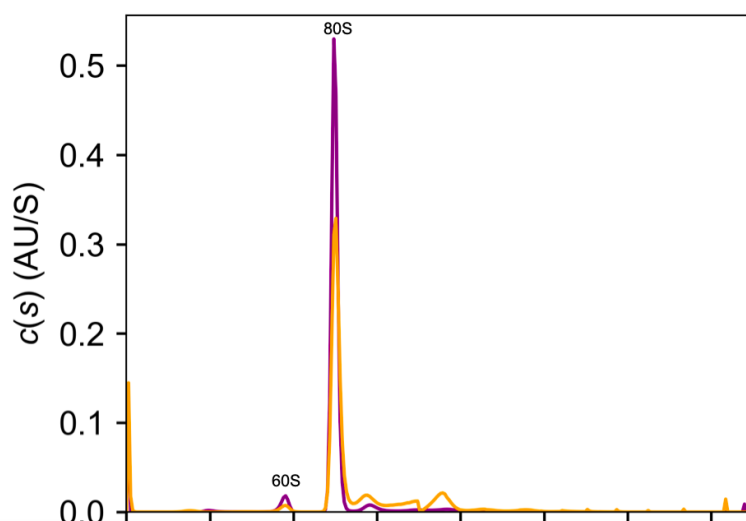


**Figure 85.** Comparison of sedimentation profiles of *C. albicans* ribosome (orange) and *S. cerevisiae* ribosome (purple).

## Crystallization

The initial conditions for crystallization were taken from the David Bruchlen's manuscript and were adapted over time to produce reproducible crystals. First screenings were carried out by the robot (Formulatrix, CBI, IGBMC) and then manually at 4 °C. All tried and tested conditions are summarized in Table 11 below.

**Table 11.** Summary of tried crystallization conditions.

Component	Concentration	Types		
		Tris	Bis-tris	
Buffers, pH 6.5 - 7.5	0 – 100 mM	Tris	Bis-tris	
Cations	0 – 600 mM	K <sup>+</sup>	NH <sub>4</sub> <sup>+</sup>	
Anions	0 – 600 mM	SCN <sup>-</sup>	Acetate <sup>-</sup>	

Magnesium	3 – 8 mM	MgOAc <sub>2</sub>		
Polyamines	0 – 8 mM	Spermidine	Spermidine	Putrescine
Precipitant	3,5 – 5%	PEG 20000		
Cryo-protective compound	2 – 40%	Glycerol		
	0,1 – 3%	Dioxane		
Detergent	2,8 mM	Deoxy Big Chap		

Other changes in crystallization conditions:

- ribosome concentration,
- volume of reservoir solution,
- ratio in the drop between sample and reservoir,
- hanging and sitting drops,
- sample incubation at 30 °C and at 37 °C
- crystallization temperature 4 °C and 20 °C.

The first crystal screenings on the robot did not lead to large crystals, so it was decided to change the crystallization parameters manually. It was found that the concentration of KSCN significantly affects the crystal shape and the volume of reservoir affects the size of crystal. Also, decrease of ribosome and spermidine concentrations directly affected on the crystal shape. As a result, the obtained crystals diffracted at 7 Å (Fig. 86).

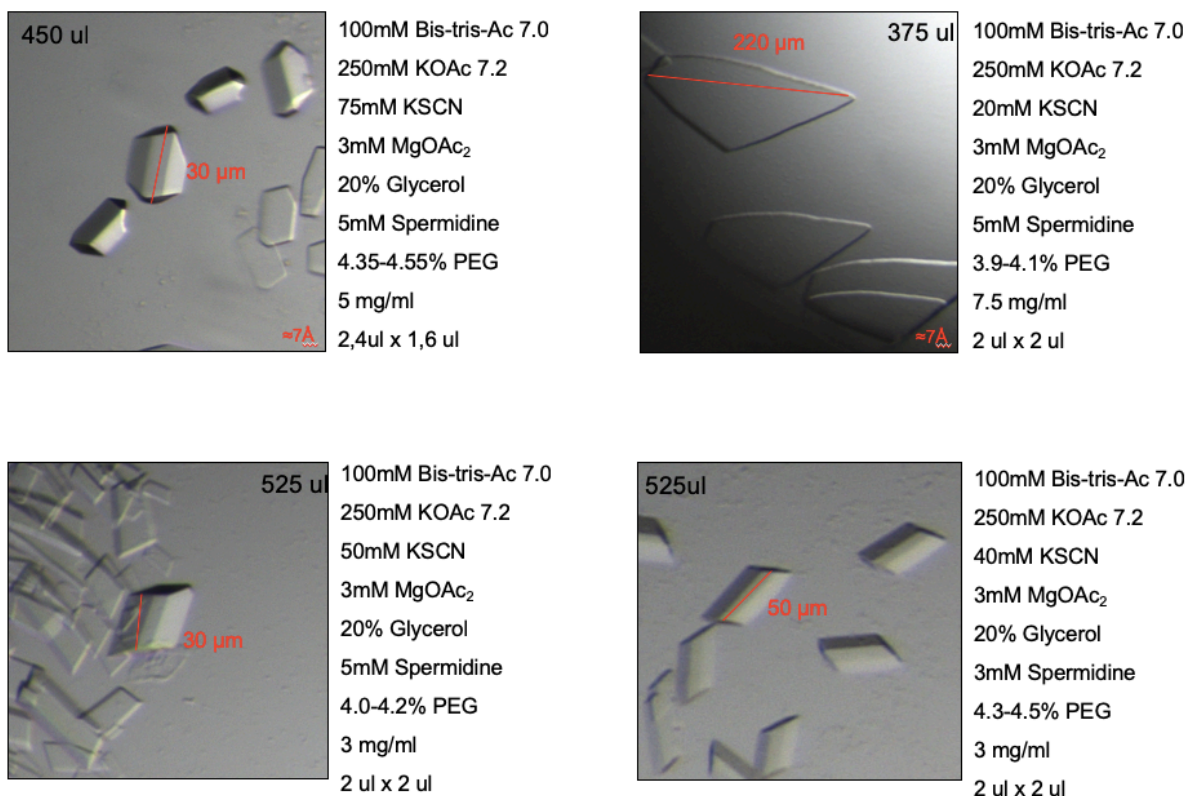


**Figure 86.** Crystals of 80S ribosome from *C. albicans*.

### Post-crystallization treatment

This stage is needed to improve the crystal stability and diffraction. For this purpose, the dehydration method was used. It is known that the reduction of the solvent content inside the crystal produces internal strengthening which can lead to an improvement in the diffraction limit. To achieve this goal, our laboratory uses a slow and stepwise increase of smaller PEG than 20K, depending on the type of which the cell parameter and the degree of conformational changes of the small ribosomal subunit can vary.

The post-crystallization treatment conditions were taken from David Bruchlen's manuscript to check the quality of crystals. Initially, the protocol was developed for *Saccharomyces cerevisiae* which was later adapted for cryoprotection of *Candida albicans*'s crystals.

The drop on cover slip was placed into a small Petri dish and the first buffer was replaced by the solution with slightly higher PEG 20K concentration (80 mM Bis-tris-Ac pH 7.0, 70 mM KSCN, 10 mM Mg(OAc)<sub>2</sub>, 20% v/v Glycerol, 5% w/v PEG 20K, 6.5 mM spermidine, 7.5 mM NH<sub>4</sub>OAc, 1.4 mM Deoxy Big Chap, 2 mM DTT). Then this solution was replaced

stepwise by solutions with increasing concentrations of PEG 6K till 20% after 5 steps (80 mM Tris-Acetate pH 7.0, 286 mM KOAc, 70 mM KSCN, 10 mM Mg(OAc)<sub>2</sub>, 18% v/v Glycerol, 5% w/v PEG 20K, 6.5 mM spermidine, 7.5 mM NH<sub>4</sub>OAc, 20% w/v PEG 6K, 2 mM DTT, without detergent). Final solution was replaced with the same solution supplemented with 2 mM osmium hexamine and the drop was kept in the Petri dish sealed with parafilm for 1 hour. The final scheme of treatment is described in Figure 87. Crystals were frozen and stored in liquid nitrogen until they shot on synchrotron.

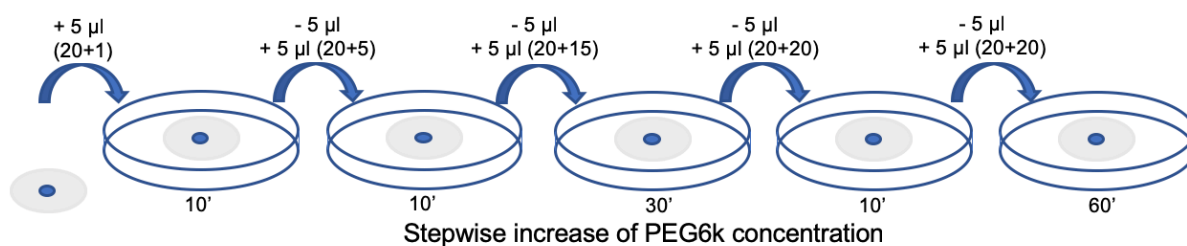


**Figure 87.** Scheme of post-crystallization treatment.

## DISCUSSION

Most antibiotics inhibit protein synthesis by binding to the ribosome, so it is necessary to know the ribosome structure for the correct understanding the mechanism of action of these compounds.

*Candida albicans* is a pathogenic yeast belonging to the Saccharomycetaceae family. The previous biochemical, structural and bioinformatics studies show a high level of structural similarity between 80S from *S. cerevisiae* and *C. albicans* (see Bruchlen's manuscript). In this regard, it was decided to use the cell growth and ribosome purification protocols developed for *S. cerevisiae* with some adaptations. After obtaining the good quality sample for 80S crystallization the protocol from *S. cerevisiae* were used (Ben Shem et al., 2011). However, the crystallization assays were unsuccessful using the related protocols from yeast, as no crystals were found in our drops. A large screening was carried out to determine the conditions for the appearance and growth of crystals. Subsequently, the crystallization conditions were changed to obtain better reproducibility. Several conditions were found under which the crystals diffracted at 6,5 - 7 Å.

It should be noted that the only successfully crystallized yeast ribosomes are vacant and do not contain any translation factors. However, these ribosomes are further stabilized by a non-ribosomal protein, a homologue of *stm1*, which occupies the mRNA tunnel in order to inhibit translation during the stress by glucose starvation (Ben Shem et al., 2011). This is another significant similarity between *S. cerevisiae* and *C. albicans* ribosomes.

## PERSPECTIVES

*Candida albicans* (*C. albicans*) is detected in the gastrointestinal tract and mouth in 40–60% of healthy adults (Kerawala et al., 2010), but despite this, mortality among patients with systemic candidiasis reaches 40% (Singh et al., 2017). Invasive candidiasis contracted in a hospital causes 2800 to 11200 deaths yearly in the USA (Pfaller et al., 2007). Nevertheless, these numbers may not truly reflect the true extent of damage this organism causes, given new studies indicating that *C. albicans* can cross the blood-brain barrier (Wu et al., 2019). Thus, there is a need to search for compounds effective against this pathogenic yeast.

Since most antibiotic targets are ribosomes, determining their structure is essential. After obtaining well-reproducible protocols for ribosome purification and crystallization, the next step is to improve diffraction of crystals.

At the same time, the predicted *C. albicans* ribosome structure allowed our collaborators to begin the development of species-specific compounds, which may be further used in *in vivo* studies. Before reaching the ribosome, the compounds must pass through the cell wall and plasma membrane. If at least one of the ribosomal inhibitors stops the growth of the strain, then it will be important to verify the non-toxicity of this molecule on human cells. This is a prerequisite for obtaining a new drug candidate, which will be a specific antifungal against *C. albicans*.

## CONCLUDING REMARKS

The structural studies of ribosome and its functional complexes are necessary and have a practical significance. Scientists from around the world are contributing to this challenge. They face the fact that not all ribosome structures have been resolved yet and, when working in this direction, they reveal many unexplored and essential features that require more detailed study. After stepwise solving every task, new important challenges arise.

The reproducible protocols are the small but significant step in ribosome structure determination from *C. albicans*. This structure will be further used to study the binding of new compounds to the *C. albicans* ribosome. To solve this problem, X-ray crystallography is the best suited. Bioinformatics data already allows our collaborators to begin the selection of new compounds specifically targets *C. albicans* ribosome, which will soon be used in our research.

# RESUME DE THESE EN FRANÇAIS

## Introduction

La synthèse des protéines est un processus hautement conservé dont le ribosome est l'acteur principal. Pendant de nombreuses années, le ribosome est resté l'un des objets de recherche les plus importants pour les scientifiques du monde entier. Les structures à haute résolution des ribosomes et de ses sous-unités obtenues par cristallographie et microscopie électronique ont révolutionné le domaine de la biologie structurale. Le ribosome est le site de synthèse de protéines, également appelé traduction. Ce processus peut être divisé en 4 étapes principales: l'initiation, l'élongation, la terminaison et le recyclage. L'étape d'initiation de la traduction est une étape limitante, impliquant l'action de nombreux composants finement régulés. De nombreux antibiotiques agissent précisément à ce stade de la synthèse des protéines. L'étape d'élongation est mieux conservée par rapport à l'initiation chez toutes les espèces et inclut la formation de la chaîne polypeptidique. Les étapes de terminaison et de recyclage sont accompagnées de la libération de la chaîne polypeptidique et de la dissociation de tous les composants de la traduction.

### *Projet de recherche 1*

La traduction chez les procaryotes a été principalement étudiée sur le modèle de bactéries gram-négatives telles qu'*Escherichia coli* (*E. coli*) et *Thermus thermophilus*. Cependant, des études récentes ont montré des différences significatives au niveau de l'étape d'initiation entre les bactéries gram négatives et les bactéries gram positives telles que *Bacillus subtilis* (*B. subtilis*) et *Staphylococcus aureus* (*S. aureus*). *S. aureus* est un agent pathogène humain fréquemment présent dans le nez, les voies respiratoires et la peau. Cette bactérie provoque des maladies telles que la pneumonie, la méningite, l'ostéomyélite et autres. Il a été signalé que 158 000 infections survenues en France en 2012 étaient dues à souche multirésistante *Staphylococcus* (Colomb-Cotinat et al., 2016). *S. aureus* présente une résistance extrêmement élevée aux antibiotiques ciblant les ribosomes.

La structure du ribosome résolue il y a trois ans présente des caractéristiques spécifiques qui ne sont pas typiques des bactéries à gram négatif (Khusainov et al., 2016). L'une des caractéristiques de l'ARN ribosomal dans la petite sous-unité ribosomal est l'extension de l'hélice 26, impliquée dans la dimérisation des ribosomes (Khusainov et al., 2017). Près de

cette hélice se lie la protéine ribosomale S1 qui, chez *E. coli*, déploie l'ARNm structuré sur le ribosome. Cependant, il a été démontré que *Bacillus stearothermophilus* (*B. stearothermophilus*) est dépourvu de protéine équivalente à *E. coli* S1 (Isono et Isono, 1975). Étant donné que S1 est très similaire chez toutes les bactéries à Gram positif et que chez *S. aureus* le site de liaison aux ribosomes a été perdu, il a été suggéré que les facteurs d'initiation (IF) pourraient probablement remplir des fonctions supplémentaires compensant le rôle de S1. De plus, les facteurs d'initiation ont aussi des caractéristiques spécifiques à l'espèce. La région C-terminale de IF2 est très conservée, tandis que la longueur de la région N-terminale dépend de l'espèce bactérienne.

En outre, chez *S. aureus*, il existe des ARN régulateurs, tels que l'ARN III, qui affectent la régulation des gènes de virulence. Il a été montré que l'ARN III réprime l'expression du gène *spa* qui code pour la protéine de surface A, l'un des principaux facteurs de virulence, et inhibe la formation du complexe d'initiation de la traduction (Patel et al., 1987, Huntzinger et al., 2005).

L'objectif principal de notre projet était de déterminer les structures par cryo-EM des complexes d'initiation de *Staphylococcus aureus*, afin de mieux comprendre certains aspects fondamentaux et spécifiques de l'initiation de la traduction de ce pathogène.

### *Projet de recherche 2*

*Candida albicans* (*C. albicans*) est l'agent pathogène humain le plus répandu dans au moins 70% de la population humaine. Du fait que les cibles cellulaires de *C. albicans* sont souvent partagées avec les humains, de nombreux effets secondaires apparaissent, rendant le traitement inefficace (Berman et Sudbery, 2002). Par conséquent, l'étude des mécanismes physiologiques de cet agent pathogène et la mise au point de nouveaux médicaments contre celui-ci ont une signification pratique.

Le ribosome est la cible des antibiotiques les plus couramment utilisés. La détermination de sa structure est une tâche prioritaire.

Les prédictions bio-informatiques montrent une différence significative dans le site E entre *C. albicans* et *S. cerevisiae*, ce qui pourrait expliquer la résistance du premier au cycloheximide (Goldway et al., 1995).

Mon objectif dans ce projet était d'optimiser les protocoles de purification et de cristallisation du ribosome *C. albicans* et de les rendre reproductibles. Une amélioration

supplémentaire de la résolution de la structure ribosomale est nécessaire pour étudier l'effet des antibiotiques.

## Résultats

### *Etude en microscopie cryo-electronique du complexe d'initiation de la traduction de S. aureus*

Notre travail comportait plusieurs étapes:

- pour la reconstruction in vitro
  - 1) purification de tous les composants: 30S, IF (IF1, IF2 et IF3), ARNm et fMet-tRNA<sup>fMet</sup>,
  - 2) détermination du meilleur rapport pour la formation de complexe,
  - 3) acquisition de données,
  - 4) résoudre la structure: traitement des données et construction du modèle atomique,
- ex vivo
  - 1) purification des complexes,
  - 2) acquisition des données,
  - 3) résoudre la structure: traitement des données et construction du modèle atomique.

Les protocoles pour les purifications des petites sous-unités ribosomales (30S) et des facteurs d'initiation (IF1, IF2 et IF3) ont été développés et validés. Les ribosomes se sont révélés purs, stables et capables de se cristalliser. Les facteurs d'initiation, l'ARNm et le fMet-tRNA<sup>fMet</sup> étaient suffisamment purs pour pouvoir être utilisés dans d'autres expériences. Les concentrations optimales de facteurs d'initiation du ribosome ont été trouvées et étaient de 3: 1 pour IF1 et IF2 et de 2: 1 pour IF3.

Après plusieurs tentatives, la structure du 30S intact a été obtenue. L'ARNr a été stabilisé par addition de spermidine. Ensuite, l'ARNm a été ajouté au 30S et les structures ont été analysées en présence et en l'absence de spermidine. Le résultat obtenu montre le rôle de la spermidine dans la stabilisation de la conformation fermée 30S, aidant ainsi à loger correctement l'ARNm dans le canal. Plusieurs structures de 30S avec l'ARNm, le fMet-tRNA<sup>fMet</sup> et l'IF3 à différentes résolutions ont été obtenues. La structure de 30S avec l'ARNm, le fMet-tRNA<sup>fMet</sup> et l'IF2 à 10 Å a également été obtenue. Dans le même temps, IF1 n'a jamais été détecté.

La stratégie expérimentale a été modifiée en faveur d'une méthode plus proche des conditions naturelles. Il a été démontré que les ribosomes eucaryotes peuvent être séparés en sous-unités par addition de GMP-PNP (Anthony et Merrick, 1992, Simonetti et al., 2016). Le

même protocole avec quelques adaptations a été utilisé dans notre cas. Au cours de l'analyse des données, il a été observé que, dans toutes les structures obtenues, l'hélice 44 était flexible, probablement en raison de la faible concentration de spermidine. Les résultats montrent la nécessité de sélectionner plus précisément la concentration de spermidine.

L'effet de l'incubation par étapes sur la formation du complexe a également été vérifié. Il a été constaté que l'incubation séparée de 30S uniquement avec l'ARNm et l'addition de facteurs juste avant la préparation de la grille permettait d'obtenir des structures avec un pourcentage plus élevé d'IF3 lié au ribosome.

Les résultats que j'ai obtenus au cours de ma thèse seront discutés en détail dans les prochains chapitres.

### *Détermination de la structure du ribosome 80S de Candida albicans par cristallographie aux rayons X*

Pour obtenir une structure ribosomique adaptée à l'étude d'antibiotiques spécifiques à l'espèce, plusieurs étapes doivent être complétées:

- 1) la croissance cellulaire et la purification des ribosomes doivent toujours être reproductibles,
- 2) une pureté d'échantillon élevée doit être obtenue,
- 3) les cristaux doivent avoir une taille suffisante pour le traitement post-cristallisation,
- 4) les cristaux avec une bonne diffraction doivent être analysés sur synchrotron.

Les protocoles de purification et de cristallisation du ribosome pour *C. albicans* ont été adaptés à partir des protocoles pour *S. cerevisiae* (Ben Shem et al., 2011).

La purification efficace du ribosome a été réalisée en plusieurs étapes: lyse cellulaire, précipitation du ribosome au polyéthylène glycol (PEG), séparation des 80S de ses sous-unités par des gradients de saccharose et dernière précipitation du PEG pour la concentration de l'échantillon. Les ribosomes obtenus se sont révélés purs, stables et susceptibles d'être cristallisés.

Le criblage à grande échelle des conditions de cristallisation a été effectué. Le changement de la température de cristallisation de + 4 ° C à + 20 ° C a affecté négativement l'apparition des cristaux. Les changements significatifs affectant la forme et la taille des cristaux étaient les concentrations de ribosome, ainsi que la concentration en sels, le rapport entre l'échantillon et le réservoir à l'intérieur de la goutte et le volume du réservoir. Une

diminution de la nucléation a été obtenue en réduisant la concentration de spermidine. Les cristaux obtenus ont atteint une longueur de 220  $\mu\text{m}$  et ont été diffractés à 6,5 - 7  $\text{\AA}$ .

Mes collègues travaillent actuellement à l'amélioration de la diffraction des cristaux.

## Conclusions

*S. aureus* est un objet intéressant pour les scientifiques en raison de la portée pratique de son étude. Sa résistance à la plupart des antibiotiques constitue un défi pour les chercheurs. La nécessité d'étudier le processus d'initiation de la traduction de cette bactérie est indéniable.

Malgré toutes les difficultés rencontrées, nous avons quand même réussi à obtenir plusieurs structures de complexes d'initiation à différentes résolutions. Les connaissances acquises au cours de nos travaux feront l'objet d'autres études et conduiront sans aucun doute à des résultats significatifs.

Un autre agent pathogène, dont le processus de traduction devrait être étudié, est *C. albicans*. En raison de la similitude du ribosome de *C. albicans* et du ribosome humain, le traitement par antibiotique n'est pas efficace. La détermination de la structure du ribosome de *C. albicans* pour le développement d'antibiotiques de nouvelle génération est essentiel.

Des protocoles bien reproductibles constituent la première étape essentielle de la détermination de la structure du ribosome. Commencer le travail de recherche avec des cristaux ayant diffractés à 7  $\text{\AA}$  est un avantage significatif.

Les connaissances acquises dans mon travail seront sans aucun doute utilisées dans les recherches futures et contribueront probablement à la lutte contre ces agents pathogènes.

## BIBLIOGRAPHY

**Agrawal, R. K., and Sharma, M. R.** (2012). Structural aspects of mitochondrial translational apparatus. *Curr. Opin. Struct. Biol.* 22, 797–803.

**Anthony, D. D., Merrick, W. C.** (1992). Analysis of 40 S and 80 S complexes with mRNA as measured by sucrose density gradients and primer extension inhibition. *J Biol Chem.* 267, 1554-1562.

**Antoun, A., Pavlov, M. Y., Lovmar, M., Ehrenberg, M.** (2006a). How initiation factors tune the rate of initiation of protein synthesis in bacteria. *EMBO* 25, 2539– 2550.

**Armache, J. P., Anger, A. M., Márquez, V., Franckenberg, S., Fröhlich, T., Villa, E., Berninghausen, O., Thomm, M., Arnold, G. J., Beckmann, R., Wilson, D. N.** (2013). Promiscuous behaviour of archaeal ribosomal proteins: implications for eukaryotic ribosome evolution. *Nucleic Acids Res.* 41, 1284–1293.

**Armachea, J., Jarascha, A., Angera, A., Villab, E., Beckera, T., Bhushana, S., Jossinetc, F., Habeckd, M., Dindara, G., Franckenberga, S., Marqueza, V., Mielkef, T., Thommh, M., Berninghausena, O., Beatrixa, B., Södinga, J., Westhof, E., Wilson, D., Beckmann, R.** (2010). Cryo-EM structure and rRNA model of a translating eukaryotic 80S ribosome at 5.5-Å resolution. *PNAS* 107, 19748–19753.

**Asherie, N.** (2004). Protein crystallization and phase diagrams. *Methods* 34, 266-272.

**Baker, L. A., Smith, E. A., Bueler, S. A., Rubinstein, J. L.** (2010). The resolution dependence of optimal exposures in liquid nitrogen temperature electron cryomicroscopy of catalase crystals. *J. Struct. Biol.* 169, 431–437.

**Ban, N., Nissen, P., Hansen, J., Moore, P. B., Steitz, T. A.** (2000). The complete atomic structure of the large ribosomal subunit at 2.4 Å resolution. *Science* 289, 905-920.

**Ban, N., Beckmann, R., Cate, J., Dinman, J., Dragon, F., Ellis, S., Lafontaine, D., Lindahl, L., Liljas, A., Lipton, J., McAlear, M., Moore, P., Noller, H., Ortega, J., Panse, V., Ramakrishnan, V., Spahn, C., Steitz, T., Tchorzewski, M., Tollervey, D., Warren, A., Williamson, J., Wilson, D., Yonath, A., Yusupov, M.** (2014). A new system for naming ribosomal proteins. *Curr. Opi. Struct. Biol.*, 165-169.

**Baudet, M., Ortet, P., Gaillard, J. C., Fernandez, B., Guérin, P., Enjalbal, C., Subra, G., De Groot, A., Barakat, M., Dedieu, A., et al.** (2010). Proteomics-based refinement of *Deinococcus deserti* genome annotation reveals an unwonted use of non-canonical translation initiation codons. *Molecular & Cellular Proteomics : MCP* 9, 415–426.

**Becker, T., Franckenberg, S., Wickles, S., Shoemaker, C. J., Anger, A. M., Armache, J. P., Sieber, H., Ungewickell, C., Berninghausen, O., Daberkow, I., Karcher, A., Thomm, M., Hopfner, K. P., Green, R., Beckmann, R.** (2012). Structural basis of highly conserved ribosome recycling in eukaryotes and archaea. *Nature* 482, 501-506.

**Beckert, B., Turk, M., Czech, A., Berninghausen, O., Beckmann, R., Ignatova, Z., Plitzko, J. M., Wilson, D. N.** (2018). Structure of a hibernating 100S ribosome reveals an inactive conformation of the ribosomal protein S1. *Nature Microbiology* 3, 1115–1121.

**Belova, L., Tenson, T., Xiong, L., McNicholas, P. M., Mankin, A. S.** (2001). A novel site of antibiotic action in the ribosome: Interaction of evernimicin with the large ribosomal subunit. *PNAS* 98, 3726-3731.

**Ben-Shem, A., Jenner, L., Yusupova, G., Yusupov, M.** (2010). Crystal structure of the eukaryotic ribosome. *Science* 330, 1230 – 1209.

**Ben-Shem, A., Garreau de Loubresse, N., Melnikov, S., Jenner, L., Yusupova, G., and Yusupov, M.** (2011). The structure of the eukaryotic ribosome at 3.0 Å resolution. *Science* 334, 1524-1529.

**Ben-Shem, A., Jenner, L., Yusupova, G., Yusupov, M.** (2010). Crystal structure of the eukaryotic ribosome. *Science* 330, 1230 – 1209.

**Benito, Y., Kolb, F. A., Romby, P., Lina, G., Etienne, J., Vandenesch, F.** (2000). Probing the structure of RNAIII, the *Staphylococcus aureus* agr regulatory RNA, and identification of the RNA domain involved in repression of protein A expression. *RNA*. 6, 668-679.

**Berman, J., Sudbery, P. E.** (2002). *Candida albicans*: a molecular revolution built on lessons from budding yeast. *Nature reviews* 3, 918 - 930.

**Binns, N., Masters, M.** (2002). Expression of the *Escherichia coli* *pcnB* gene is translationally limited using an inefficient start codon: a second chromosomal example of translation initiated at AUU. *Molecular Microbiology* 44, 1287–1298.

**Biou, V., Shu, F., Ramakrishnan, V.** (1995). X-ray crystallography shows that translational initiation factor IF3 consists of two compact alpha/beta domains linked by an alpha-helix. *EMBO* 14, 4056–4064.

**Blanchard, S. C., Kim, H. D., Gonzalez, R. L. Jr., Puglisi, J. D., Chu, S.** (2004). tRNA dynamics on the ribosome during translation. *PNAS* 101, 12893–12898.

**Blattner, F. R., Plunkett, G., Bloch, C. A., Perna, N. T., Burland, V., Riley, M., Collado-Vides, J., Glasner, J. D., Rode, C. K., Mayhew, G. F., et al.** (1997). The complete genome sequence of *Escherichia coli* K-12. *Science* 277, 1453–1462.

**Boileau, G., Butler, P., Hershey, J. W., Traut, R. R.** (1983). Direct cross-links between initiation factors 1, 2, and 3 and ribosomal proteins promoted by 2-iminothiolane. *Biochemistry* 22, 3162–3170.

**Bokov, K., Steinberg, S. V.** (2009). A hierarchical model for evolution of 23S ribosomal RNA. *Nature* 457, 977 – 980.

**Bondi, A. Jr., Dietz, C. C.** (1945). Penicillin resistant staphylococci. *Proc. Soc. Exp. Biol. Med.* 6, 55-58.

**Caldas, T., Laalami, S., Richarme, G.** (2000). Chaperone properties of bacterial elongation factor EF-G and initiation factor IF2. *The Journal of Biological Chemistry* 275, 855–860.

**Campbell, E. A., Korzheva, N., Mustaev, A., Murakami, K., Nair, S., Goldfarb, A., Darst, S. A.** (2001). Structural mechanism for rifampicin inhibition of bacterial rna polymerase. *Cell* 104, 901-912.

**Carter, P., Clemons, W. M., Brodersen, D. E., Morgan-Warren, R. J., Hartsch, T., Wimberly, B. T., Ramakrishnan, V.** (2001). Crystal structure of an initiation factor bound to the 30S ribosomal subunit. *Science* 291, 498–501.

**Caserta, E., Tomsic, J., Spurio, R., La Teana, A., Pon, C. L., Gualerzi, C. O.** (2006). Translation initiation factor IF2 interacts with the 30 S ribosomal subunit via two separate binding sites. *Journal of Molecular Biology* 362, 787–799.

**Caskey, C. T., Beaudet, A. L., Scolnick, E. M., Rosman, M.** (1971). Hydrolysis of fMet-tRNA by Peptidyl Transferase. *Proc. Natl. Acad. Sci.* 68, 3163–3167.

**Celano, B., Pawlik, R. T., and Gualerzi, C. O.** (1988). Interaction of Escherichia coli translation-initiation factor IF-1 with ribosomes. *FEBS* 178, 351–355.

**Chambers, H. F., Deleo, F. R.** (2009). Waves of resistance: Staphylococcus aureus in the antibiotic era. *Nat. Rev. Microbiol.* 7, 629-641.

**Chen, C., Tang, J., Dong, W., Wang, C., Feng Y., Wang, J., Zheng, F., Pan, X., Liu., D., Li, M., et al.** (2007). A glimpse of streptococcal toxic shock syndrome from comparative genomics of *S. suis* 2 chinese isolates. *PLoS One* 2, e315.

**Choi, S. K., Lee, J. H., Zoll, W. L., Merrick, W. C., Dever, T. E.** (1998). Promotion of met- tRNA<sup>iMet</sup> binding to ribosomes by yIF2, a bacterial IF2 homolog in yeast. *Science* 280, 1757–1760.

**Clemons, W. M. Jr., May, J. L., Wimberly, B. T., McCutcheon, J. P., Capel, M. S., Ramakrishnan, V.** (1999). Structure of a bacterial 30S ribosomal subunit at 5.5 Å resolution. *Nature* 400, 833-40.

**Cole, J. L., Lary, J. W., Moody, T., Laue, T. M.** (2008). Analytical ultracentrifugation: sedimentation velocity and sedimentation equilibrium. *Methods Cell Biol.* 84, 143-179.

**Cory, S., Marcker, K. A., Dube, S. K., Clark, B. F.** (1968). Primary structure of a methionine transfer RNA from Escherichia coli. *Nature* 220, 1039–1040.

**Cox, G., Thompson, G. S., Jenkins, H. T., Peske, F., Savelsbergh, A., Rodnina, M. V., Wintermeyer, W., Homans, S. W., Edwards, T. A., O'Neill, A. J.** (2012). Ribosome clearance by FusB-type proteins mediates resistance to the antibiotic fusidic acid. *Proc. Natl. Acad. Sci.* 109, 2102 – 2107.

**Cundliffe, E., McQuillen, K.** (1967). Bacterial protein synthesis: the effects of antibiotics. *J Mol Biol.* 30, 137 - 146.

**Dallas, A., Noller, H. F.** (2001). Interaction of translation initiation factor 3 with the 30S ribosomal subunit. *Molecular Cell* 8, 855–864.

**Davidovich, C., Bashan, A., Auerbach-Nevo, T., Yaggie, R. D., Gontarek, R. R., Yonath, A.** (2007). Induced-fit tightens pleuromutilins binding to ribosomes and remote interactions enable their selectivity. *Proc. Natl. Acad. Sci.* 104, 4291 – 4296.

**Day, L. E.** (1966). *J Bacteriol*, 91.

**De Smit, M. H., Van Duin, J.** (2003). Translational standby sites: how ribosomes may deal with the rapid folding kinetics of mRNA. *Journal of Molecular Biology* 331, 737–743.

**Debey, P., Hui Bon Hoa, G., Douzou, P., Godefroy-Colburn, T., Graffe, M., Grunberg- Manago, M.** (1975). Ribosomal subunit interaction as studied by light scattering. Evidence of different classes of ribosome preparations. *Biochemistry* 14, 1553–1559.

**Dinos, G., Wilson, D. N., Teraoka, Y., Szaflarski, W., Fucini, P., Kalpaxis, D., Nierhaus, K. H.** (2004). Dissecting the ribosomal inhibition mechanisms of edeine and pactamycin: the universally conserved residues G693 and C795 regulate P-site RNA binding. *Mol. Cell.* 13, 113-124.

**Dreyfus, M.** (1988). What constitutes the signal for the initiation of protein synthesis on *Escherichia coli* mRNAs? *Journal of Molecular Biology* 204, 79–94.

**Dube, S. K., Marcker, K. A., Clark, B. F., Cory, S.** (1968). Nucleotide sequence of N- formyl-methionyl-transfer RNA. *Nature* 218, 232–233.

**Dubochet, J., Lepault, J., Freeman, R., Berriman, J. A., Homo, J. C.** (1982). Electron microscopy of frozen water and aqueous solutions. *Journal of Microscopy* 128, 219-237.

**Dumitru, R., Hornby, J. M., Nickerson, K. W.** (2004). Defined anaerobic growth medium for studying *Candida albicans* basic biology and resistance to eight antifungal drugs. *Antimicrob. Agents Chemother* 48, 2350 - 2354.

**Duval, M., Korepanov, A., Fuchsbauer, O., Fechter, P., Haller, A., Fabbretti, A., Choulier, L., Micura, R., Klaholz, B. P., Romby, P., Springer, M., Marzi, S.** (2013). *Escherichia coli* ribosomal protein S1 unfolds structured mRNAs onto the ribosome for active translation initiation. *PLoS Biology* 11, e1001731

**Escaich, S., Prouvensier, L., Saccomani, M., Durant, L., Oxoby, M., Gerusz, V., Moreau, F., Vongsouthi, V., Maher, K., Morrissey, I., Soulama-Mouze, C.** (2011). The MUT056399 inhibitor of FabI is a new antistaphylococcal compound. *Antimicrob. Agents Chemother.* 55, 4692-4697.

**Fabbretti, A., Pon, C. L., Hennelly, S. P., Hill, W. E., Lodmell, J. S., Gualerzi, C. O.** (2007). The real-time path of translation factor IF3 onto and off the ribosome. *Molecular Cell* 25, 285–296.

**Fahnestock, S. R.** (1977). Reconstitution of active 50 S ribosomal subunits from *Bacillus licheniformis* and *Bacillus subtilis*. *Arch Biochem Biophys.* 182, 497-505.

**Faruqi, A. R., McMullan, G.** (2011). Electronic detectors for electron microscopy. *Q Rev Biophys.* 44, 357-390.

**Farwell, M. A., Roberts, M. W., Rabinowitz, J. C.** (1992). The effect of ribosomal protein S1 from *Escherichia coli* and *Micrococcus luteus* on protein synthesis in vitro by *E. coli* and *Bacillus subtilis*. *Mol. Microbiol.* 6, 3375-3383.

**Fortier, P. L., Schmitter, J. M., Garcia, C., Dardel, F.** (1994). The N-terminal half of initiation factor IF3 is folded as a stable independent domain. *Biochimie* 76, 376-383.

**Fourmy, D., Mechulam, Y., Brunie, S., Blanquet, S., Fayat, G.** (1991). Identification of residues involved in the binding of methionine by *Escherichia coli* methionyl-tRNA synthetase. *FEBS Letters* 292, 259-263.

**Freistroffer, D. V., Pavlov, M. Y., MacDougall, J., Buckingham, R. H., Ehrenberg, M.** (1997). Release factor RF3 in *E. coli* accelerates the dissociation of release factors RF1 and RF2 from the ribosome in a GTP-dependent manner. *EMBO* 16, 4126-4133.

**Fujii, K., Susanto, T. T., Saurabh, S., Barna, M.** (2018). Decoding the Function of Expansion Segments in Ribosomes. *Mol Cell.* 72, 1013-1020.

**Garcia, C., Fortier, P. L., Blanquet, S., Lallemand, J. Y., Dardel, F.** (1995a). 1H and 15N resonance assignments and structure of the N-terminal domain of *Escherichia coli* initiation factor 3. *FEBS* 228, 395-402.

**Garcia, C., Fortier, P. L., Blanquet, S., Lallemand, J. Y., Dardel, F.** (1995b). Solution structure of the ribosome-binding domain of *E. coli* translation initiation factor IF3. Homology with the U1A protein of the eukaryotic spliceosome. *Journal of Molecular Biology* 254, 247-259.

**Garreau de Loubresse, N., Prokhorova, I., Holtkamp, W., Rodnina, M. V., Yusupova, G., Yusupov, M.** (2014). Structural basis for the inhibition of the eukaryotic ribosome. *Nature* 513, 517-522.

**Gaur, R., Grasso, D., Datta, P. P., Krishna, P. D. V, Das, G., Spencer, A., Agrawal, R. K., Spremulli, L., Varshney, U.** (2008). A single mammalian mitochondrial translation initiation factor functionally replaces two bacterial factors. *Molecular Cell* 29, 180-190.

**Ghooi, R. B., Thatte, S. M.** (1995). Inhibition of cell wall synthesis--is this the mechanism of action of penicillins? *Med. Hypotheses.* 44, 127-131.

**Gillum, A. M., Tsay, E. Y., Kirsch, D. R.** (1984). Isolation of the *Candida albicans* gene for orotidine-5'-phosphate decarboxylase by complementation of *S. cerevisiae* *ura3* and *E. coli* *pyrF* mutations. *Mol. Gen. Genet.* 198, 179-182.

**Giuliodori, A. M., Brandi, A., Gualerzi, C. O., Pon, C. L.** (2004). Preferential translation of cold-shock mRNAs during cold adaptation. *RNA* 10, 265-276.

**Giuliodori, A. M., Brandi, A., Giangrossi, M., Gualerzi, C. O., Pon, C. L.** (2007). Cold- stress-induced de novo expression of *infC* and role of IF3 in cold-shock translational bias. *RNA* 13, 1355-1365.

**Glaeser, R. M., Hall, R. J.** (2011). Reaching the information limit in cryo-EM of biological macromolecules: experimental aspects. *Biophys J.* 100, 2331-2337.

**Goldway, M., Teff, D., Schmidt, R., Oppenheim, A. B., Koltin, Y.** (1995). Multidrug resistance in *Candida albicans*: disruption of the BENr gene. *Antimicrob. Agents Chemother* 39, 422–426.

**Gómez, M. I., Lee, A., Reddy, B., Muir, A., Soong, G., Pitt, A., Cheung, A., Prince, A.** (2004). Staphylococcus aureus protein A induces airway epithelial inflammatory responses by activating TNFR1. *Nat Med.* 10, 842-848.

**Gourse, R. L., Gaal, T., Bartlett, M. S., Appleman, J. A., Ross, W.** (1996). rRNA transcription and growth rate-dependent regulation of ribosome synthesis in *Escherichia coli*. *Annu. Rev. Microbiol.* 50, 645-677.

**Goyal, A., Belardinelli, R., Rodnina, M. V.** (2017). Non-canonical binding site for bacterial initiation factor 3 on the large ribosomal subunit. *Cell Rep* 20, 3113-3122.

**Gray, N. K., Hentze, M. W.** (1994). Iron regulatory protein prevents binding of the 43S translation pre-initiation complex to ferritin and eALAS mRNAs. *EMBO* 13, 3882–3891.

**Grunberg-Manago, M., Dessen, P., Pantaloni, D., Godefroy-Colburn, T., Wolfe, D., and Dondon, J.** (1975). Light-scattering studies showing the effect of initiation factors on the reversible dissociation of *Escherichia coli* ribosomes. *Journal of Molecular Biology* 94, 461–478.

**Gualerzi, C. O., and Pon, C. L.** (1990). Initiation of mRNA translation in prokaryotes. *Biochemistry* 29, 5881–5889.

**Guca, E., Hashem, Y.** (2018). Major structural rearrangements of the canonical eukaryotic translation initiation complex. *Curr. Opin. Struct. Biol.* 53, 151 – 158.

**Guenneugues, M., Caserta, E., Brandi, L., Spurio, R., Meunier, S., Pon, C. L., Boelens, R., Gualerzi, C. O.** (2000). Mapping the fMet-tRNA(f)(Met) binding site of initiation factor IF2. *EMBO* 19, 5233–5240.

**Haggerty, T. J., Lovett, S. T.** (1997). IF3-mediated suppression of a GUA initiation codon mutation in the recJ gene of *Escherichia coli*. *Journal of Bacteriology* 179, 6705– 6713.

**Hansen, P. K., Wikman, F., Clark, B. F., Hershey, J. W., Uffe Petersen, H.** (1986). Interaction between initiator Met-tRNA<sup>fMet</sup> and elongation factor EF-Tu from *E. coli*. *Biochimie* 68, 697–703.

**Hartleib, J., Köhler, N., Dickinson, R. B., Chhatwal, G. S., Sixma, J. J., Hartford, O. M., Foster, T. J., Peters, G., Kehrel, B. E., Herrmann, M.** (2000). Protein A is the von Willebrand factor binding protein on *Staphylococcus aureus*. *Blood.* 96, 2149-56.

**Hartmann, G., Honikel, K. O., Knüsel, F., Nüesch, J.** (1967). The specific inhibition of the DNA-directed RNA synthesis by rifamycin. *Biochim Biophys Acta.* 145, 843-844.

**Hartz, D., McPheeters, D. S., Gold, L.** (1989). Selection of the initiator tRNA by *Escherichia coli* initiation factors. *Genes and Development* 3, 1899–1912.

**Hartz, D., Binkley, J., Hollingsworth, T., Gold, L.** (1990). Domains of initiator tRNA and initiation codon crucial for initiator tRNA selection by *Escherichia coli* IF3. *Genes Dev.* 4, 1790-1800.

**Hermann, T.** (2005). Drugs targeting the ribosome. *Curr. Opin. Struct. Biol.* 15, 355-366.

**Hershey, J. W., Monro, R. E.** (1966). A competitive inhibitor of the GTP reaction in protein synthesis. *J Mol Biol.* 18, 68-76.

**Hershey, J. W., Yanov, J., Johnston, K., Fakunding, J. L.** (1977). Purification and characterization of protein synthesis initiation factors IF1, IF2, and IF3 from *Escherichia coli*. *Archives of Biochemistry and Biophysics* 182, 626–638.

**Hirokawa, G., Kiel, M. C., Muto, A., Selmer, M., Raj, V. S., Liljas, A., Igarashi, K., Kaji, H., Kaji, A.** (2002). Post-termination complex disassembly by ribosome recycling factor, a functional tRNA mimic. *EMBO* 21, 2272–2281.

**Huntzinger, E., Boisset, S., Saveanu, C., Benito, Y., Geissmann, T., Namane, A., Lina, G., Etienne, J., Ehresmann, B., Ehresmann, C., Jacquier, A., Vandenesch, F., Romby P.** (2005). *Staphylococcus aureus* RNAIII and the endoribonuclease III coordinately regulate spa gene expression. *EMBO* 24, 824–835.

**Hussain, T., Llácer, J. L., Wimberly, B. T., Kieft, J. S., Ramakrishnan, V.** (2016). Large-Scale Movements of IF3 and tRNA during Bacterial Translation Initiation. *Cell* 167, 133-144.

**Isono, S., Isono, K.** (1975). Role of ribosomal protein S1 in protein synthesis: effects of its addition to *Bacillus stearothermophilus* cell-free system. *Eur J Biochem.* 56, 15-22.

**Jenner, L., Demeshkina, N., Yusupova, G., Yusupov, M.** (2010). Structural rearrangements of the ribosome at the tRNA proofreading step. *Nat. Struct. Mol. Biol.* 17, 1072-1078.

**Jenner, L., Starosta, A. L., Terry, D. S., Mikolajka, A., Filonava, L., Yusupov, M., Blanchard, S. C., Wilson, D. N., Yusupova, G.** (2013). Structural basis for potent inhibitory activity of the antibiotic tigecycline during protein synthesis. *PNAS* 110, 3812 – 3816.

**Jin, H., Zhao, Q., Gonzalez de Valdivia, E. I., Ardell, D. H., Stenström, M., Isaksson, L.** (2006). Influences on gene expression in vivo by a Shine-Dalgarno sequence. *Molecular Microbiology* 60, 480–492.

**Johnson, M. D., Decker, C. F.** (2008). Antimicrobial agents in treatment of MRSA infections. *Dis Mon.* 54, 793-800.

**Julián, P., Milon, P., Agirrezabala, X., Lasso, G., Gil, D., Rodnina, M. V, Valle, M.** (2011). The Cryo-EM structure of a complete 30S translation initiation complex from *Escherichia coli*. *PLoS Biology* 9, e1001095.

**Kalpaxis, D. L., Coutsogeorgopoulos, C.** (1989). Type of inhibition of peptide bond formation by chloramphenicol depends on the temperature and the concentration of ammonium ions. *Mol. Pharmacol.* 36, 615-619.

**Kapralou, S., Fabbretti, A., Garulli, C., Gualerzi, C. O., Pon, C. L., and Spurio, R.** (2009). Characterization of *Bacillus stearothermophilus* infA and of its product IF1. *Gene* 428, 31–35.

**Kapralou, S., Fabbretti, A., Garulli, C., Spurio, R., Gualerzi, C. O., Dahlberg, A. E., Pon, C. L.** (2008). Translation initiation factor IF1 of *Bacillus stearothermophilus* and *Thermus thermophilus* substitute for *Escherichia coli* IF1 in vivo and in vitro without a direct IF1- IF2 interaction. *Molecular Microbiology* 70, 1368–1377.

**Karimi, R., Pavlov, M. Y., Buckingham, R. H., Ehrenberg, M.** (1999). Novel roles for classical factors at the interface between translation termination and initiation. *Molecular Cell* 3, 601–609.

**Kerawala, C., Newlands, C.** (2010). *Oral and maxillofacial surgery.* Oxford University Press. 446-447.

**Khusainov, I., Vicens, Q., Bochler, A., Grosse, F., Myasnikov, A., Menetret, J., Chicher, J., Marzi, S., Romby, P., Yusupova, G., Yusupov, M., Hashem, Y.** (2016). Structure of the 70S ribosome from human pathogen *Staphylococcus aureus*. *Nucleic Acids Research* 44, 10491–10504.

**Khusainov, I., Vicens, Q., Ayupov, R., Usachev, K., Myasnikov, A., Simonetti, A., Validov, S., Kieffer, B., Yusupova, G., Yusupov, M., Hashem, Y.** (2017). Structures and dynamics of hibernating ribosomes from *Staphylococcus aureus* mediated by intermolecular interactions of HPF. *EMBO* 36, 2073–2087.

**Kim, D. H., Kang, S. J., Lee, K. Y., Jang, S. B., Kang, S. M., Lee, B. J.** (2017). Structure and dynamics study of translation initiation factor 1 from *Staphylococcus aureus* suggests its RNA binding mode. *Biochim Biophys Acta Proteins Proteom.* 1865, 65-75.

**Klaholz, B. P.** (2011). Molecular recognition and catalysis in translation termination complexes. *Trends Biochem Sci.* 36, 282-292.

**Klinge, S., Voigts-Hoffmann, F., Leibundgut, M., Arpagaus, S., Ban, N.** (2011). Crystal structure of the eukaryotic 60S ribosomal subunit in complex with initiation factor 6. *Science* 334, 941–948.

**Koutmou, K. S., McDonald, M. E., Brunelle, J. L., Green R.** (2014). RF3:GTP promotes rapid dissociation of the class 1 termination factor. *RNA* 20, 609-620.

**Kozak, M.** (1999). Initiation of translation in prokaryotes and eukaryotes. *Gene* 234, 187–208.

**Kyrpides, N. C., Woese, C.R.** (1998). Universally conserved translation initiation factors. *Proceedings of the National Academy of Sciences of the United States of America* 95, 224–228.

**La Teana, A., Pon, C. L., Gualerzi, C. O.** (1996). Late events in translation initiation. Adjustment of fMet-tRNA in the ribosomal P-site. *Journal of Molecular Biology* 256, 667–675.

**Laalami, S., Putzer, H., Plumbridge, J., Grunberg-Manago, M.** (1991). A severely truncated form of translational initiation factor 2 supports growth of *Escherichia coli*. *Journal of Molecular Biology* 220, 335–349.

**Laursen, B. S., Sørensen, H. P., Mortensen, K. K., Sperling-Petersen, H. U.** (2005). Initiation of Protein Synthesis in Bacteria. *Microbiology and molecular biology reviews* 69, 101–123.

**Le Loir, Y., Baron, F., Gautier, M.** (2003). *Staphylococcus aureus* and food poisoning. *Genet Mol Res.* 2, 63-76.

**Le, K. Y., Otto, M.** (2015). Quorum-sensing regulation in staphylococci-an overview. *Front Microbiol.* 6, 1174.

**Leshner, G. Y., Froelich, E. J., Gruett, M. D., Bailey, J. H., Brundage, R. P.** (1962). 1,8-Naphthyridine derivatives. A new class of chemotherapeutic agents. *J Med Chem.* 5, 1063–1065.

**Li, X., Mooney, P., Zheng, S., Booth, C. R., Braunfeld, M. B., Gubbens, S., Agard, D. A., Cheng, Y.** (2013). Electron counting and beam-induced motion correction enable near-atomic-resolution single-particle cryo-EM. *Nat Methods.* 10, 584-590.

**Liu, Y., Huynh, D. T., Yeates, T. O.** (2019). A 3.8 Å resolution cryo-EM structure of a small protein bound to an imaging scaffold. *Nat. Commun.* 10, 1864.

**Lockwood, H., Chakraborty, P. R., Maitra, U.** (1971). A complex between initiation factor IF2, guanosine triphosphate, and fMet-tRNA: an intermediate in initiation complex formation. *Proceedings of the National Academy of Sciences of the United States of America* 68, 3122–3126.

**Lomakin, I. B., Shirokikh, N. E., Yusupov, M. M., Hellen, C. U. T., Pestova, T. V.** (2006). The fidelity of translation initiation: reciprocal activities of eIF1, IF3 and YciH. *EMBO* 25, 196–210.

**Luchin, S., Putzer, H., Hershey, J. W., Cenatiempo, Y., Grunberg-Manago, M., Laalami, S.** (1999). In vitro study of two dominant inhibitory GTPase mutants of *Escherichia coli* translation initiation factor IF2. Direct evidence that GTP hydrolysis is necessary for factor recycling. *The Journal of Biological Chemistry* 274, 6074–6079.

**Lundgren, D. H., Hwang, S. I., Wu, L., Han, D. K.** (2010). Role of spectral counting in quantitative proteomics. *Expert. Rev. Proteomics.* 7, 39-53.

**Lyon, B. R., Skurray, R.** (1987). Antimicrobial resistance of *Staphylococcus aureus*: genetic basis. *Microbiol Rev.* 51, 88-134.

**Ma, J., Campbell, A., Karlin, S.** (2002). Correlations between Shine-Dalgarno sequences and gene features such as predicted expression levels and operon structures. *Journal of Bacteriology* 184, 5733–5745.

**Maar, D., Liveris, D., Sussman, J. K., Ringquist, S., Moll, I., Heredia, N., Kil, A., Bläsi, U., Schwartz, I., Simons, R. W.** (2008). A single mutation in the IF3 N-terminal domain perturbs the fidelity of translation initiation at three levels. *Journal of Molecular Biology* 383, 937–944.

**Majumdar, A., Bose, K. K., Gupta, N. K.** (1976). Specific binding of *Escherichia coli* chain Initiation factor 2 to fMet-tRNA<sup>fMet</sup>. *The Journal of Biological Chemistry* 251, 137–140.

**Mayer, C., Köhrer, C., Kenny, E., Prusko, C., RajBhandary, U. L.** (2003). Anticodon sequence mutants of *Escherichia coli* initiator tRNA: effects of overproduction of aminoacyl-tRNA synthetases, methionyl-tRNA formyltransferase, and initiation factor 2 on activity in initiation. *Biochemistry* 42, 4787–4799.

**McCarthy, J. E., Brimacombe, R.** (1994). Prokaryotic translation: the interactive pathway leading to initiation. *Trends in Genetics* : TIG 10, 402–407.

**McCutcheon, J. P., Agrawal, R. K., Philips, S. M., Grassucci, R., Gerchman, S. E., Clemons, W. M., Ramakrishnan, V., Frank, J.** (1999). Location of translational initiation factor IF3 on the small ribosomal subunit. *Proceedings of the National Academy of Sciences of the United States of America* 96, 4301–4306.

**McMullan, G., Chen, S., Henderson, R., Faruqi, A. R.** (2009). Detective quantum efficiency of electron area detectors in electron microscopy. *Ultramicroscopy* 109, 1126–1143

**Mechulam, Y., Schmitt, E., Maveyraud, L., Zelwer, C., Nureki, O., Yokoyama, S., Konno, M., Blanquet, S.** (1999). Crystal structure of *Escherichia coli* methionyl-tRNA synthetase highlights species-specific features. *Journal of Molecular Biology* 294, 1287–1297.

**Mechulam, Y., Guillon, L., Yatime, L., Blanquet, S., Schmitt, E.** (2007). Protection-based assays to measure aminoacyl-tRNA binding to translation initiation factors. *Methods Enzymol.* 430, 265-281.

**Meinzel, T., Sacerdot, C., Graffe, M., Blanquet, S., Springer, M.** (1999). Discrimination by *Escherichia coli* initiation factor IF3 against initiation on non-canonical codons relies on complementarity rules. *Journal of Molecular Biology* 290, 825–837.

**Melnikov, S., Ben-Shem, A., Garreau de Loubresse, N., Jenner, L., Yusupova, G., Yusupov, M.** (2012). One core, two shells: bacterial and eukaryotic ribosomes. *Nat. Struct. Mol. Biol.* 19, 560 – 567.

**Mikolajka, A., Liu, H., Chen, Y., Starosta, A. L., Márquez, V., Ivanova, M., Cooperman, B. S., Wilson, D. N.** (2011). Differential effects of thiopeptide and orthosomycin antibiotics on translational GTPases. *Chem Biol.* 18, 589-600.

**Milac, T. I., Randolph, T. W., Wang, P.** (2012). Analyzing LC-MS/MS data by spectral count and ion abundance: two case studies. *Stat. Interface.* 5, 75-87.

**Milazzo, A. C., Cheng, A., Moeller, A., Lyumkis, D., Jacovetty, E., Polukas, J., Ellisman, M. H., Xuong, N. H., Carragher, B., Potter, C. S.** (2011). Initial evaluation of

a direct detection device detector for single particle cryo-electron microscopy. *J Struct Biol.* 176, 404-408.

**Milon, P., Tischenko, E., Tomsic, J., Caserta, E., Folkers, G., La Teana, A., Rodnina, M. V, Pon, C. L., Boelens, R., Gualerzi, C. O.** (2006). The nucleotide-binding site of bacterial translation initiation factor 2 (IF2) as a metabolic sensor. *Proceedings of the National Academy of Sciences of the United States of America* 103, 13962–13967.

**Milon, P., Konevega, L., Peske, F., Fabbretti, A., Gualerzi, C., Rodnina, M.** (2007). Transient kinetics, fluorescence and FRET in studies of initiation of translation in bacteria. *Methods in Enzymology* 430, 1 – 30.

**Milón, P., Maracci, C., Filonava, L., Gualerzi, C. O., Rodnina, M. V.** (2012). Real-time assembly landscape of bacterial 30S translation initiation complex. *Nat Struct Mol Biol.* 19, 609-615.

**Monro, R. E., Marcker, K. A.** (1967). Ribosome-catalysed reaction of puromycin with a formylmethionine-containing oligonucleotide. *J Mol Biol.* 25, 347-350.

**Moreau, M., De Cock, E., Fortier, P. L., Garcia, C., Albaret, C., Blanquet, S., Lallemand, J. Y., Dardel, F.** (1997). Heteronuclear NMR studies of *E. coli* translation initiation factor IF3. Evidence that the inter-domain region is disordered in solution. *Journal of Molecular Biology* 266, 15–22.

**Morgan, M.** (2011). Treatment of MRSA soft tissue infections: an overview. *Injury* 42.

**Nissen, P., Kjeldgaard, M., Thirup, S., Polekhina, G., Reshetnikova, L., Clark, B. F., Nyborg, J.** (1995). Crystal structure of the ternary complex of Phe-tRNAPhe, EF-Tu, and a GTP analog. *Science* 270, 1464–1472.

**Noeske, J., Wasserman, M. R., Terry, D. S., Altman, R. B., Blanchard, S. C., Cate, J. H.** (2015). High-resolution structure of the *Escherichia coli* ribosome. *Nat. Struct. Mol. Biol.* 22, 336-341.

**Novick, R. P., Geisinger, E.** (2008). Quorum Sensing in *Staphylococci*. *Annu. Rev. Genet.* 42, 541 – 564.

**O'Donnell, S. M., Janssen, G. R.** (2002). Leaderless mRNAs bind 70S ribosomes more strongly than 30S ribosomal subunits in *Escherichia coli*. *J Bacteriol.* 184, 6730-6733.

**Odds, F. C.** (1988). *Candida and candidosis*. Baillière Tindall, London.

**Olsson, C. L., Graffe, M., Springer, M., Hershey, J. W.** (1996). Physiological effects of translation initiation factor IF3 and ribosomal protein L20 limitation in *Escherichia coli*. *Molecular and General Genetics* 250, 705–714.

**Omotajo, D., Tate, T., Cho, H., Choudhary, M.** (2015). Distribution and diversity of ribosome binding sites in prokaryotic genomes. *BMC Genomics.* 14, 16:604.

**Patel, A. H., Nowlan, P., Weavers, E. D., Foster, T.** (1987). Virulence of protein A-deficient and alpha-toxin-deficient mutants of *Staphylococcus aureus* isolated by allele replacement. *Infect Immun.* 55, 3103-10.

**Pawel, A., Penczek.** (2010). Image Restoration in Cryo-electron Microscopy. *Methods Enzymol.* 482, 35–72.

**Payne, D. J., Miller, W. H., Berry, V., Brosky, J., Burgess, W. J., Chen, E., DeWolf, W. E. Jr., Fosberry, A. P., Greenwood, R., Head, M. S., et al.** (2002). Discovery of a novel and potent class of FabI-directed antibacterial agents. *Antimicrob. Agents Chemother.* 46, 3118-3124.

**Perlroth, J., Choi, B., Spellberg, B.** (2007). Nosocomial fungal infections: epidemiology, diagnosis, and treatment. *Med. Mycol.* 45, 321 - 346.

**Peske, F., Rodnina, M. V., Wintermeyer, W.** (2005). Sequence of steps in ribosome recycling as defined by kinetic analysis. *Molecular Cell* 18, 403–412.

**Peske, F., Kuhlenkoetter, S., Rodnina, M. V., Wintermeyer, W.** (2014). Timing of GTP binding and hydrolysis by translation termination factor RF3. *NAR* 42, 1812-1820.

**Pestova, T. V, Lomakin, I. B., Lee, J. H., Choi, S. K., Dever, T. E., Hellen, C. U.** (2000). The joining of ribosomal subunits in eukaryotes requires eIF5B. *Nature* 403, 332–335.

**Petrelli, D., LaTeana, A, Garofalo, C., Spurio, R., Pon, C. L., Gualerzi, C. O.** (2001). Translation initiation factor IF3: two domains, five functions, one mechanism? *EMBO* 20, 4560–4569.

**Pfaller, M. A., Diekema, D. J.** (2007). Epidemiology of Invasive Candidiasis: A Persistent Public Health Problem. *Clinical Microbiology Reviews.* 20, 133–163.

**Plumbridge, J., Howe, J. G., Springer, M., Touati-Schwartz, D., Hershey, J. W., Grunberg-Manago, M.** (1982). Cloning and mapping of a gene for translational initiation factor IF2 in *Escherichia coli*. *Proceedings of the National Academy of Sciences of the United States of America* 79, 5033–5037.

**Polard, P., Prère, M. F., Chandler, M., Fayet, O.** (1991). Programmed translational frameshifting and initiation at an AUU codon in gene expression of bacterial insertion sequence IS911. *Journal of Molecular Biology* 222, 465–477.

**Polikanov, Y. S., Blaha, G. M., Steitz, T. A.** (2012). How hibernation factors RMF, HPF, and YfiA turn off protein synthesis. *Science* 336, 915-918.

**Prevost, G., Bouakham, T., Piemont, Y., Monteil, H.** (1995). Characterisation of a synergohymenotropic toxin produced by *Staphylococcus intermedius*. *FEBS Lett.* 376, 135-40.

**Rabl, J., Leibundgut, M., Ataide, S.F., Haag, A., Ban, N.** (2011). Crystal structure of the eukaryotic 40S ribosomal subunit in complex with initiation factor 1. *Science* 331, 730–736.

**RajBhandary, U. L., Ghosh, H. P.** (1969). Studies on polynucleotides. XCI. Yeast methionine transfer ribonucleic acid: purification, properties, and terminal nucleotide sequences. *J Biol Chem.* 244, 1104-1113.

**RajBhandary, U.** (1994). Initiator transfer RNAs. *Journal of Bacteriology* 176, 547–552.

**Rayner, C., Munckhof, W. J.** (2005). Antibiotics currently used in the treatment of infections caused by *Staphylococcus aureus*. *Intern Med J.* 35.

**Rich, A., RajBhandary, U.L.** (1976). Transfer RNA: molecular structure, sequence, and properties. *Annual Review of Biochemistry* 45, 805–860.

**Rodnina, M. V.** (2013). The ribosome as a versatile catalyst: Reactions at the peptidyl transferase center. *Curr Opin Struct Biol* 23, 595–602.

**Rodnina, M.** (2018). Translation in prokaryotes. *Cold Spring Harb Perspect Biol.*

**Roll-Mecak, A., Cao, C., Dever, T. E., Burley, S. K.** (2000). X-Ray structures of the universal translation initiation factor IF2/eIF5B: conformational changes on GDP and GTP binding. *Cell* 103, 781–792.

**Romby, P., Vandenesch, F., Wagner, E. G. H.** (2006). The role of RNAs in the regulation of virulence-gene expression. *Curr. Opin. Microbiol.* 9, 229 – 236.

**Ruhnke, M., Maschmeyer, G.** (2002). Management of mycoses in patients with hematologic disease and cancer -- review of the literature. *European journal of medical research* 7, 227 - 235.

**Ruiz, J., Pons, M. J., Gomes, C.** (2012). Transferable mechanisms of quinolone resistance. *Int J Antimicrob Ag.* 40, 196–203.

**Sabol, S., Sillero, M. A., Iwasaki, K., Ochoa, S.** (1970). Purification and properties of initiation factor F3. *Nature* 228, 1269–1273.

**Sakai, T. T., Cohen, S. S.** (1976). Regulation of ornithine decarboxylase activity by guanine nucleotides: in vivo test in potassium-depleted *Escherichia coli*. *Proc. Natl. Acad. Sci.* 73, 3502-3505.

**Sanbonmatsu, K. Y., Joseph, S., Tung, C. S.** (2005). Simulating movement of tRNA into the ribosome during decoding. *PNAS* 102, 15854–15859.

**Sardi, J. C. O.** (2016). "Candida species: current epidemiology, pathogenicity, biofilm formation, natural antifungal products and new therapeutic options". *Journal of Medical Microbiology.*

**Savelsbergh, A., Rodnina, M. V., Wintermeyer, W.** (2009). Distinct functions of elongation factor G in ribosome recycling and translocation. *RNA* 15, 772–780.

**Scheres, S. H. W.** (2014). Beam-induced motion correction for sub-megadalton cryo-EM particles *eLife.* 3, e03665.

**Schlünzen, F., Zarivach, R., Harms, J., Bashan, A., Tocilj, A., Albrecht, R., Yonath, A., Franceschi, F.** (2001). Structural basis for the interaction of antibiotics with the peptidyl transferase centre in eubacteria. *Nature* 413, 814-821.

**Schmeing, T. M., Ramakrishnan, V.** (2009). What recent ribosome structures have revealed about the mechanism of translation. *Nature* 461, 1234–1242.

**Schmitt, E., Mechulam, Y., Ruff, M., Mitschler, A., Moras, D., Blanquet, S.** (1996a). Crystallization and preliminary X-ray analysis of *Escherichia coli* methionyl-tRNA(fMet) formyltransferase. *Proteins* 25, 139–141.

**Schmitt, E., Blanquet, S., Mechulam, Y.** (1996b). Structure of crystalline *Escherichia coli* methionyl-tRNA(f)Met formyltransferase: comparison with glycinamide ribonucleotide formyltransferase. *EMBO* 15, 4749–4758.

**Schmitt, E., Panvert, M., Blanquet, S., Mechulam, Y.** (1998). Crystal structure of methionyl-tRNA<sup>fMet</sup> transformylase complexed with the initiator formyl-methionyl-tRNA<sup>fMet</sup>. *EMBO* 17, 6819–6826.

**Schneider, T. D., Stormo, G. D., Gold, L., Ehrenfeucht, A.** (1986). Information content of binding sites on nucleotide sequences. *Journal of Molecular Biology* 188, 415–431.

**Schuwirth, B. S., Borovinskaya, M. A., Hau, C. W., Zhang, W., Vila-Sanjurjo, A., Holton, J. M., and Cate, J. H. D.** (2005). Structures of the bacterial ribosome at 3.5 Å resolution. *Science* 310, 827–834.

**Schweisguth, D. C., Moore, P. B.** (1997). On the conformation of the anticodon loops of initiator and elongator methionine tRNAs. *Journal of Molecular Biology* 267, 505–519.

**Segal, E.** (2005). *Candida*, still number one--what do we know and where are we going from there? *Mycoses* 48, 3 - 11.

**Seong, B. L., RajBhandary, U. L.** (1987). *Escherichia coli* formylmethionine tRNA: mutations in GGGCCC sequence conserved in anticodon stem of initiator tRNAs affect initiation of protein synthesis and conformation of anticodon loop. *Proceedings of the National Academy of Sciences of the United States of America* 84, 334–338.

**Serna, M.** (2019). Hands on Methods for High Resolution Cryo-Electron Microscopy Structures of Heterogeneous Macromolecular Complexes. *Front. Mol. Biosci.*, 15, 6-33.

**Sette, M., Van Tilborg, P., Spurio, R., Kaptein, R., Paci, M., Gualerzi, C. O., and Boelens, R.** (1997). The structure of the translational initiation factor IF1 from *E. coli* contains an oligomer-binding motif. *EMBO* 16, 1436–1443.

**Shine, J., Dalgarno, L.** (1974). The 3'-terminal sequence of *Escherichia coli* 16S ribosomal RNA: complementarity to nonsense triplets and ribosome binding sites. *Proceedings of the National Academy of Sciences of the United States of America* 71, 1342–1346.

**Simonetti, A., Marzi, S., Myasnikov, A. G., Fabbretti, A., Yusupov, M., Gualerzi, C. O., Klaholz, B. P.** (2008). Structure of the 30S translation initiation complex. *Nature* 455, 416-420.

**Simonetti, A., Marzi, S., Billas, I. M., Tsai, A., Fabbretti, A., Myasnikov, A. G., Roblin, P., Vaiana, A. C., Hazemann, I., Eiler, D., Steitz, T. A., Puglisi, J. D., Gualerzi, C. O., Klaholz, B. P.** (2013). Involvement of protein IF2 N domain in ribosomal

subunit joining revealed from architecture and function of the full-length initiation factor. *Proc. Natl. Acad. Sci.* 110, 15656-15661.

**Simonetti, A., Brito Querido, J., Myasnikov, A. G., Mancera-Martinez, E., Renaud, A., Kuhn, L., Hashem, Y.** (2016). eIF3 Peripheral Subunits Rearrangement after mRNA Binding and Start-Codon Recognition. *Molecular Cell* 63, 206–217.

**Singh, N. S., Das, G., Seshadri, A., Sangeetha, R., Varshney, U.** (2005). Evidence for a role of initiation factor 3 in recycling of ribosomal complexes stalled on mRNAs in *Escherichia coli*. *Nucleic Acids Research* 33, 5591–5601.

**Singh, N. S., Ahmad, R., Sangeetha, R., Varshney, U.** (2008). Recycling of ribosomal complexes stalled at the step of elongation in *Escherichia coli*. *Journal of Molecular Biology* 380, 451–464.

**Singh, R., Chakrabarti, A.** (2017). *Invasive Candidiasis in the Southeast-Asian Region*. Springer International Publishing 27.

**Skipkin, E., McConnell, T. S., DeVito, J., Lawrence, L., Ippolito, J. A., Duffy, E. M., Sutcliffe, J., Franceschi, F.** (2008). R chi-01, a new family of oxazolidinones that overcome ribosome-based linezolid resistance. *Antimicrob. Agents Chemother.* 52, 3550-3557.

**Sohmen, D., Harms, J. M., Schlunzen, F., Wilson, D. N.** (2009). SnapShot: Antibiotic inhibition of protein synthesis I. *Cell* 138, 1248.

**Sørensen, H. P., Hedegaard, J., Sperling-Petersen, H. U., Mortensen, K. K.** (2001). Remarkable conservation of translation initiation factors: IF1/eIF1A and IF2/eIF5B are universally distributed phylogenetic markers. *IUBMB Life.* 51, 321-327.

**Spahn, C., Jan, E., Mulder, A., Grassucci, R., Sarnow, P., Frank, J.** (2004). Cryo-EM Visualization of a Viral Internal Ribosome Entry Site Bound to Human Ribosomes: The IRES Functions as an RNA-Based Translation Factor. *Cell* 118, 465–475.

**Spurio, R., Brandi, L., Caserta, E., Pon, C. L., Gualerzi, C. O., Misselwitz, R., Krafft, C., Welfle, K., Welfle, H.** (2000). The C-terminal subdomain (IF2 C-2) contains the entire fMet-tRNA binding site of initiation factor IF2. *The Journal of Biological Chemistry* 275, 2447–2454.

**Steffensen, S. A., Poulsen, A. B., Mortensen, K. K., Sperling-Petersen, H. U.** (1997). *E. coli* translation initiation factor IF2--an extremely conserved protein. Comparative sequence analysis of the *infB* gene in clinical isolates of *E. coli*. *FEBS Letters* 419, 281–284.

**Steitz, J. A.** (1969). Polypeptide chain initiation: nucleotide sequences of the three ribosomal binding sites in bacteriophage R17 RNA. *Nature* 224, 957–964.

**Stringer, E. A., Sarkar, P., Maitra, U.** (1977). Function of initiation factor 1 in the binding and release of initiation factor 2 from ribosomal initiation complexes in *Escherichia coli*. *The Journal of Biological Chemistry* 252, 1739–1744.

**Studer, S. M., Joseph, S.** (2006). Unfolding of mRNA secondary structure by the bacterial translation initiation complex. *Molecular Cell* 22, 105–115.

**Subramanian, K. S., Meranger, J. C., MacKeen, J. E.** (1983). Graphite furnace atomic absorption spectrometry with matrix modification for determination of cadmium and lead in human urine. *Anal. Chem.* 55, 1064-1067.

**Sundari, R. M., Stringer, E. A., Schulman, L. H., Maitra, U.** (1976). Interaction of bacterial initiation factor 2 with initiator tRNA. *The Journal of Biological Chemistry* 251, 3338–3345.

**Sussman, J. K., Simons, E. L., Simons, R. W.** (1996). Escherichia coli translation initiation factor 3 discriminates the initiation codon in vivo. *Molecular Microbiology* 21, 347–360.

**Szkaradkiewicz, K., Zuleeg, T., Limmer, S., Sprinzl, M.** (2000). Interaction of fMet-tRNA<sup>fMet</sup> and fMet-AMP with the C-terminal domain of Thermus thermophilus translation initiation factor 2. *European Journal of Biochemistry / FEBS* 267, 4290–4299.

**Tabor, C. W.** (1962). Stabilization of protoplasts and spheroplasts by spermine and other polyamines. *J Bacteriol.* 83, 1101-1111.

**Tapprich, W. E., Goss, D. J., Dahlberg, E.** (1989). Mutation at position 791 in Escherichia coli 16S ribosomal RNA affects processes involved in the initiation of protein synthesis. *Proceedings of the National Academy of Sciences of the United States of America* 86, 4927–4931.

**Taylor, T. A., Unakal, C. G.** (2019). Staphylococcus Aureus. *StatPearls*, id NBK441868.

**Tenson, T., Mankin, A.** (2006). Antibiotics and the ribosome. *Mol. Microbiol.* 59, 1664-1677.

**Thon, F.** (1966). Zur Defokussierungsabhängigkeit des Phasenkontrastes bei der elektronenmikroskopischen Abbildung. *Zeitschrift für Naturforschung* 21a 476.

**Tomsic, J., Vitali, L., Daviter, T., Savelsbergh, A., Spurio, R., Striebeck, P., Wintermeyer, W., Rodnina, M. V, Gualerzi, C. O.** (2000). Late events of translation initiation in bacteria: a kinetic analysis. *EMBO* 19, 2127–2136.

**Tu, D., Blaha, G., Moore, P., Steitz, T.** (2005). Structures of MLSBK antibiotics bound to mutated large ribosomal subunits provide a structural explanation for resistance. *Cell* 121, 257–270.

**Umekage, S., Ueda, T.** (2006). Spermidine inhibits transient and stable ribosome subunit dissociation. *FEBS Lett.* 580, 1222-1226.

**Varshney, U., Lee, C. P., RajBhandary, U. L.** (1993). From elongator tRNA to initiator tRNA. *Proceedings of the National Academy of Sciences of the United States of America* 90, 2305–2309.

**Vellanoweth, R. L., Rabinowitz, J. C.** (1992). The influence of ribosome-binding-site elements on translational efficiency in Bacillus subtilis and Escherichia coli in vivo. *Mol. Microbiol.* 6, 1105-1114.

**Voorhees, R. M., Ramakrishnan, V.** (2013). Structural basis of the translational elongation cycle. *Annu Rev Biochem.* 82, 203-236.

**Walsh, C.** Where will new antibiotics come from? *Nature Rev. Microbiol.* 1, 65–70.

**Weiel, J., and Hershey, J. W.** (1982). The binding of fluorescein-labeled protein synthesis initiation factor 2 to *Escherichia coli* 30 S ribosomal subunits determined by fluorescence polarization. *The Journal of Biological Chemistry* 257, 1215–1220.

**Wilson, D. N.** (2009). The A-Z of bacterial translation inhibitors. *Crit. Rev. Biochem. Mol. Biol.* 44, 393-433.

**Wilson, D. N.** (2014). Ribosome-targeting antibiotics and mechanisms of bacterial resistance. *Nature reviews Microbiol.* 12, 35 – 48.

**Wintermeyer, W., Gualerzi, C.** (1983). Effect of *Escherichia coli* initiation factors on the kinetics of N-Acph-e-tRNAPhe binding to 30S ribosomal subunits. A fluorescence stopped-flow study. *Biochemistry* 22, 690–694.

**Wolfrum, A., Brock, S., Mac, T., Grillenbeck, N.** (2003). Expression in *E. coli* and purification of *Thermus thermophilus* translation initiation factors IF1 and IF3. *Protein Expression and Purification* 29, 15–23.

**Wu, Y., Du, S., Johnson, L., Tung, H., Landers, C., Liu, Y., Seman, B. G., Wheeler, R. T., Costa-Mattioli, M.** (2019). Microglia and amyloid precursor protein coordinate control of transient *Candida cerebritis* with memory deficits. *Nature Communications.* 10, 58.

**Yamamoto, H., Qin, Y., Achenbach, J., Li, C., Kijek, J., Spahn, C. M., Nierhaus, K. H.** (2014). EF-G and EF4: translocation and back-translocation on the bacterial ribosome. *Nat Rev Microbiol.* 12, 89–100.

**Yonath, A., Muessig, J., Tesche, B., Lorenz, S., Erdmann, V. A., Wittmann, H. G.** (1980). Crystallization of the large ribosomal subunit from *B. stearothermophilus*, *Biochem Int.* 1, 428-435.

**Yusupov, M. M., Yusupova, G. Z., Baucom, A., Lieberman, K., Earnest, T. N., Cate, J. H., Noller, H. F.** (2001). Crystal structure of the ribosome at 5.5 Å resolution. *Science* 292, 883-896.

**Yusupova, G. Z., Yusupov, M. M., Cate, J. H., Noller, H. F.** (2001). The path of messenger RNA through the ribosome. *Cell* 106, 233-241.

# Cryo-electron microscopy study of translation initiation complexes from *Staphylococcus aureus*

## Résumé

La synthèse des protéines, également appelée traduction de l'ARNm, est un processus conservé dans toutes les cellules vivantes. L'initiation de la traduction est une étape hautement régulée qui peut avoir plusieurs caractéristiques propres aux bactéries dites «à Gram positif». Un exemple de bactérie à Gram positif est le *S. aureus*, qui provoque de nombreuses infections nosocomiales et développe une résistance aux antibiotiques les plus couramment utilisés. Dans la plupart des cas, le ribosome est la cible d'antibiotiques pouvant agir à l'étape d'initiation de la traduction. Chez *S. aureus*, cette étape, présente des caractéristiques propres telles que l'absence de protéine ribosomale S1, l'extension de l'hélice 26 de l'ARNr 16S, des ARNm spéciaux impliqués dans la virulence et éventuellement d'autres caractéristiques affectant la synthèse des protéines. En conséquence, les structures obtenues des complexes d'initiation aideront à approfondir nos connaissances des aspects spécifiques de la synthèse protéique de cette bactérie.

Les connaissances acquises au cours de mes travaux pourront permettre de renforcer lutté contre cet agent pathogène.

**Mots clés:** *S. aureus*, ribosome, initiation de la traduction, cryo-EM

## Résumé en anglais

Protein synthesis, also called mRNA translation, is a conserved process in all living cells. It can be divided into 4 main steps: initiation, elongation, termination and recycling. Translation initiation is a highly regulated step that has several features unique to gram-positive bacteria. One example of gram-positive bacteria is a human pathogen *Staphylococcus aureus* that causes several nosocomial infections and develops resistance to most commonly used antibiotics. Often, the ribosome is the target of antibiotics that can act at the translation initiation step. This step in *S. aureus* has its own characteristics like the absence of r-protein S1, extension of the helix 26 of 16S rRNA, special virulence mRNAs and possibly other features affecting protein synthesis. As a result, obtained structures of the initiation complexes will help in gaining deeper insight on the species-specific features of protein synthesis of this bacterium.

The knowledge gained during my work will be used in further research and will hopefully contribute to the fight against this pathogen.

**Key words:** *Staphylococcus aureus*, ribosome, translation initiation, cryo-EM